ACTIVITY REMOVAL AND TRANSPORT STUDIES IN SUPPORT OF PWR IN-PILE LOOP OPERATIONS

by

Philippe Borys

Ingénieur Physicien, Ecole Nationale Supérieure de Physique de Grenoble

(July 1990)

SUBMITTED TO THE DEPARTMENT OF
NUCLEAR ENGINEERING IN PARTIAL FULFILLMENT OF
THE REQUIREMENTS FOR THE DEGREE OF
MASTER OF SCIENCE
at the
MASSACHUSETTS INSTITUTE OF TECHNOLOGY
February 1991

Signature of Author_____
Department of Nuclear Engineering
December 20, 1990

Certified by_____
Michael J. Driscoll Thesis Advisor
Professor Emeritus, Nuclear Engineering

Certified by_____
Otto K. Harling Thesis Advisor
Professor, Nuclear Engineering

Accepted by_____
Allan F. Henry
Chairman, Department Committee on Graduate Students

ACTIVITY REMOVAL AND TRANSPORT STUDIES IN SUPPORT OF

PWR IN-PILE LOOP OPERATIONS

by

Philippe Borys

Submitted to the Department of Nuclear Engineering on the 20th of December 1990, in partial fulfillment of the requirements for the Degree of Master of Science in Nuclear Engineering

ABSTRACT

An in-pile loop has been constructed at the MIT Nuclear Reactor Laboratory for PWR coolant chemistry studies. The first two experimental campaigns using this facility are now complete and a third is underway; the loop has become a significant resource for associated research in several areas which can provide data to better understand corrosion product transport mechanisms.

In the present work, data acquisition was a major task. In particular, decontamination methods were developed to assay, before and after in-pile runs, the inventory of deposited corrosion products and their associated radionuclides. As well, charging water and loop materials were analyzed for composition and impurity content, using different analysis techniques such as Neutron Activation Analysis, Atomic Absorption, High Performance Liquid Chromatography, and Colorimetry. In addition, the state-of-the-art computer codes, CRUDSIM, CORA and PACTOLE were applied to the MIT loop; predictions and experimental results were compared.

Results from the assay of radionuclides on loop surfaces suggest that PWR operation at $pH_{300°C}$ higher than 7.1 would be beneficial (lower ex-core activity deposition, hence lower maintenance doses) compared to operation at pH lower than 7.0. Computer codes, especially PACTOLE, were in relatively good agreement with MIT loop data when used to predict the effect of pH on the transport and deposition of transition metals species and radionuclides such as Co-60 and Co-58.

Initial crud inventories on preconditioned loop surfaces before the in-pile run were found to be representative of full-scale PWRs. Loop Inconel, Stainless Steel and Zircaloy-4 compositions were within specifications. It is worth noting that NAA showed 0.7 ppm Co in commercial Zr samples, and consequently, a recommendation was made to the ASTM to lower the specification for Co in Zircaloy from 20 to 2 ppm. Finally, water analyses showed that loop water was within EPRI guidelines values, and contained no unusual impurities.

Thesis Supervisor:	Dr. Michael J. Driscoll
Title:	Professor Emeritus of Nuclear Engineering
Thesis Supervisor:	Dr. Otto K. Harling
Title:	Professor of Nuclear Engineering

ACKNOWLEDGEMENTS

The author would like to sincerely thank Professor Emeritus Michael J. Driscoll for his continuous assistance, invaluable guidance, and understanding throughout the conduct of this work. My sincere thanks also goes to Prof. Otto K. Harling for his time and valuable comments.

The author would like to thank all of those people involved with the loop project , for their continuous help, guidance and cooperation, including Dr Gordon Khose, Mike Ames, Ernesto Cabello, Rene Sanchez and Chan Bock Lee.

The author would like to also thank Dr Pierre Beslu for his time and valuable comments.

Particular acknowledgement is due to Dr Ilhan Olmez for his cooperation. Thanks also, to Ms D. Eichel and R. Morton for their help.

I express gratitude to the MIT-Electric Utility Program, EPRI, ESEERCO, and NUPEC for their financial support for this work.

Finally, I thank my mother for her support.

TABLE OF CONTENTS

LIST OF FIGURES

LIST OF TABLES

1 INTRODUCTION

1.1 Foreword

The chemical environment in the primary circuit of a Pressurized Water Reactor (PWR) nuclear power plant is sufficiently corrosive to merit concern over materials integrity and the resulting need for maintenance, while at the same time creating circumstances which interfere with repair. In particular, from the various metals used throughout the system, corrosion products are released into the coolant and transported onto core surfaces where they are activated. Re-release followed by deposition, which forms what is called "crud" (transition metal oxides: eg nickel ferrites), on the out-of-core components creates a significant radiation dose, leading to significant maintenance problems.

Steady decline of the maintenance dose rate has been seen over the past few years. However, in view of the work remaining to do in this area, an in-pile facility has been developed at the MIT Nuclear Reactor Laboratory to evaluate how to reduce dose rates by improving PWR coolant chemistry. The work reported here is part of the effort to acquire data from the experiments already completed to better understand corrosion product transport mechanisms.

1.2 Background

As the wetted surfaces around the primary coolant loop corrode, the corrosion products of iron, nickel, chromium and cobalt, which are the main constituents of metal such as stainless steel and Inconel, are released into the coolant. The resulting water borne corrosion products may be soluble (ions) or insoluble particles. These corrosion products can deposit on fuel surfaces in the reactor core and capture neutrons to become radioactive. Figure 1.1 shows the main mechanisms of activation of corrosion products. Some of the product radionuclides are then released into the coolant and eventually re-deposit on out of core surfaces. This radioactivity on out of core surfaces, especially steam generator tubing and channel heads, has become the main source of plant worker exposure for PWR units. A schematic of the transport of corrosion products in PWRs is presented in Fig. 1.2.

The main radioactive species of concern are Co58 and Co60. Co58 is dominant during the first year of a new reactor and because of its short half life ($T_{1/2}$=71 days) tends to saturate after about a year. On the other hand, the long-lived Co60 ($T_{1/2}$=5.26 years) increases, until stabilizing after about 5 years. In PWRs, after a few years of operation, the respective activities of both species are comparable, even though the relative fraction of each species differs from plant to plant due in part to the high variability of Co59 (natural Cobalt and the parent of Co60) from stellites used in wear-susceptible surfaces such as valves, or

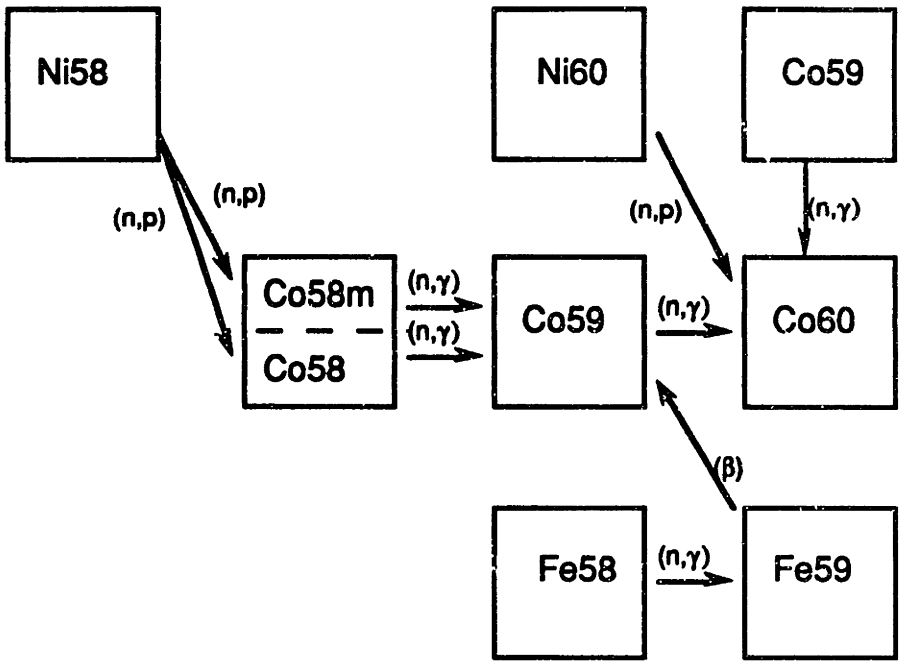

Fig 1.1 Principal Corosion Product Radioisotope Production Schemes (K-1)

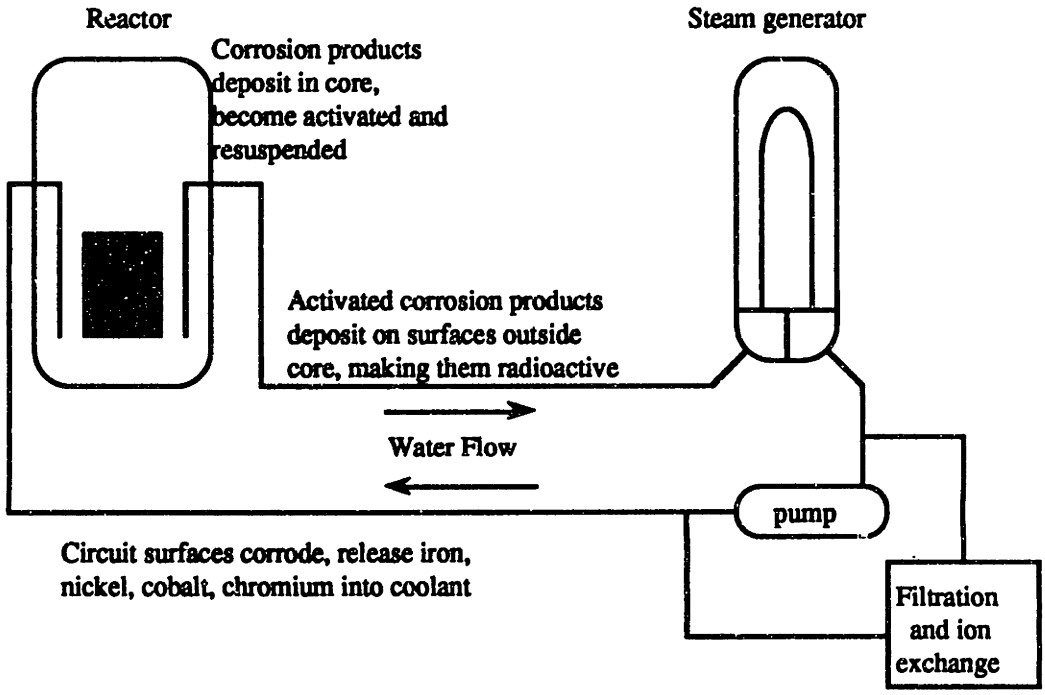

Fig 1.2 Transport of Corrosion Products in PWRs

from cobalt contamination in Nickel alloys used in the spacer grits of some older fuel assembly designs and of course the heat exchangers . Co58, on the other hand, is produced by (n,p) reaction with Ni58 (68.3% of natural nickel) which is a major constituent of both Inconel and Stainless Steel

An in-pile loop, the PWR Coolant Chemistry Loop (PCCL), has been constructed at the MIT Nuclear Reactor Laboratory (Fig 1.3) to simulate a PWR primary circuit in order to study corrosion product transport. The initial conceptual design of the facility was carried out under MIT Electric Utility Program, and the EUP has continued to support complementary research on the PCCL, including much of the effort reported in this thesis. Subsequently, construction and operation were undertaken under Electric Power Research Institute (EPRI) and Empire State Electric Energy Research Corporation (ESEERCO) sponsorship. The Japanese Nuclear Power Engineering Test Center (NUPEC) has also contracted for a series of three 3000 hour runs using the PCCL during the next three years. As of fall 1990, seven runs have been completed under EPRI and ESEERCO sponsorship. The purpose of these month long runs was the optimization of $LiOH/H_3BO_3$ pH control to minimize deposition of activated corrosion products on the out-of-core surfaces. At the end of each run, each loop is sacrified and studied. As noted earlier, the main purpose of the work presented in this thesis is development and application of data collection methods to loop components. In

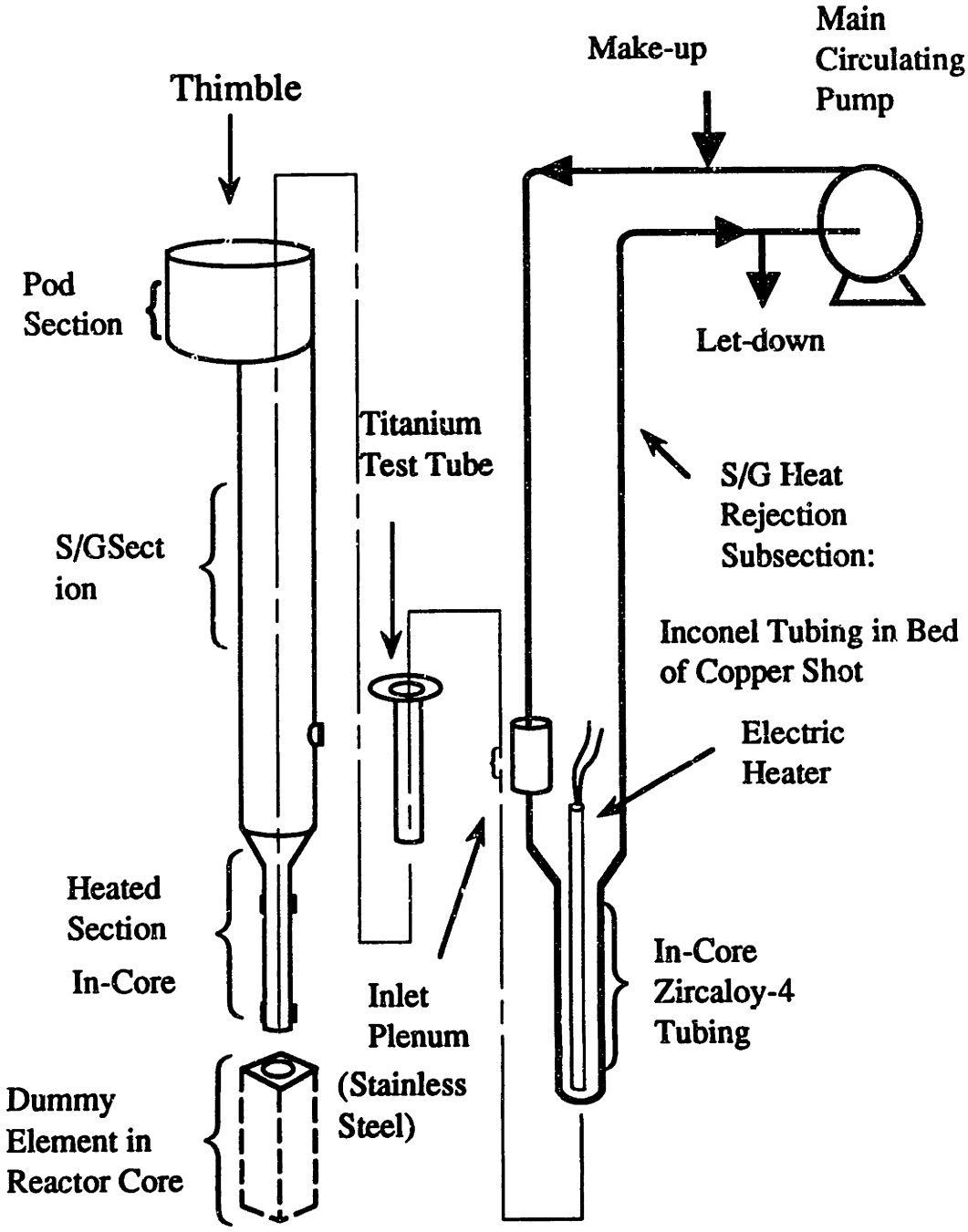

Fig 1.3 Diagram of Major PCCL Components (S-2)

addition, significant work was also done in the area of post shut down experiments, and comparison between code predictions and experimental results.

The basic idea of the PWR Coolant Chemistry Loop (PCCL) is to simulate a unit-flow cell of a PWR (one steam generator tube and one core flow channel -see Fig 1.3-) in order to study chemistry control strategies such as the effect of lithium hydroxide and boric acid control of pH on radionuclide deposition. The hydraulic diameters and lengths are about 1/3 of those of a real PWR. The heat fluxes, ratio of Zircaloy/Inconel/Stainless Steel surfaces exposed to the coolant and coolant velocity are scaled to match as closely as possible those of a full scale PWR. Each loop is compact, therefore inexpensive, and can be sacrified for analysis at the end of each run. At the end of each run, one of the principal objectives is to analyze the components for their radionuclide inventories. On one hand, the Inconel steam generator section is directly scanned using a HpGe detector (C-1)(S-1), on the other hand, for the bottom of the steam generator section, the stainless steel plenum and the core section, it was necessary to develop descaling methods in order to separate the crud from the activated base metal. Beginning with the earlier work by Cabello (C-1), and continuing with the effort reported here, methods were developed from already existing chemical or mechanical decontamination procedures used in plants to reduce the amount of radioisotopes.

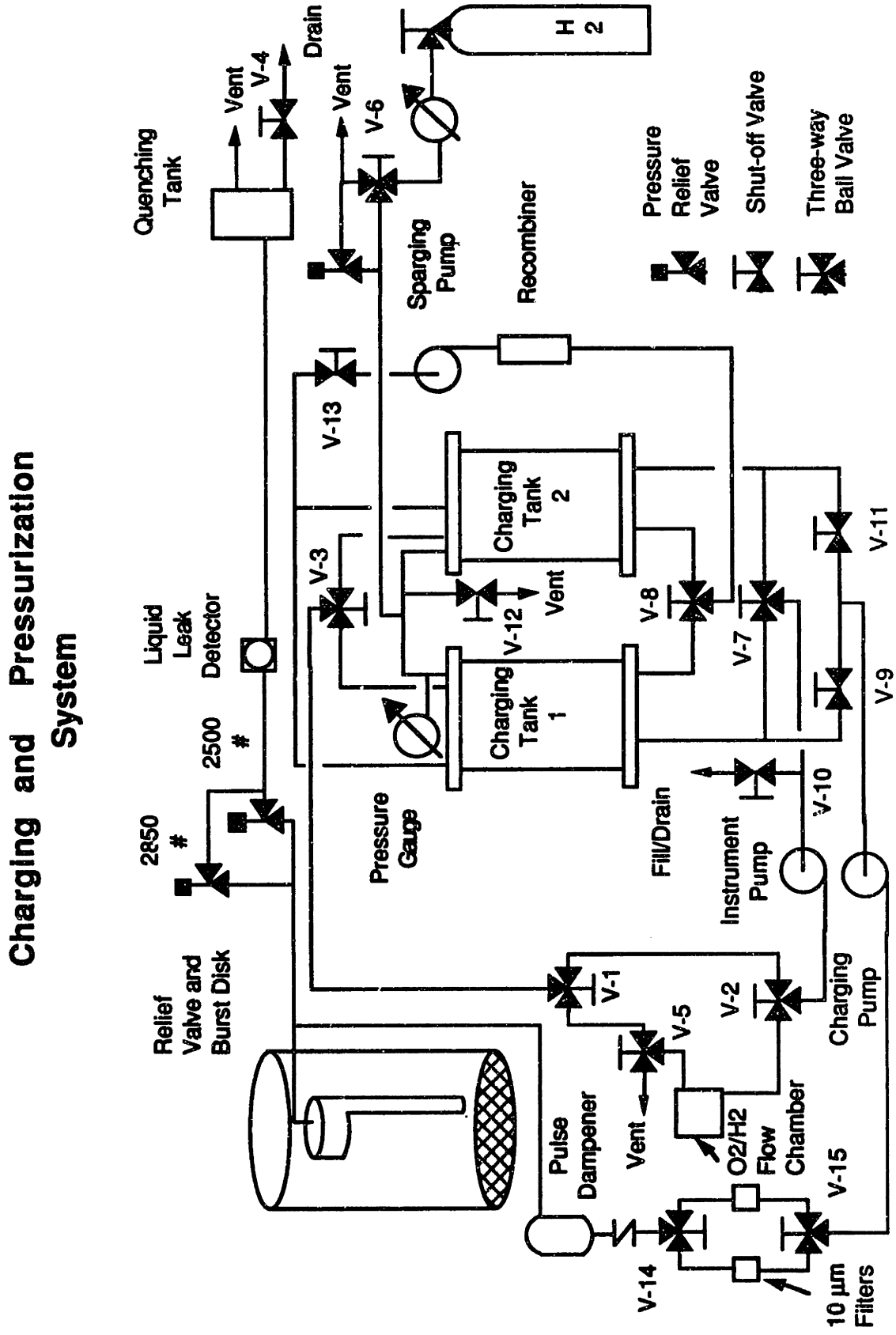

Fig 1.4 PCCL Charging System (S-2)

Also of concern was the importance of the charging system (see Fig 1.4), which is mostly made of stainless steel and is run at room temperature, where the solubilities are much higher than at 300°C. PACTOLE code predictions suggested that more than 60% of both PWR and PCCL corrosion products originate from the charging system surfaces. In the present work, coolant analyses have been performed to investigate such predictions.

Analyses of the materials used to build the PCCL were done using Neutron Activation Analysis (NAA), not only to check the representativity of these materials but also to explain the origin of some radionuclides measured in PCCL coolant or surface samples.

Also of interest is the fact that the loops were prefilmed together for one month out-of-pile using PWR reference chemistry (1.41 ppm Li, 600 ppm Boron) and preconditioned separately for one month under chemistry identical to that used in its one month long in-pile run. Chemistry for the seven in pile runs are as follows:

PR1: 1.84 ppm Li, 800 ppm B	$pH_{300°C}=7.0$
PR2: 1.84 ppm Li, 800 ppm B	$pH_{300°C}=7.0$
PH1: 6.26 ppm Li, 800 ppm B	$pH_{300°C}=7.5$
PL1: 0.56 ppm Li, 800 ppm B	$pH_{300°C}=6.5$
PBR: 3.00 ppm Li, 800 ppm B	$pH_{300°C}=7.2$
PBL: 0.46 ppm Li, 0 ppm B	$pH_{300°C}=7.2$
PNZ: 3.00 ppm Li, 800 ppm B, "less Zinc"	$pH_{300°C}=7.2$

At the end of each preconditioning it was necessary, from a modelling point of view, for each run, to measure the inventory of corrosion product species on the loop surfaces. To do this, tubes

and coupons were descaled and the solutions analyzed using Atomic Absorption (AA) and NAA. Finally, end-of-run assays of both chemical and radioactive species were compared with state-of-the-art computer programs such as PACTOLE (B-2)(B-3)(B-4), CRUDSIM (B-5) and CORA (K-1).

Table 1.1 summarizes the PCCL run histories; the hot hours (ie temperature at the outlet of the core > 550°F) and the MW-Hours are shown for each run. References (S-2) and (D-1) provide additional details.

Table 1.1 Summary of PCCL Tests (D-1)

Run	Chemistry			Operation		Transients*		
Code	$pH_{300°C}$	B (ppm)	Li (ppm)	Hot Hours	MW-Hours	A	B	C
PR1	7.0	800	1.84	889	2328	1	-	2
PR2	7.0	800	1.84	536	1871	1	-	5
PL1	6.5	800	0.56	478	2115	2	-	-
PH1	7.5	800	6.26	533	2288	-	-	-
PBR	7.2	800	3.00	728	1569	-	-	-
PBL	7.2	0	0.46	711	1656	-	1	1
PNZ	7.2	800	3.00	232	842	-	3	-

* The number of transients after the beginning of operation is given:
A- Controlled shutdown
B- Automatic shutdown, no boiling
C- Automatic Shutdown, boiling

1.3 Organization of Present Work

This thesis is divided into seven chapters. The present chapter presents the introduction to the work reported in this report.

Chapter two describes the chemical analyses performed on the water samples taken from the loop coolant as well as analyses done on the materials used to build not only the seven EPRI/ESEERCO loops but also the three NUPEC loops. The choice of the technique of analysis depended on the analysis but Atomic Absorption (AA), Neutron Activation Analysis (NAA), High Performance Liquid Chromatography (HPLC) and Colorimetry were used.

Chapter three discusses all the decontamination techniques used to descale the PCCL components, and reports the final inventory of radionuclides in each area around the loop (steam generator, plenum and core).

Post-shutdown studies are described and results reported in chapter four. Tubes from the steam generator and core section underwent treatment to reproduce the high release of radionuclides seen in plants during cooldown and aeration.

Chapter five reports the work performed to determine the initial (ie. at the beginning of the in-pile run) inventory on loop surfaces. This work was valuable for computer code studies because code predictions depend on the initial inventory.

Chapter six summarizes the work done using the computer codes available at MIT (PACTOLE, CRUDSIM, CORA). Predictions are compared to experimental results.

Finally, chapter seven provides a summary of the work reported in this thesis and conclusions which follow from it. Recommendations for future work are also given in this chapter.

2 CHEMICAL ANALYSES

2.1 Introduction

The main task of the work presented in this thesis was to evaluate the contributions to, and inventory of, corrosion products in the subject in-pile experiments. To do so, it was necessary to characterize the water provided to the loop by the loop charging system as well as to characterize the different materials (ie Stainless Steel, Inconel and Zircaloy) used to build the loop.

Concerns about the transition metal input from the charging system tubing grew when initial PACTOLE code predictions (B-1) suggested that more than 60% of the transition metals in the water were coming from the charging system for the EPRI/ESEERCO runs. High predicted solubilities in the room temperature charging lines were causing this effect, and therefore it was necessary to make actual measurements to check the predictions and to take adequate measures to get rid of this input for the NUPEC runs. Accordingly, measurements of high purity source waters and samples from the PCCL charging system were made. Means of analyses were mainly Neutron Activation Analysis (NAA), High Performance Liquid Chromatography (HPLC), Atomic Absorption (AA) and Colorimetry. Descriptions of the techniques, experiments and results are presented in the following sections of this chapter.

In addition, characterization of the tubing materials, and more particularly their cobalt content, was needed to be sure that

they were within specification, but also to understand the source of the corrosion products and the radionuclides. This has been done using NAA. The technique is described in detail in section 2. Results are presented in section 7 of the present chapter.

Finally, preconcentration methods using chelating ion-exchange papers, a useful tool for these investigations, were developed and are presented in section 6 of this chapter.

2.2 Neutron Activation Analysis

In Neutron Activation Analysis (NAA), the sample to be analyzed is exposed to a high neutron flux. Because of the lack of Coulomb barrier between neutrons and the target nucleus, the probability of having a nuclear reaction with neutrons is rather large compared to other particles. The most important nuclear reaction for NAA is the (n,γ) type, in which the excited nucleus decays to a lower energy state by the emission of γ rays.

If we irradiate an isotope with neutrons, the activity produced can be calculated using the following equation:

$$A = \phi\sigma n(1-e^{-\lambda t_i})e^{-\lambda t_c} \qquad (2.1)$$

where ϕ = neutron flux (n/sec.cm^2)

σ = cross section (cm^2)

n = number of target nuclei

t_i = irradiation time (min)

t_c = cooling time (min)

λ = decay constant (min^{-1})

Using this equation one can calculate the amount of material in a given matrix. But since ϕ is not well defined, a "comparative method" is employed, where a standard with accurately known composition is irradiated along with the unknown sample. Then, the composition of the unknown can be calculated from:

$$\text{Wt (in sample)} = ([\text{A (sample)}]/[\text{A (std)}]) * \text{Wt (in std)} \quad (2.2)$$

Semiconductor (GeLi or HpGe) detectors are commonly used in NAA because of their high resolution.

When a predominantly thermal-spectrum nuclear reactor is used to irradiate the sample, we speak of thermal NAA. Activation is effected primarily by (n,γ) reactions. Since, activation cross sections of most of the elements are high for thermal neutrons, low detection limits can be achieved.

2.3 High Performance Liquid Chromatography

The HPLC technique takes its roots from liquid chromatography and gas chromatography techniques. In the original methods an adsorbent, for instance alumina or silica, is packed into a column and is eluted with a suitable liquid. A mixture to be separated is introduced at the top of the column and is washed through the column by the eluting liquid. If a component of the mixture (a solute) is adsorbed weakly onto the surface of the solid stationary phase it will travel down the column faster than another solute that is more strongly adsorbed. Thus separation of the solutes is possible if there are differences in their strength of adsorption by the solid.

HPLC was developed in the 1960's. The particle size of the stationary phase material (in the column) was reduced; this had the effect of improving the efficiency of the method. Today microparticulate columns, commonly porous silica particles, are used. The mechanisms of separation can be described as the adsorption of elements by chemical elements bonded to the silica particle. At present, 75% of the work done by HPLC uses columns with C-18 Alkyl groups attached to the surface of silica particles.

The mobile phase (eluent) typically has a flow rate between 0.5 and 5 cc/min. In all the applications described in this report a constant flow rate was used. For a given eluent and a given flow rate, the retention time of solutes (ie the time taken for a solute to pass through the chromatographic system) is a constant.

After passing through the column, the separated solutes are sensed by an in-line detector. The output of the detector is an electrical signal. UV and conductivity detectors can be used, depending on the nature of the species involved.

The basic components of a HPLC are described in Fig 2-1 (adapted from (L-2)).

2.4 Atomic Absorption Technique

Atomic spectroscopy has its origins in the flame test in which many elements can be identified by the characteristic colors which their salts give to a flame. (see Fig. 2-2).

With the development of the Bunsen burner, which gives a relatively colorless flame and consequently doesn't produce intrinsic interferences, the technique of atomic absorption has been improved.

In atomic absorption, high temperatures are needed to generate free atoms. Once atoms are generated, photons can interact with them. Under certain conditions their interaction can lead to a photon being absorbed by an atom.

Since the energy levels in an atom are quantified, they can only have certain well defined values. The absorption process is described in Fig. 2-3.

The photon energy, $h\upsilon$, must be exactly equal to the energy which separates two levels.

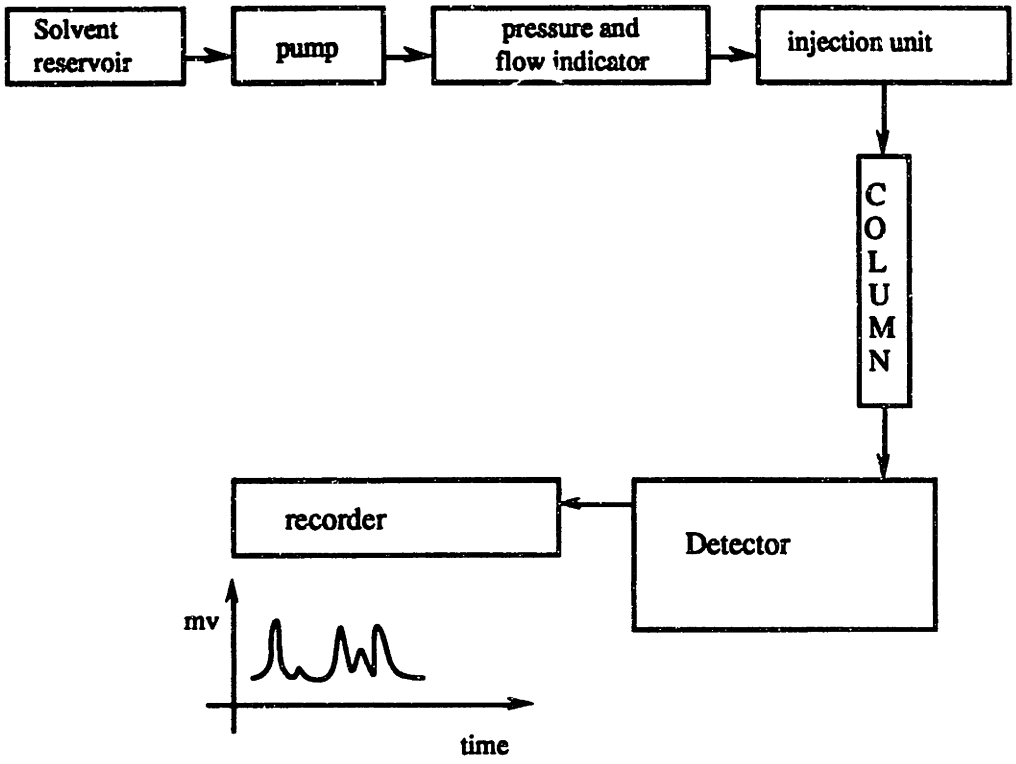

Fig 2.1 Basic components of a HPLC (adapted from L-2)

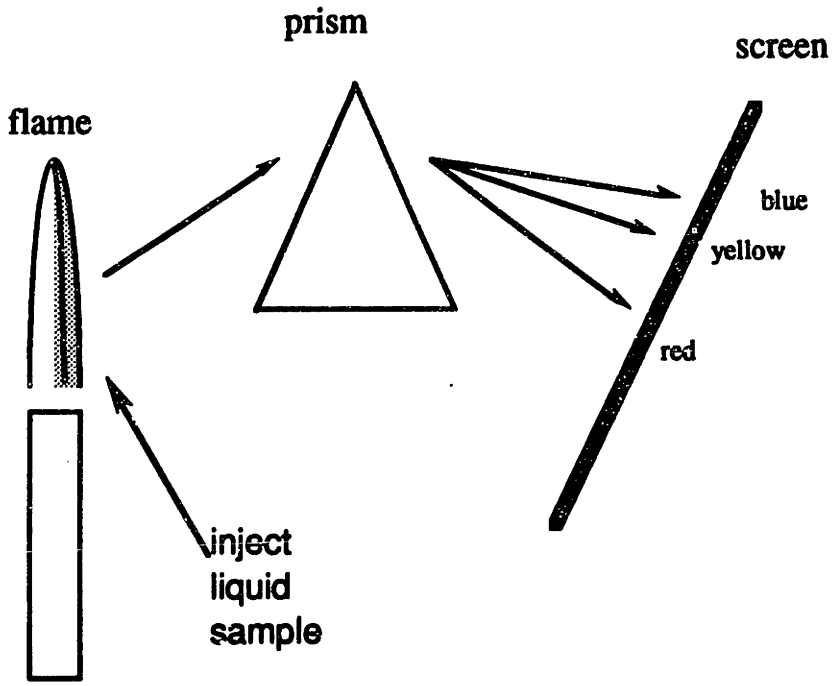

Fig 2.2 Dispersion of light emitted from a flame.(M-1)

The determination, in an analysis, of hυ allows us to recognize a specific element in our sample. For instance, at 589 nm, electrons of sodium atoms move from the 3s orbitals to the 3p orbitals. Consequently, if one measures the light absorbed by a sample at 589 nm, and compares it with absorption by a standard, it is easy, using Beer's law, to compute the sodium concentration of a sample.

2.5 Colorimetry

When light passes through a medium, the different wavelengths of the beam may be preferentially absorbed. For example, a liquid colored red will only allow the wavelength of red light to pass through without being absorbed.

In any medium the absorbed wavelengths are called the "absorption peaks".

A determination of the wavelength vs absorption spectrum of any medium , if there is absorption of light by this medium, provides a characterization of the substance. Consequently, we are sometimes able to detect a compound in a medium. Moreover, the intensity of an absorption peak can be used for quantitative analyses. A spectrometer permits quantitative determination of light transmitted by a sample, to carry out qualitative and quantitative analyses (I-2).

A schematic representation of a colorimeter is shown in Fig 2.5.

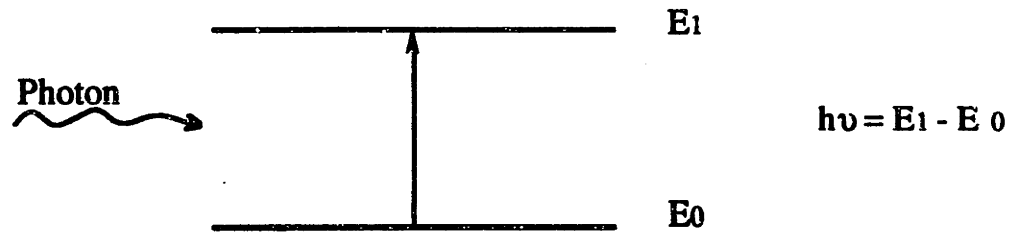

Fig 2.3 Representation of an atomic absorption process

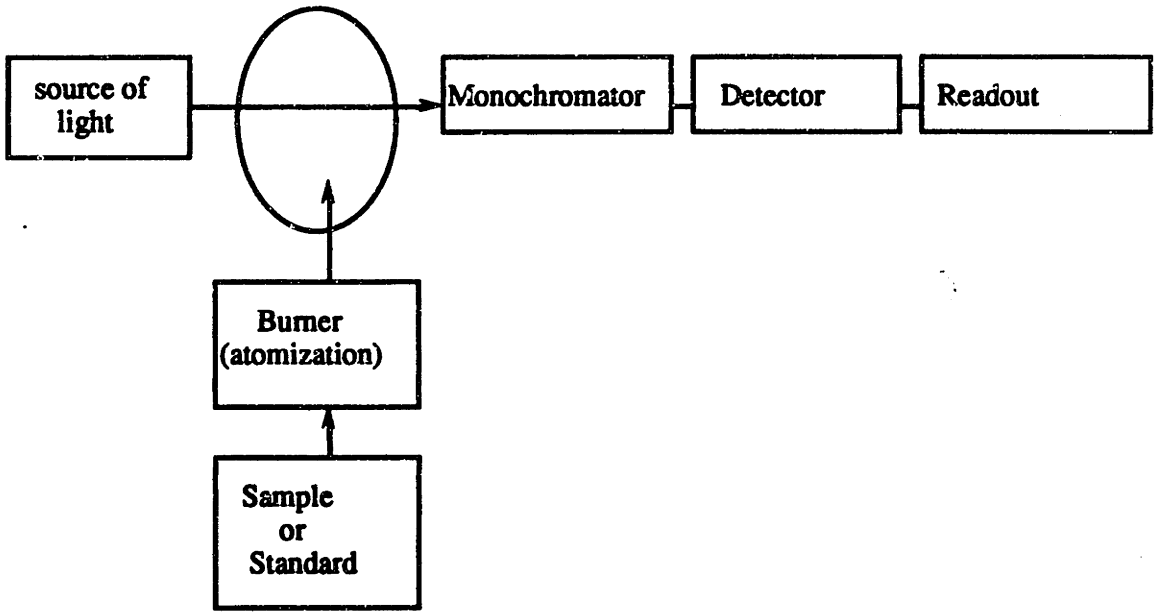

Fig 2.4 Main features of the atomic absorption technique (M-1)

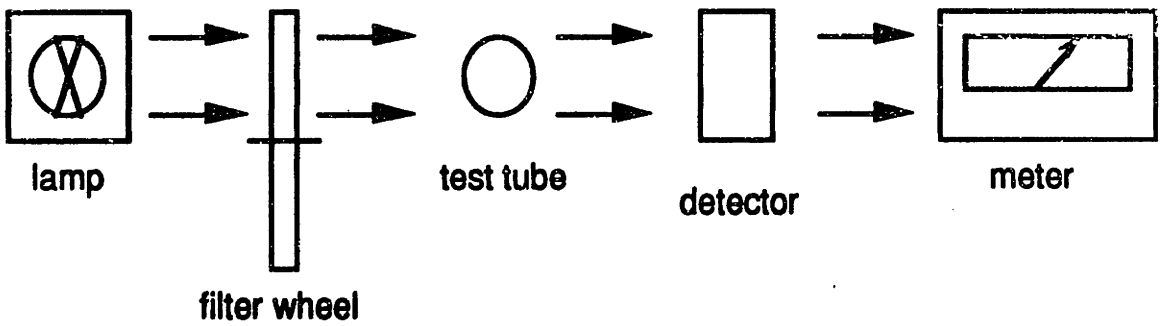

Fig 2.5 Basic components of a colorimeter

To obtain quantitative results, Beer's law can be applied:

$$\log_{10}(I_0/I)=KLC$$

where I_0=solvent transmittance
I=sample transmittance
K=constant
L=path length through the sample
C=concentration

The term $\log_{10}(I_0/I)$ is called absorbance. As can be seen, the absorbance is linearly related to the concentration and thus, is very useful for quantitative studies.

Usually, a calibration curve of absorbance vs concentration is plotted by measuring some known samples. It is, then, easy to determine an unknown concentration by measuring the absorbance of the sample.

2.6 Ion-Exchange Papers

Cation, anion and chelating 47mm Ø filter paper disks were purchased from Sumitomo Chemical Industries, Co (Cat. No EXPAPIER NF-1, NF-2, NF-3). The projected use of these papers was in a system to clean the loop charging water for the NUPEC PCCL runs. However, the chelating paper also appeared to be suitable for chemical analyses of current interest. As received,

cation, anion and chelating papers were in the Na, Cl and Cu forms respectively. Depending on the application, pretreatment was sometimes needed to change the form of the paper. For the scope of this thesis, only one paper was used, the chelating one. Tests were performed in order to characterize its ability to remove transition metals from solutions and therefore concentrate them.

2.6.1 Description of the Tests

For these tests, papers were prepared following the procedure recommended by Mitsubishi. This procedure was aimed at using the papers to clean PWR type waterchemistry without affecting the boron and lithium contents. The procedure, for the chelating paper (F-1) is described below. The filter holder apparatus was purchased from Millipore (cat. no XX43 047 00).

- Preparation of the chelating papers:

1-soak a maximum of 10 papers overnight in 200ml of 2N-HCl

2-mount two sheets of papers in the filtering apparatus.

3-elute twice with 50ml, 2N-HCL (Filtration flow rate: 10ml/min).

4-Rinse 6 times with 50 ml each of pure water.

5-Treat with 2.5 liters of LiOH solution (2 ppm Li).

6-Rinse twice with 50 ml of pure water.

7-Store in sealed polyethylene bag (to keep the papers wet).

The purpose of the first set of tests was not only to check the ability of the papers to remove transition metals, but also to check the capacity of the papers. Different solutions were pumped using a peristaltic pump through two prepared filters placed in series in two different holders. Filters were then analyzed by NAA. Table 2.1 describes the test procedures.

A similar test was done to check that a chelating paper would not modify the pH of a PWR chemistry solution. PWR type chemistry was pumped through two chelating papers and the pH of grab samples was checked, using a Cole Parmer Chemcadet® pH meter (model no 5984-50, serial no 507631), at different times during the experiment, and compared to the pH of the input solution.

2.6.2 Results and Conclusions

Results of the tests described above are presented in tables 2.2 and 2.3.

The STD-1 and STD-2 papers were nominally capable of absorbing 0.5 mg of cobalt; the subject measurements showed the ability of the chelating papers to pick up transition metals, and a capacity of a few mg.

These results showed also that the use of chelating papers to clean up solutions of PWR type chemistry could lead to pH

Table 2.1 Test Procedures

Test purpose	characterize the ability of picking up transition metals	Test the capacity of the papers
number of papers and description	2 STD-1 (first paper) STD-2 (second paper)	2 CAP-1 (first paper) CAP-2 (second paper)
number of filter holders	2	2
solution	1 ppm Co	1 ppm Co
Volume of solution pumped through the papers	0.5 liter (ie 0.5 mg of Co)	5 liters (ie 5 mg of Co)
mode of analysis of the papers	NAA	NAA

Table 2.2 Results of the Chelating paper tests

	Cobalt content (mg)
STD-1	0.49 +/- 0.005
STD-2	0.01 +/- 0.0001
CAP-1	2.86 +/- 0.03
CAP-2	1.49 +/- 0.02

Table 2.3 pH study results

Volume of chemistry already filtered when sample when taken	pH
0	6.57 (before filtration)
500 ml	6.35
1 liter	6.51
1.5 l	6.54
2.0 l	6.57
2.5 l	6.54

changes in small samples; however, after filtration of 2 liters of chemistry, this effect no longer takes place.

Other experiments, beyond the scope of this thesis, indicated that the papers, if used as-prepared for cleaning PWR type chemistry, are inadequate because they release undesirable chloride ions to the water. Furthermore, NAA done on the chelating paper showed non negligible traces of sodium. Consequently, it was decided not to use these papers for the next (NUPEC) campaign of PCCL runs because of their potential release of undesirable species. On the other hand, they have been shown to be adequate for concentrating transition metals for trace analyses using NAA.

2.7 Materials and Water Analyses

2.7.1 Description of the Experiments

The main purpose of these analyses was to measure the levels of impurities in the charging chemistry of the PCCL loop, and also, to determine the compositions of the materials used to construct the PCCL. To check for impurities in the PCCL water, two different techniques were used: HPLC for transition metals and anions, and NAA (using a freeze-dry process, or concentrating the species by filtering a sample through a chelating ion-exchange paper). Table 2.4 summarizes the analytic capabilities presently available at the MITNRL. The process of freeze-drying is used to

dry the sample. The samples are first frozen and then put under vacuum. From a phase diagram for H_2O, one can see that at low temperatures under vacuum, water goes from the solid phase to gas without being liquified. One of the advantages of this approach over high temperature evaporation is that it is done under vacuum and therefore minimizes contamination from dust from the air.

Stainless steel, Inconel, and Zircaloy, the main alloys constituting the wetted surfaces of the PCCL loop were analyzed by NAA. Small pieces (a few milligrams), of the material to be analyzed were cut, and in order to avoid contamination from the cutting tool, the outside surface was dissolved away using aqua regia (1vol HNO_3 + 3 vol HCl +2vol H_2O) or, in the case of Zircaloy, ammonium bifluoride. The surfaces were then cleaned using HNO_3 (30%) followed by a final rinse using DI H_2O. However, the surfaces of two Zircaloy pieces were also analyzed to confirm that the surface was not different from the bulk metal. These two pieces were shaved using a diamond coated scraper; the scraps were then analyzed following the regular procedure. The samples, together with standards, were irradiated in the 1PH1 port of the MIT Nuclear Reactor. The flux there is approximately 7.35 10^{12} n/cm^2sec when the reactor is at 4.5 MW. The irradiation time was varied with the material to be tested: 10 minutes and 4 hours were usually adequate for the Stainless Steel or Inconel and Zircaloy, respectively. Samples were then counted using either the PCCL HpGe detector (C-1) (S-1) or one of the GeLi detectors in the NRL Radiochemistry Laboratory operated by Dr Ilhan Olmez,

which offered high efficiencies, high resolution and automatic analysis by NAA software (ND9900 Workstation - Nuclear Data Inc.- used on a Micro Vax/VSM). Table 2.5 summarizes the main reactions that were used to determine the amounts of metals in each sample.

2.7.2 Results and Conclusions

• Results of Makeup Water Analyses and Conclusions

First, in tables 2.6 through table 2.8 are presented the results of the analyses of the high purity water sources available at the MIT NRL. Usually, DI water from the AA Lab, located in Building NW13 Room 247, was used to prepare PCCL makeup water chemistry batches. This system consists of 5 Cole Parmer ion-X-Changer filter cartridges. One adsorber cartridge (cat.# N-01506-15) removes most organic compounds, free chlorine and chloramines, phosphate complexes and turbidity. Two Universal cartridges (cat# N-01506-25) remove all ionized constituents except free carbon dioxide and silica. Finally, two Research cartridges remove all ionized minerals down to a level of 4 ppb or less (C-2).

Second, in tables 2.9 through 2.11 are presented the results of the analyses of the PWR type chemistry used for the PCCL runs. These solutions were made using Mallinckrodt H_3BO_3 analytical reagent, which claims 0.0001% of iron (this represents

Table 2.4 Analysis capabilities at the NRL

	Prof Ballinger's Waters HPLC	NRL Dionex HPLC	HACH DR2000 Colorimeter	AA flame or graphite furnace	NAA
elements measured with these techniques	Na^+, Li^+, NH_4^+, K^+ Co^{2+}, Fe^{2+}, Ni^{2+}, Co^{2+}, Pb^{2+}, Mn^{2+}, Cu^{2+}, Cd^{2+}	F^-, Br^-, Cl^-, SO_4^{2-}, NO_3^- NO_2^-	Fe^{2+}, Ni^{2+}, SiO_2	Ca, B, Li, Co, Fe, Zn, Cu, Ni, Cr, Pb	Co, Ni, Cr, Mn, Fe

table 2.5 Main reactions used for NAA

Element	Nuclear Reactions	Radionuclide	γ Energies	Half Life
Ni	Ni64(n,γ)Ni65	Ni65	1.4818 MeV 1.1155 MeV	2.520 hours
Mn	Mn55(n,γ)Mn56	Mn56	0.84675 MeV	2.580 hours
Fe	Fe58(n,γ)Fe59	Fe59	1.0992 MeV 1.2916 MeV	44.6 days
Co	Co59(n,γ)Co60	Co60	1.3325 MeV 1.1732 MeV	5.27 years
W	W186(n,γ)W187	W187	0.68581 MeV 0.47953 MeV	23.9 hours
Zn	Zn64(n,γ)Zn65	Zn65	1.1155 MeV	243.8 days

Table 2.6 Results of NAA using freeze-dry process

(ppb)	Radiation Lab DI Water	AA Lab DI water
Iron	250 +/- 70	476 +/- 164 <353
Sodium	454 +/- 30	325 +/- 21
Tungsten	<0.26	0.2 +/- 0.1
Bromine	2.0 +/- 0.6	2.6 +/- 0.7
Chromium	3.9 +/- 0.7	2.1 +/- 0.9
Cobalt	2.1 +/- 0.2	1.8 +/- 0.4
Zinc	<19.7	<47

Table 2.7 Results of NAA using Chelating Papers

(ppb)	double DI water from AA Lab
Zinc	0.7 +/- 0.4
Cobalt	<0.02
Iron	<8
Chromium	0.13 +/- 0.1

Table 2.8 Additional Results of NAA using freeze-dry technique

(ppb)	DI water from BCCL system	DI water from reactor system	DI water from Prof Ballinger's Lab system	DI water from AA Lab
Zinc	9.6 +/- 1.3	4.1 +/- 0.6	2.7 +/- 0.6	9.6 +/- 1.3
Cobalt	<0.01	<0.01	<0.01	<0.01
Iron	4 +/- 3	10 +/- 3	<6	<6
Chromium	0.35 +/- 0.07	1.4 +/- 0.1	<0.1	<0.1

Table 2.9 HPLC Measurements of Makeup Water Trace Elements

(ppb)	PR1	PR2	PL1	PH1	PBR
Zinc	13 (12.3)	52 (47.3	26 (15.1)	19	16
Nickel	106 (53.3)	68 (40.7)	142 (68.2)	58 {<10}	88
Cobalt	~4 (<4)	(~9)	~10 (~7.6)	~4 {<10}	~4 [1.8 ± 0.1]
Chromium				{<4}	[0.7 ± 0.5]
Iron (II)	116 (54.2)	83 (57.2)	210 (82.9)	89 {130}	92 [91 ± 35]
Manganese	23 (<4)	20 (8)	29 (14.3)	23 {5}	30 [10 ± 1.4]

note: Values in () are results measured on December 1989

Values in [] are results of NAA measurements (performed by R. Sanchez using Bio-Rad Analytical Grade Chelating Resin - Chelex™ 100 - catalogue # 142-2842)

Values in {} are Inductively Coupled Plasma (ICP) results (performed in France by P. Beslu)

Table 2.10 Further Results of NAA using freeze-dry process

(ppb)	PL1 Outlet of the charging line	PBR Outlet of the charging line
Iron	326 +/- 108 <300	250 +/- 70
Sodium	334 +/- 22	297 +/- 19
Tungsten	0.1 +/- 0.05	<0.15
Bromine	2 +/- 0.5	2.5 +/- 0.7
Chromium	7.3 +/- 1.1	4.3 +/- 0.7
Cobalt	1.3 +/- 0.3	2.0 +/- 0.3
Zinc	<43.7	19.5 +/- 14

Table 2.11 Additional Results of NAA using Chelating Papers

(ppb)	PNZ (Charging tank)
Zinc	3.5 +/- 0.5
Cobalt	0.15 +/- 0.01
Iron	6 +/- 3
Chromium	0.9 +/- 0.1

about 5 ppb of iron in a 800ppm boron solution), and Fluka Chemie AG $LiOH.H_2O$ which claims less than 0.005% of iron and zinc (this represents less than 1ppb of iron and zinc in a 2ppm Lithium solution).

Note that the ion chromatograph measurements of transition metals reported here are suspected to be high due to some contamination from the Waters IC unit stainless steel injection system.

The results show that PCCL makeup water adds a non-negligible input of transition metals. However, the most recent NAA results, using chelating papers to concentrate the species and to minimize contamination during handling, seem to indicate that this source is not dominant. As will be discussed later, total transition metal input is small compared to the measured crud inventory on loop surfaces. Also, it should be noted that all these measurements have been performed on grab samples, some of them after a few months; this made accurate measurement of ppb levels of species difficult.

• Results of Materials Analyses

Results of the analyses of commercial vendor Zircaloy, as well as of the MIT PCCL Zircaloy 4 are presented in table 2.12. Cobalt content appears to be on average about 1 ppm, far below the ASTM (B353-83) specification of 20 ppm, a result which ruled out a hypothetical important participation of the cobalt from the

table 2.12 Results of Zircaloy Neutron Activation Analyses

(ppm)	Cr	Fe	Co	Sb	Eu	Hf	Ta	Ni	W
Vendor 1									
Sample A	1010 ±32	1915 ±105	1.1 ±0.1	2.7 ±0.4		48 ±4			
Sample B #1	1070 ±34	2290 ±100	1.1 ±0.1	1.1 ±0.2	0.06 ±0.01	45 ±4	0.79 ±0.14		
Sample B #2	1140 ±20	2380 ±100	0.72 ±0.06	1.3 ±0.1		51 ±3	1.4 ±0.1	<26	1.6
Sample B surface	1184 ±32	2597 ±423	<2.1						
Sample C	75 ±4	1070 ±90	1.0 ±0.1	12.6 ±1.6		70 ±6	5.1 ±0.9		
Sample D	1030 ±33	1950 ±95	1.6 ±0.1	8.9 ±1.1		41 ±4	0.31 ±0.07		
Vendor 2									
Sample A	1070 ±39	2290 ±115	0.48 ±0.09	2.1 ±0.6	0.076 ±0.025	40 ±4	0.70 ±0.32		
Sample B	1045 ±38	2180 ±100	0.55 ±0.09	2.2 ±0.5		43 ±4	0.59 ±0.26		
Sample C	1105 ±40	2145 ±125	0.79 ±0.11	1.4 ±0.5		45 ±4			
Sample D	930 ±34	1840 ±125	0.68 ±0.13	2.1 ±0.6	0.14 ±0.03	43 ±4			
Sample E	965 ±30	1940 ±90	1.1 ±0.1	1.7 ±0.2		43 ±3			
Vendor 3									
Sample A	1110 ±40	2230 ±145	0.58 ±0.16	1.8 ±0.6		40 ±4	0.90 ±0.44		
Sample B	1130 ±40	2340 ±140	0.9 ±0.18	<1.0		44 ±4	0.56 ±0.28		
Vendor 4									
Sample A	1060 ±20	1990 ±90	0.71 ±0.06	1.1 ±0.1		51 ±3		<34	<1
Sample B	1050 ±20	2005 ±90	0.59 ±0.05	1.2 ±0.2		52 ±4		<30	<1
Sample C	1040 ±40	1890 ±90	0.66 ±0.06	1.3 ±0.1		53 ±4		<35	<1
Sample D	1160 ±21	2430 ±110	0.43 ±0.06	0.51 ±0.07		46 ±3	0.29 ±0.05	<35	65
Sample E	930 ±17	1880 ±80	0.4 ±0.04	0.35 ±0.06		34 ±2	0.37 ±0.05	<25	0.08

Table 2.12 (cont'd)

(ppm)	Cr	Fe	Co	Sb	Eu	Hf	Ta	Ni	W
MIT PCCL									
Zir2	984 ±18	1450 ±70	0.5 ±0.07			48 ±4			
Zir4 #1	1029 ±19	2180 ±100	0.72 ±0.08			52 ±4			
Zir4 #2	1060 ±20	2070 ±90	0.67 ±0.05	2.1 ±0.2		54 ±4	0.59 ±0.06	<25	0.62
Zir4 #3	1070 ±20	2080 ±90	0.68 ±0.04	2.2 ±0.2		54 ±4	0.57 ±0.06	<25	0.48
Zir4 #4	1111 ± 22	2360 ± 177	<0.85						
Zir 4 surface	1184 ± 32	2597 ± 428	<2.7						
ASTM Specification for Zir2	500 -1500	700 -2000	<20			<100		300 - 800	<100
ASTM Specification for Zir4	700 -1300	1800- 2400	<20			<100		<70	<100

Zircaloy oxide in crud transport. Our data compares well with the values of 0.86 ± 0.06 ppm and 1.76 ± 0.14 ppm reported in reference (A-1). 1 ppm is also mentioned in ref. L-1. Cabello's calculations (C-1) show that 1 ppm Co in Zircaloy would make the cobalt in the ZrO_2 corrosion film represent about 10% of the cobalt in the crud at the end of an average PCCL run. Thus in-situ cobalt is not significant compared to the crud cobalt. Therefore, in the data acquisition and interpretation process, separation of the two components will not be needed.

It should be noted that most of these analyses were done on bulk metal. Further analyses were then needed to confirm that the bulk was not different from the surface. The results of two surface analyses confirmed this supposition.

In the future, if high pH chemistry is adopted in PWRs, cobalt in Zircaloy may become of growing concern, not only because of higher Zircaloy corrosion rates due to high lithium concentration, but also, because of solubility gradients that would transport the cobalt from the core to the steam generators. Therefore, it has been recommended, in a paper presented by MIT at the ANS Fall 1990 conference (O-1) that the ASTM specifications on cobalt in nuclear service Zircaloy be lowered to 2 ppm and that NAA be specified as a standard test to monitor these lower limits.

In table 2.13, the results of the measurements made on EPRI/ESEERCO Loop materials are presented. These results confirm that these materials are within specifications, and representative of actual full scale PWR materials.

Similar analyses were performed on the newly purchased NUPEC Loop materials and the results, presented in table 2.14, show similar trends as for the EPRI/ESEERCO materials.

W-187 is a principal activity in the PCCL water (~ 1. E-3 μCi/cc). Sanchez carried out an experiment to prove that the tungsten present in solution was almost entirely in soluble (and anionic) form (S-2). It was estimated that as little as 20ppb W dissolved in loop coolant could explain the measured W-187 activity. Here, by looking at the W content in the loop components, two sources for the tungsten are suggested:

(1) Loop Plenum steel, with a measured content of about 400 ppm W (welding rod used to attach plenum end caps can have even higher W content)

(2) Inconel, with a measured content of about 160 ppm W.

If one estimates realistic corrosion release rates, however, this much tungsten cannot sustain 20 ppb in PCCL coolant; only if in core residence times are comparable to those estimated for other transition metal (~50 hours) can one account for the observed W-187 activity. It is then difficult to reconcile longer in-core deposition with the apparently soluble nature of the water borne W-187.

To compound the uncertainty with respect to the origin of W/W-187, other sources of tungsten do not appear plausible. Makeup water which may contain W from the Hastelloy C check

Table 2.13 Results of analyses on EPRI loop materials

	Ni	Cr	Fe	Co	Mn	W
Inconel 600 (NAA-1990)	/	19.3 ± 0.2 %	9.7 ± 3 %	380 ±130 ppm	0.4 ± 0.02 %	/
Inconel 600 (NAA-1990)	75.7 ± 3.5 %	19.6 ± 0.1%	7.7 ± 1.2 %	510 ±130 ppm	0.42 ± 0.01 %	161 ± 37 ppm
Inconel 600 (NAA-1989)	81.2 %	12.5 %	6.3 %	369 ppm	/	23 ppm
Inconel 600 (NAA-1988)	78.4 %	14.1 %	7.5 %	234 ppm	/	/
Inconel 600 Mitsubishi analyses (1989)	75.1 %	15.7 %	8.18 %	400 ppm	0.27 %	/
Inconel 600 manuf. analyses	74.6 %	15.75 %	/	/	0.26 %	/
Inconel 600 manuf. spec	72 %	14 - 17 %	6 - 10 %	/	/	/
Stainless Steel 316 (plenum) (NAA-1990)	15.4 ± 3.5 %	22.7 ± 0.1 %	70.4 ± 6 %	931 ± 270 ppm	1.80 ± 0.03 %	434 ± 66 ppm
Stainless Steel 316 (NAA-1989)	/	12.8 %	51 %	742 ppm	/	352 ppm
Stainless Steel 316 (NAA-1988)	/	6.4 %	47.9 %	524 ppm	/	/
Stainless Steel 316 manuf. analyses (plenum)	11.56 %	16.33 %	67.6 %	/	1.68 %	/
Stainless Steel 304 (line from plenum to zircaloy) (NAA-1990)	/	20.0 ± 0.2 %	76. ± 8 %	600 ± 200 ppm	1.44 ± 0.05 %	/
Stainless Steel 304 manuf. analyses (line from plenum to zircaloy)	9.16 %	18.24 %	71.0 %	/	1.10 %	/
Stainless Steel 316 manuf. analyses (AE Pump)	10.28 %	16.44 %	68.7 %	/	1.75 %	/

note: manufacturer analyses and specifications are presented in appendix A

Table 2.14 Results of analyses on NUPEC loop materials

	Ni	Cr	Fe	Co	Mn	W
Inconel (NAA-2)	75.3 ± 2.4 %	19.8 ± 0.1 %	7.8 ± 1.7 %	420 ± 100 ppm	0.21 ± 0.006 %	150 ± 11 ppm
Inconel manuf. analyses	77.05	15.17	7.10	/	0.23	/
Inconel manuf. spec.	bal.	14.0 - 17.0 %	6.0 - 10.0 %	/	<1.0 %	/
Stainless Steel (NAA-1)	/	17.4 ± 0.2 %	67.4 ± 7 %	1000 ± 300 ppm	1.06 ± 0.04 %	/
Stainless Steel (NAA-2)	8.5 ± 1.5 %	20.7 ± 0.2 %	63.3 ± 5 %	1665 ± 317 ppm	1.05 ± 0.008 %	636 ± 20 ppm
Stainless Steel manuf. analyses	11.15	16.15	/	/	1.13	/
Stainless Steel manuf. spec.	11.0 - 14.0 %	16.0 - 18.0 %	bal.	/	<2.0 %	/
Titanium (NAA)	/	76 ± 2 ppm	444 ± 53 ppm	0.40 ± 0.2 ppm	/	/
Titanium manuf. spec.	/	/	350 ppm	/	/	/

note: manufacturer analyses and specifications are presented in appendix A

valve balls (4 wt% W) in the LEWA charging pump, or impurities in boric acid have been ruled out in view of the analyses presented in table 2.10. Also, Zircaloy is ruled out after confirming that the W content is less than 1 ppm.

2.8 Chapter Summary

In this chapter, it has been determined that the charging water chemistry was a potential source of impurities for the MIT PCCL. It should be remarked at this point that the input from the CVCS in actual PWR units is also not well known because of the difficulties of sampling. Consequently, it was decided that for the NUPEC runs, this input should be minimized, and to do so a titanium charging line will be used, together with ion-exchange resins to maintain purity. In addition, special high purity boric acid (from Japan) will be used to prepare the chemistry.

Material analyses showed that the Inconel, Stainless steel and Zircaloy used for the PCCL were within specification. Also noted was a much lower cobalt content (~ 1 ppm) in the Zircaloy than allowed by the ASTM specification (<20 ppm); and it was recommended that this specification be lowered. It is suggested that the tungsten content of the Inconel and Stainless steel may be the source of the appreciable W187 activity measured in the PCCL coolant.

3 DECONTAMINATION STUDIES

3.1 Introduction

Because, in the PCCL experiment, the whole loop is in the reactor core tank, some of its parts become activated and consequently, direct measurement of final crud radionuclide inventory is impossible. This is the case for the bottom of the Inconel steam generator section, the plenum, and of course, the Zircaloy core section. For these parts, descaling processes had to be developed to separate the crud from the activated base metal. State-of-the-art decontamination procedures were tested, modified and qualified for our purposes. The present chapter describes the methods used to descale the activated regions of the PCCL, as well as to determine the radionuclide inventories in the regions of major interest.

3.2 Steam generator decontamination

3.2.1 Description of the methods

Direct measurement of the crud surface-deposited activity on the Inconel steam generator tubes is possible using a HpGe detector (C-1) (S-1). However, in the PCCL experiment, the bottom of the steam generator section is located only about 1meter above the core and thus is activated by the neutrons leaking from the

reactor core. This makes direct measurement impossible and separation of the crud from the activated base metal necessary.

Since chemical decontamination was quite unsuccessful (C-1) a combination of mechanical and electrochemical descaling methods was developed.

Ultrasound is a decontamination technique commonly used in plants; however, due to the small size of baths commercially available, it can only be used to decontaminate small pieces. This was not a problem in our case since the tubes to be decontaminated were cut into 3 cm long pieces. Ultrasound is the name given to high frequency mechanical vibrations, which are known to have a strong effect on solid-liquid interfaces (L-3). Bubble formation (cavitation) is induced by the ultrasonic waves; reference R-1 indicates that pressures and temperatures can reach 1.E4 psi and 1.1E4 °C, respectively. This results in a vigorous scrubbing action at the surface to be cleaned. Factors influencing the effectiveness of the process are numerous, but the following ones are to be noted. The temperature at which cavitation force is at the maximum is about 15°C below the normal boiling point of the solution. Aluminum or steel baskets can reduce the efficiency; glass is prefered. Soft materials absorb the ultrasonic energy (R-1). It is recommended in reference R-1 to use a concentration of chemicals added to the water on the order of 2 to 5 % by weight. Furthermore the temperature should be in the range of 65 to 77°C.

Based on these remarks, a method was developed for our purposes. Tests were done to find a suitable cleaning solution as

well as adequate operation time and temperature. Figure 3.1 describes the set-up used for the primary tests and the decontamination of the actual tubes. Tests showed that the following procedure was suitable for descaling all tubes except PL1 S/G inlet Inconel where the crud appeared to be "tougher". Base metal removal tests were also performed. The procedure selected consisted in a 3 minute ultrasound treatment using 5% nitric acid at 60°C.

Electrochemical decontamination is also employed in plants for decontamination of reactor components. It involves use of a voltage supply to drive a current in order to remove a small amount of the metallic surface in a controlled manner. Usually, the system uses an anode and a cathode plus an electrically conducting solution. The anode is the component to be decontaminated; the cathode can be stainless steel, for example, and the most common electrolyte at present is phosphoric acid because of its stability, safety and applicability to a variety of alloy systems (R-1). Reported decon factors are large, since this method can remove all crud and oxide layers. The most detrimental factor for our application is that this method removes, in every case, some base metal, therefore introducing the need to minimize this dissolution.

Factors affecting the process are reported as being mostly the temperature of the electrolyte, its concentration and the current densities employed. Reference R-1 recommends

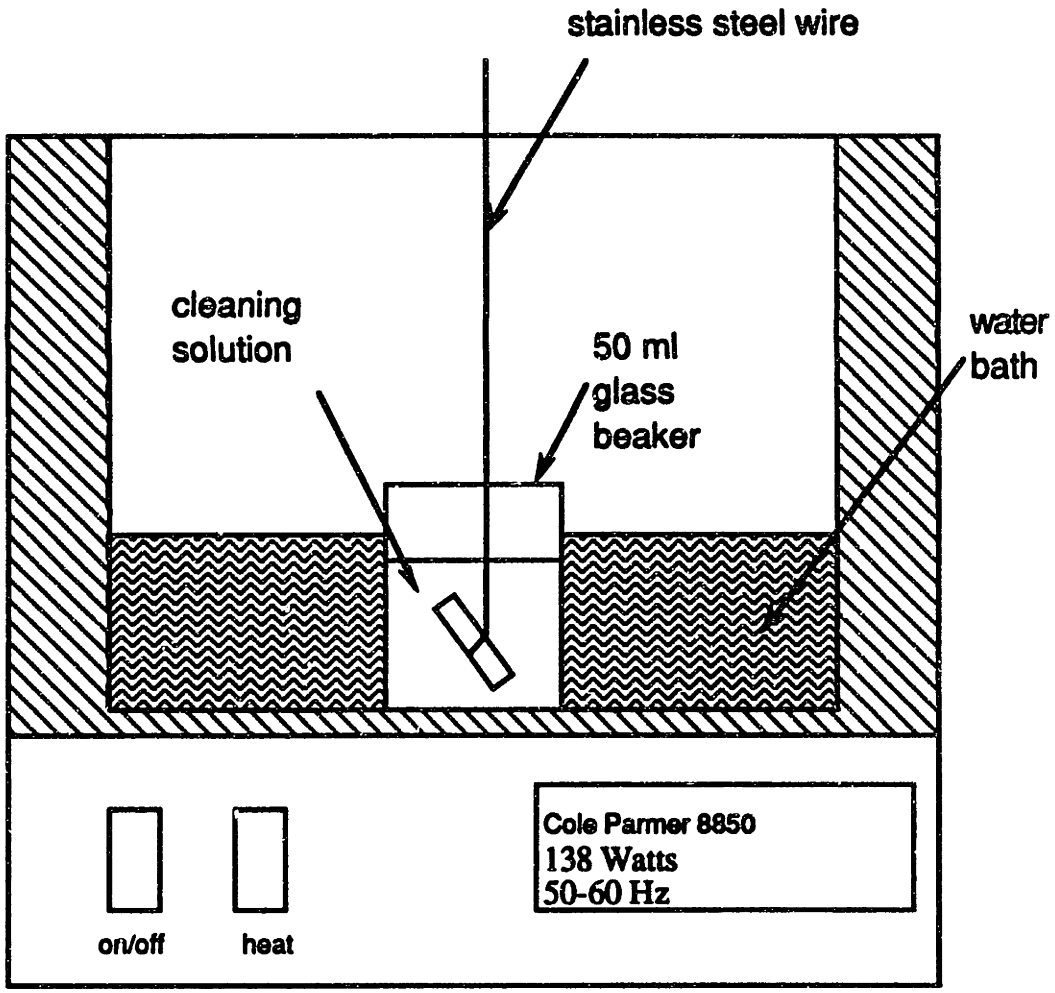

Fig 3.1 Ultrasound Setup Used in the Present Work

phosphoric acid concentrations of 40 to 80% with the temperature controlled between 40 and 80°C. Current densities should be in the range 50 to 250 A/ft^2 (0.054 to 0.269 A/cm^2). In our work, preliminary tests were done to optimize the conditions. The setup for these tests and the actual decontamination experiments is shown in Fig. 3.2 (C-1). The procedure selected consisted of a 2 minute step using 0.7 Amperes (0.117 A/cm^2) in H_3PO_4 (70%) at 70°C.

Because two descaling procedures, electrochemical and mechanical, became available, they were used on several pairs of activated tubes as a cross check, and therefore qualified each other. The qualification of the two processes was achieved by taking two adjacent tube segments from each run. On one, ultrasound was used, on the other one, electrolysis. Results were compared, and because the results were virtually identical, the two methods were considered valid and applied on the activated sections of the Inconel. Following this qualification, the method judged best suited case-by-case was used to descale the crud from the steam generator surfaces and allow one, by measuring the specific activities of the decontamination solutions, to find the radionuclide surface-deposited activity on the activated Inconel surfaces. It must be noted that visual inspection appeared to be an accurate enough gauge of efficiency: a shiny tube was a clean tube. Consequently, at times the descaling process was continued longer because of black oxide remaining on the inside of the tube.

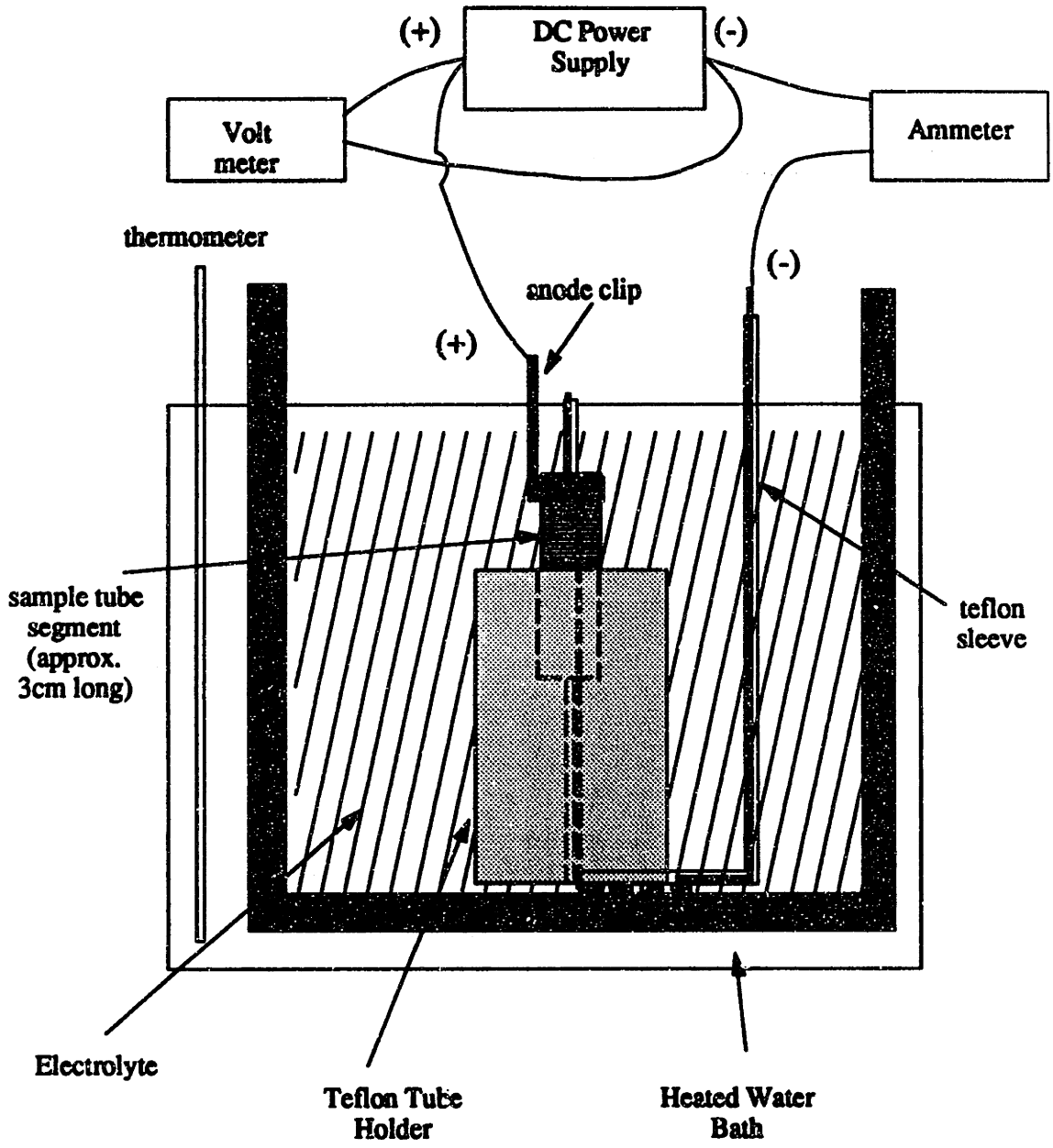

Fig 3.2 Electropolishing Setup Used in The Present Work

3.2.2 Results

First presented, in Fig. 3.3, is the way PCCL steam generator tubes are numbered. Throughout the presentation of the results, this figure will be needed to find the location of origin of a given sample.

For ultrasound, the development of the method involved the right choice for the cleaning solution, operating time and operating temperature. A summary of the tests performed to optimize the operating conditions is presented in table 3.1. From these results it can be seen that the temperature, as well as the nature of the solution, has an effect. 5% nitric acid at 60°C for 3 minutes appears to be the right choice for PR1, PR2, PH1 and the PL1 cold leg. The PL1 hot leg was more resistant for some unexplained reason. Also, it can be remarked that the use of abrasive particles (320 mesh) in conjunction with ultrasound or the use of concentrated acids do not seem to be beneficial. On the other hand, tests were performed to show that ultrasonic treatment did not remove a significant amount of base metal.

Electrolysis, as expected, proved capable of removing all the crud and oxide under any conditions. 3 minutes in 70% phosphoric acid using 0.7 Amp. (ie ~ 0.12 Amp/cm^2) was prefered.

Data on tests of the two processes are presented in table 3.2. Essentially, this table shows that the two processes lead to the same result on activated pieces, and consequently both were considered as qualified, and both subsequently applied to the activated regions from the first campaign of PCCL runs. Since

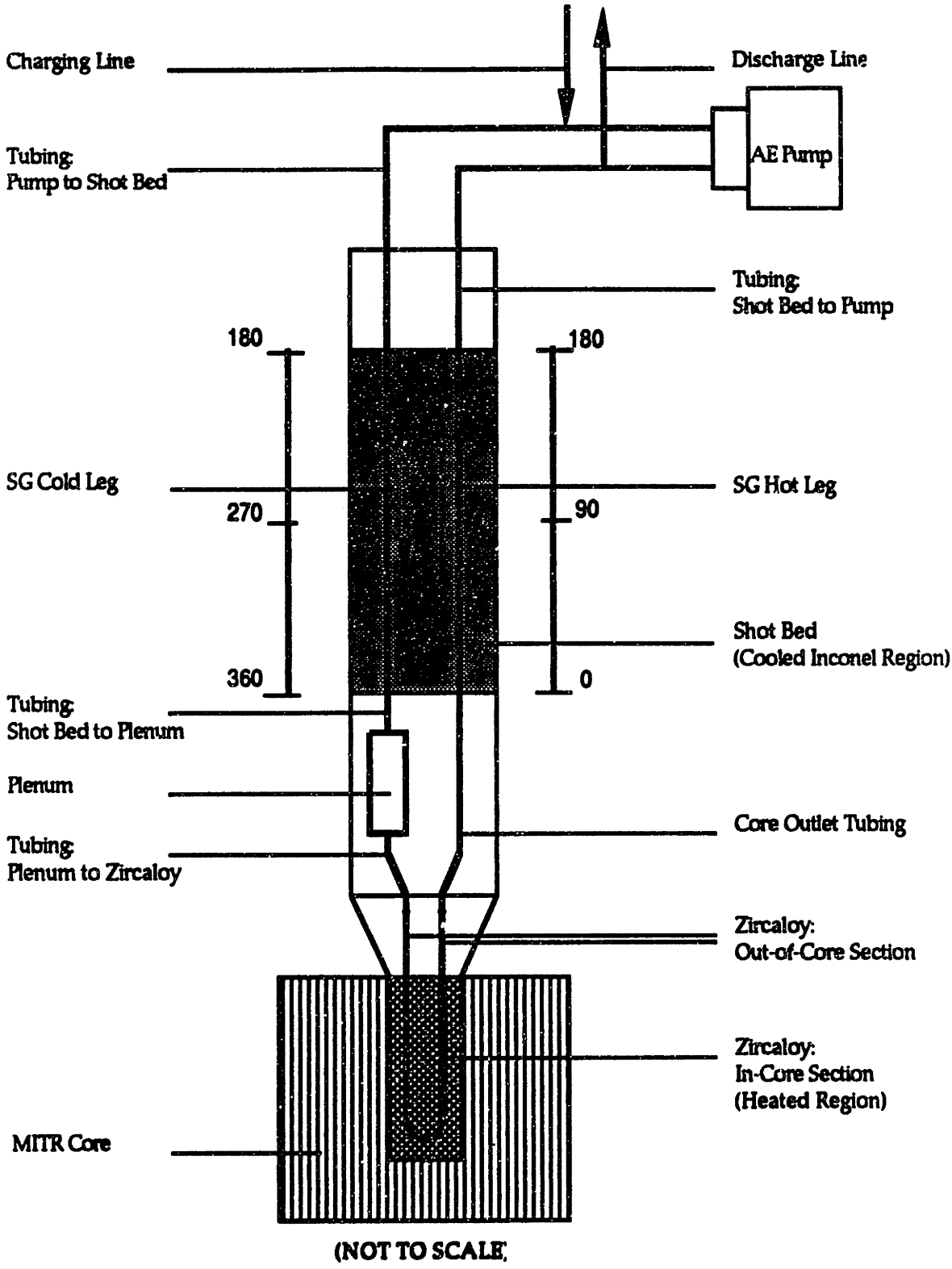

Fig 3.3 Inconel Steam Generator Schematic Showing Tube Segment Locations

Table 3.1 Ultrasonic Decontamination Test Result

Tube designation	Ultrasound solution	Time (min)	Temperature (°C)	Decontamination Factor (DF)
PR1 139-142	DI water	5	25	1.2
		35	25	1.3
		155	25	1.5
PR2 294-297	DI water	20	60	2.2
PR1 294-297	DI water	20	60	2.0
PL1 142-145	DI water	15	25	2.3
PR2 142-145	DI water	5	25	1.2
	+	35	25	1.2
	320 mesh	155	25	1.4
PR2 136-139	3% citric acid	5	25	1.1
		35	25	1.4
		155	25	1.7
PR2 151-154	10% nitric acid	1	60	2.9
		3	60	>80
PR2 154-157	5% nitric acid	3	60	>80
PR1 99-102	5% nitric acid	3	60	>70
PH1 139-142	5% nitric acid	3	60	>50
PL1 145-148	5% nitric acid	3	60	2.2
		10	60	3.5
		25	60	4.1
PL1 301-304	5% nitric acid	5	60	26
PL1 154-157	35% nitric acid	3	60	1.8

Table 3.2 Ultrasonic Decontamination Qualification Test Results

Tube Identification	Descaling Process	Co58 crud activity (nCi/cm^2) (corrected for base metal removal when neccessary)
PR1 354-357	Ultrasound 6 min. 3.5% HNO3 60°C	9.5
PR1 351-354	Electrolysis 4 min. 70% H_3PO_4 70°C 0.7Amp	9.25
PR2 354-357	Ultrasound 3 min. 3.5% HNO3 60°C	14.6
PR2 351-354	Electrolysis 2 min. 70% H_3PO_4 70°C 0.7Amp	14.2
PH1 354-357	Ultrasound 3 min. 3.5% HNO3 60°C	9.9
PH1 351-354	Electrolysis 2.3 min. 70% H_3PO_4 70°C 0.7Amp	9.6
PL1 3-6	Ultrasound	not successful
PL1 6-9	Electrolysis 5 min. 70% H_3PO_4 70°C 0.7Amp	~ 235

ultrasound was the process which removed the least base metal, and therefore did not require any correction for base metal removal, it was used whenever possible. Thus all the tubes from the four first PCCL runs were descaled using ultrasound, except for the PL1 hot leg, which was electrolyzed. Results of the descaling process, along with the results obtained by direct counting of the tube, are presented in Figs. 3.4 and 3.5. First, these results showed that there is no discontinuity between the activated and the non-activated region. As a consequence, the activated regions of the last campaign of runs (PBR, PBL and PNZ) were not descaled. Second, data from the hot leg (Fig.3.4) show clearly that operating at low pH (PL1, $pH_{300°C}$=6.5) is detrimental; and because of experimental uncertainties $pH_{300°C}$=7.5 and $pH_{300°C}$=7.2 appear to be comparably beneficial. Third, data from the cold leg is more difficult to interpret because the surface activities are very similar for all the runs. Fourth, if one examines PBL ($pH_{300°C}$=7.2, no boron) and PBR ($pH_{300°C}$=7.2, 800 ppm boron) traverses, the beneficial effect of the boron is clear. Finally, it is interesting to note that there is a heat flux effect (see Fig. 3.4, Co58) that can not be readily explained: activities increase at the outlet of the cooled region for all the runs, except for PL1 for which they decrease. On this issue, further work is in progress and SEM pictures of the crud layer will be taken in the cooled and adiabatic region and published in ref Z-1.

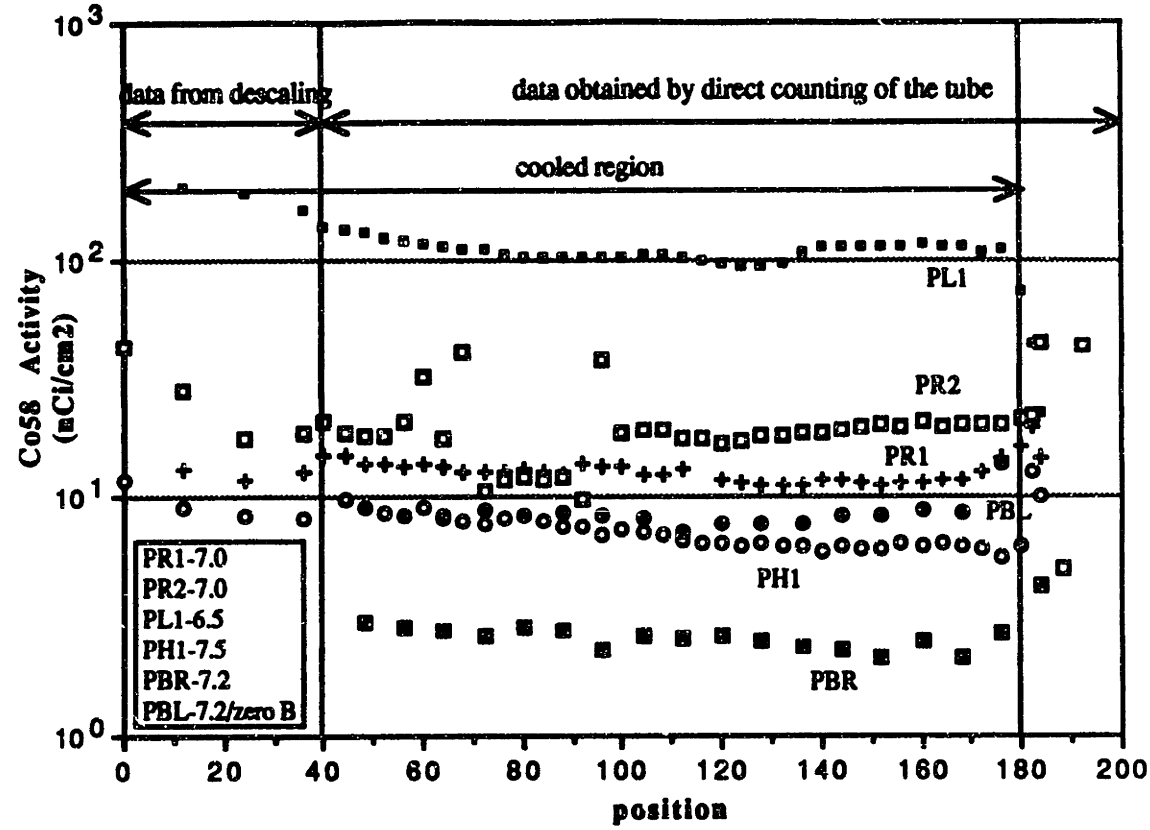

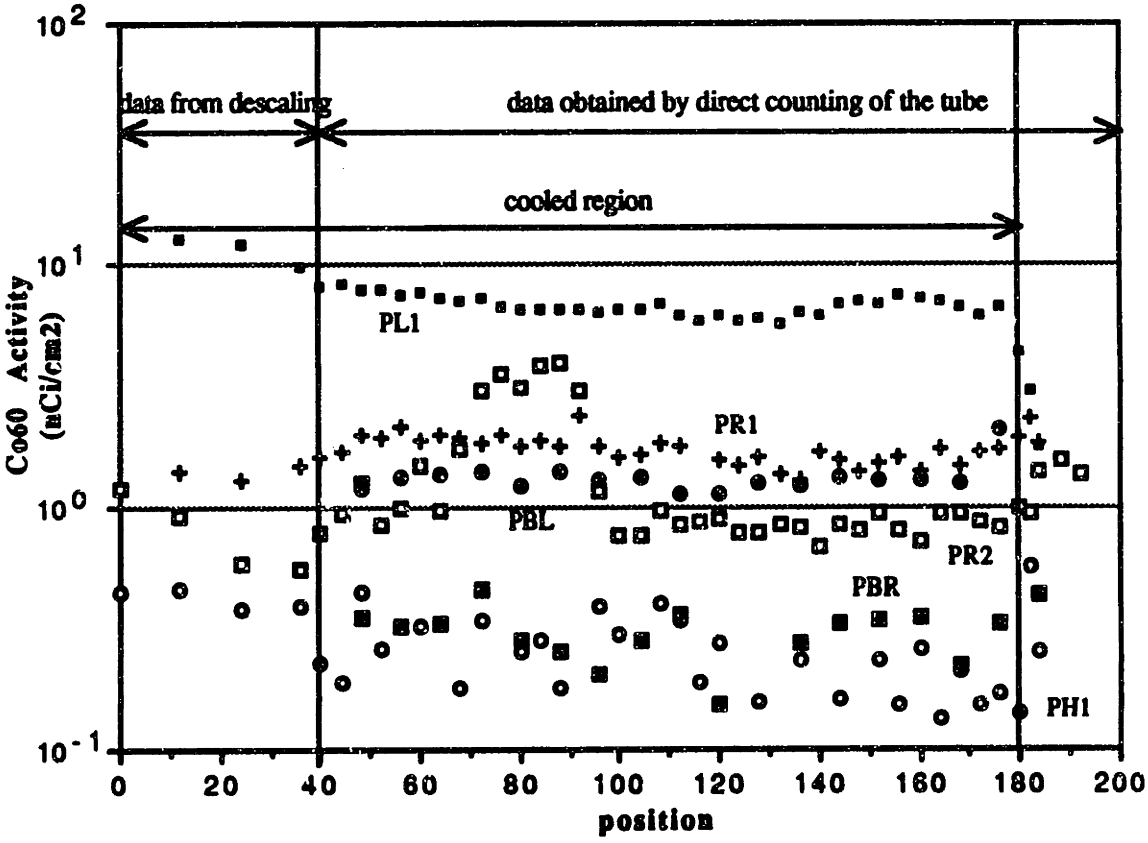

Fig 3.4 Radionuclide deposition in the PCCL Steam Generator Hot Leg

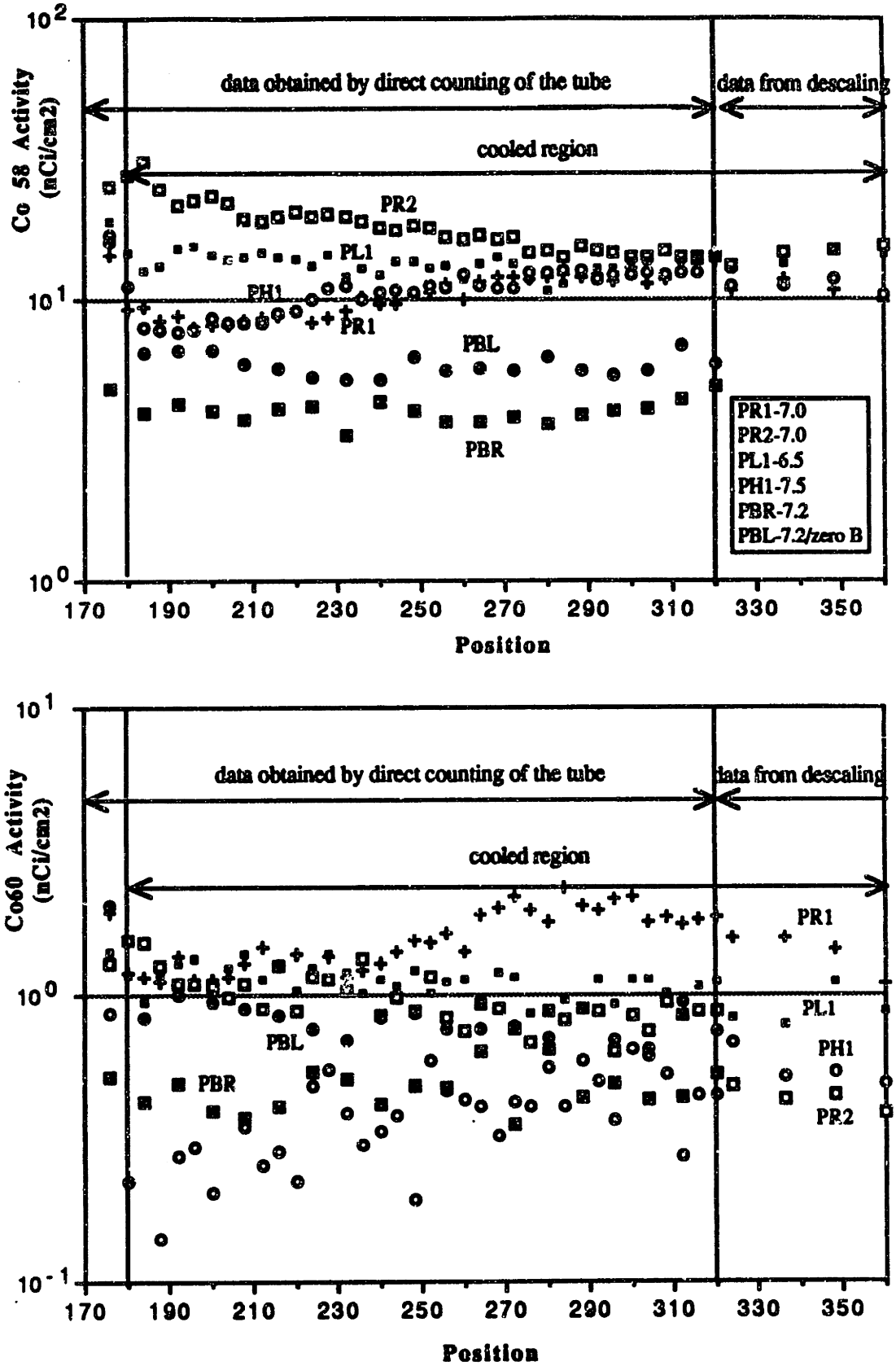

Fig 3.5 Radionuclide deposition in the PCCL Steam Generator Cold Leg

3.3 Plenum decontamination

3.3.1 Description of the method

The MIT PCCL plenum is made of 316 Stainless Steel, the composition of which is 67.62% Fe, 16.33% Cr, 11.56% Ni, 2.05% Mo and 1.680% Mn (from the manufacturers material certificate (T-1)). It is about 24.5 cm in length and has a 2.54 cm inside diameter. During fabrication the inner surface was honed to a mirror finish (a Sunnen P28J57 honing stone, grit size 220, was first used, followed by a Sunnen P28J95 stone, grit size 380, which gave an approximate 12 microinch surface finish). Figure 3.6 shows the dimensions of the PCCL plenum. In an assembled loop, it is located in the PCCL thimble about 0.5 meter above the top of the MITR-II core. Thus, during a PCCL run, it becomes activated by leakage neutrons from the core (as is the bottom of the steam generator section). This complicates the evaluation of crud radionuclide deposition on the walls. Therefore an adequate de-scaling method is needed.

Since the plenum has a 0.95 cm thick wall, the problem of cutting it into segments for analysis was not negligible. Sawing was ruled out because of possible contamination of the inner surface of the plenum, the environment and the saw due to creation of small radioactive particles. A conventional tubing cutter was difficult to use since the wall was thick and the contact dose rate was (for the more recent plena) over 80 mrem/hr. Hence a special purpose tool was built based upon use

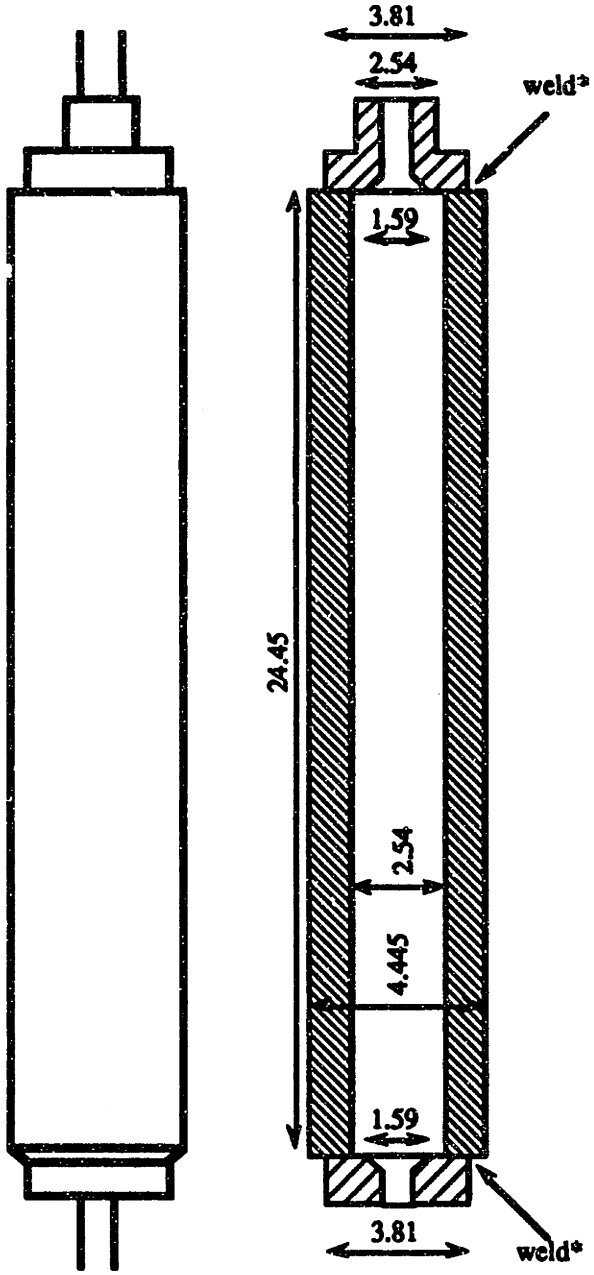

(all dimensions in cm)

* note: plena for first two runs used screw-on caps in lieu of end weld

Fig 3.6 PCCL Plenum Schematic

of a rotating machine (lathe) and commercially available cutting wheel, as shown in Fig 3.7. Protection against contamination was provided by covering with paper all potentially exposed surfaces. One drop of oil was used per cut; this made an average of 10 cuts per wheel possible before replacement was necessary.

Figure 3.8 shows how the PCCL plena were cut. The slices were cut as identical as possible, however, some are different due to incidents such as wheel breakage during a cut. Only 3 slices per plenum were analyzed, the others were archived for other experiments or in case of failure of the de-scaling process on a given slice.

A de-scaling process had to be developed since the plenum base metal activity was too high to apply the same method as used for the activated Inconel (see chapter 3 section 1). Application of Faraday's law indicates that a 2 minute anodic electropolishing step will dissolve, if a 2 Amp current is maintained, 72 mg of base metal distributed over the 16 cm^2 inner surface of an average slice. This will release 144 nCi of Co58 in some of the plena: an amount which could exceed the amount of Co58 in the crud deposited on the slice. Consequently, the anodic step had to be shorter. A series of tests were performed based on information provided in reference I-1. In this reference, it is claimed that using a square wave current (ie a succession of cathodic and anodic electropolishing steps), one can prevent the dissolution of base metal during the process. The major claim of the article is that the cathodic process causes reduction of the electrode surface (oxide and crud in our

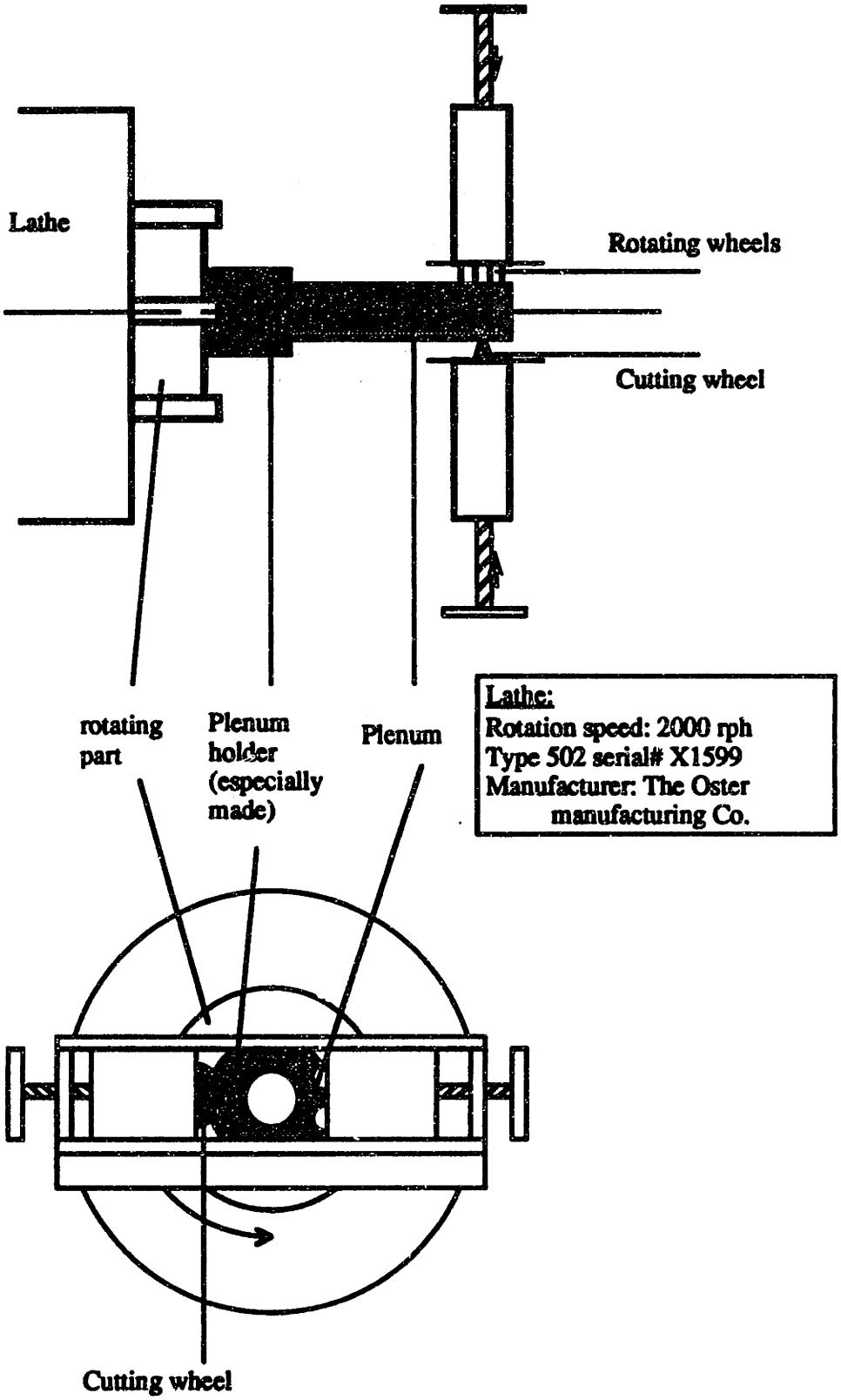

Fig 3.7 Plenum Cutter Schematic

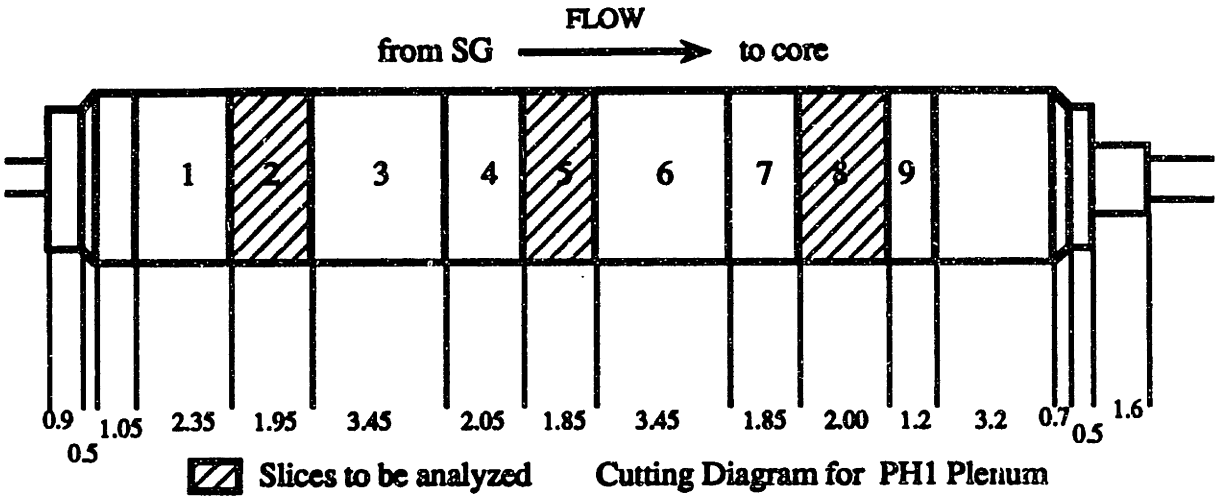

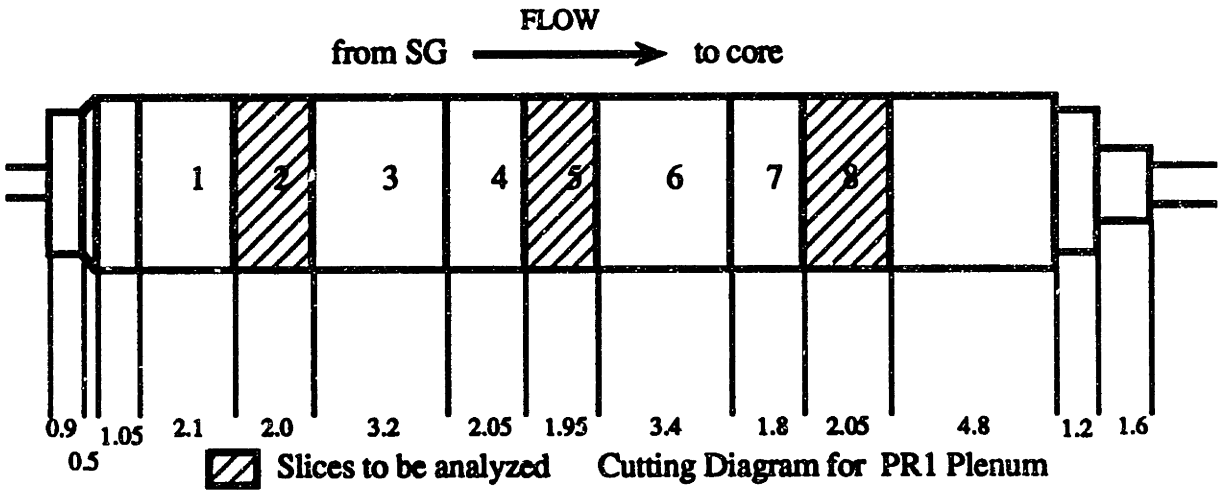

Fig 3.8 Cutting Diagrams for Loop Plena

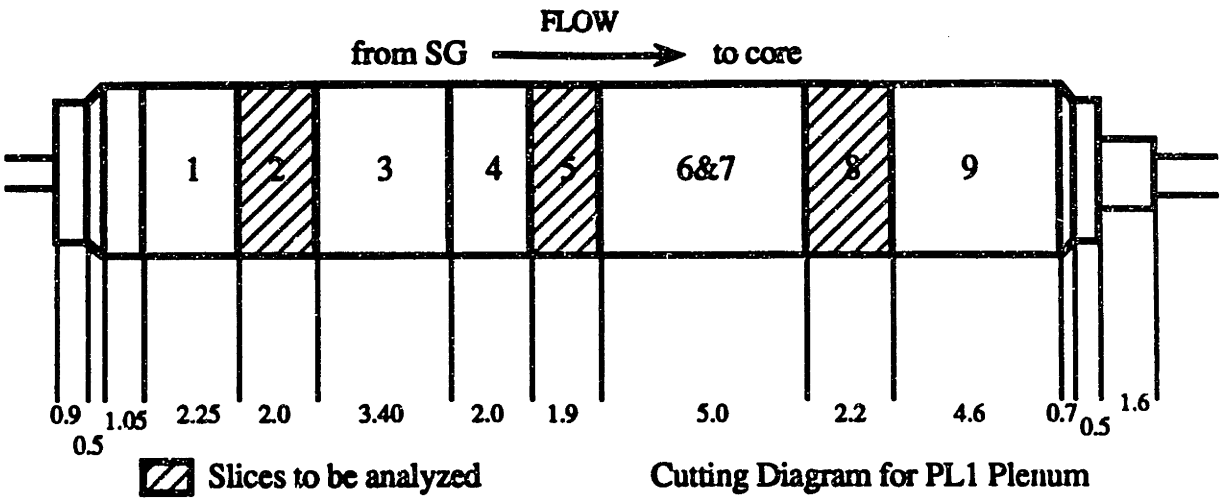

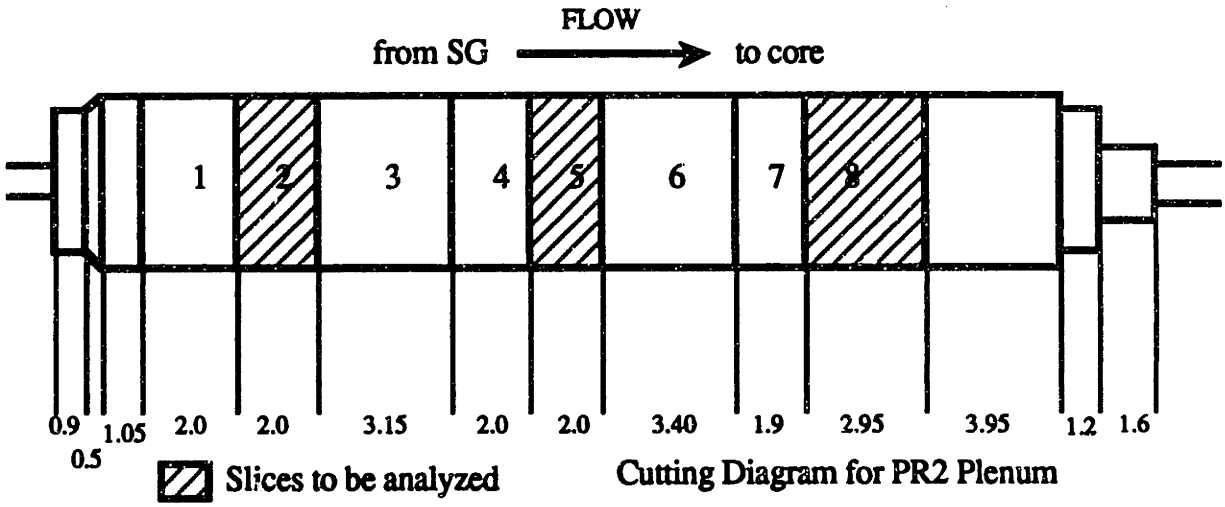

Fig 3.8 Cutting Diagrams for Loop Plena (cont'd)

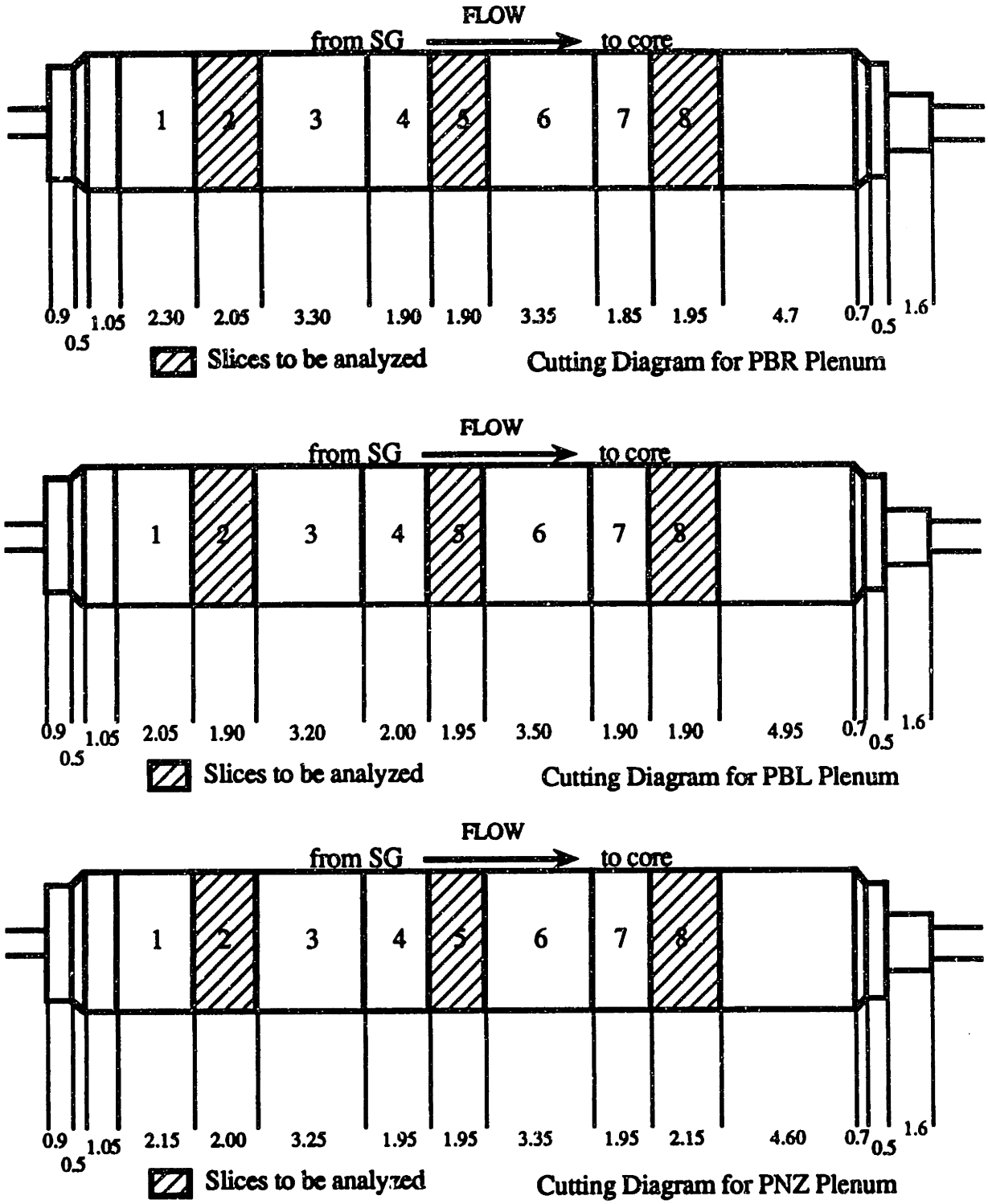

Fig 3.8 Cutting Diagrams for Loop Plena (cont'd)

application) while the anodic step causes its oxidation. The two steps involve the following reactions:

1) cathodic step:

$$Fe_3O_4 + 8H^+ + 2e^- \text{ ---- } 3Fe^{2+} + 4H_2O$$

(This reaction is slow and could not remove the entire oxide film in a short time)

$$Fe_3O_4 + 2e^- \text{ ---- } 3FeO + O^{2-}$$

$$FeO + 2e^- \text{ ---- } Fe + O^{2-}$$

2) anodic step:

$$Fe \text{ ---- } Fe^{2+} + 2e^-$$

As a result, a cathodic step followed by an anodic step would allow one to de-scale without dissolving significant base metal. Reference I-1 recommends a 60 second cathodic step followed by a 30 second anodic step. The electrolyte used is 1.7 molar Na_2SO_4, which is only mildly basic, and therefore eases handling and waste disposal. The whole process is at room temperature, and a 0.3 Amp/cm^2 current is recommended. Using these parameters as a base case, a series of tests were performed to check, to adapt and to improve the method for our application. The tests and their results are described in table 3.3; all were done on 1cm thick

slices from a plenum that had undergone a prefilming step to acquire an oxide layer.

Based on these results the following decontamination procedure was proposed:

- 2 cm thick slice
- Room Temperature
- Cathodic step

  4 minutes

  Electrolyte: Na_2SO_4 (saturated-1.7 mol/l)

  2 Amperes

  Electrode: graphite
- Anodic step.

  15 seconds

  Electrolyte: Na_2SO_4 (saturated-1.7 mol/l)

  2 Amperes

  Electrode: graphite
- Ultrasonic treatment

  HNO_3 (5%)

  Until all oxide is removed (Typically 4-6 minutes): visual examination readily reveals the presence of black oxide on the underlying silvery metal surface.

- Mix nitric acid and Na_2SO_4 solutions to dissolve any precipitate (The geometric calibration of the counting system requires that the sample is homogeneous)
- Count the solution using a standard HpGe detector system: see references (C-1) and (S-1).

Table 3.3 Summary of Descaling Methods Development Tests

Test number	Test description	Result
1	•Cathodic step 4min 1Amp in Na_2SO_4 •Anodic step 15sec 1Amp in Na_2SO_4 •Ultrasound 1min in HNO_3 (5%)	oxide removed
2	•Anodic step 15sec 1Amp in Na_2SO_4 •Ultrasound 1min in HNO_3 (5%) Followed by •Anodic step 5sec 1Amp in Na_2SO_4 •Ultrasound 1min in HNO_3 (5%)	still oxide on the wall oxide removed
3	•Cathodic step 4min 1Amp in Na_2SO_4 •Anodic step 5sec 1Amp in Na_2SO_4 •Ultrasound 4min in HNO_3 (5%)	oxide removed
4	•Cathodic step 10min 1Amp in Na_2SO_4 •Anodic step 5sec 1Amp in Na_2SO_4 •Ultrasound 4min in HNO_3 (5%)	oxide was removed
5	•Cathodic step 4min 1Amp in H_3SO_4 •Anodic step 10sec 1Amp in H_3SO_4 •Ultrasound 4min in HNO_3 (5%)	still oxide on the wall
6	•Cathodic step 4min 1Amp in Na_2SO_4 •Anodic step 10sec 1Amp in Na_2SO_4 •Ultrasound 4min in HNO_3 (5%)	oxide was removed
7 Base metal removal	•Anodic step 10sec 1Amp in Na_2SO_4 on a $10cm^2$ slice •Ultrasound 4hrs in HNO_3 (5%)	3mg removed 0.00027 mg/min.cm^2 of base metal removed

Note: The ultrasonic bath employed was a Cole Parmer 8850 model 8850-10, 138 Watts, 50-60 Hz.

In addition, before starting the decontamination procedure, scrap samples are taken from each slice, dissolved in aqua regia and the solutions are counted in order to evaluate the specific activity of the base metal and to evaluate whether any correction due to base metal removal is required.

Since we were not only interested in the crud activity, but also in the crud composition, it was important to avoid any contamination from metals not from the crud or the oxide layers. Therefore each slice was, prior to starting the decon process, painted with microstop paint (Clear Microstop Paint, manufacturer: Tobler Division Pyramid Plastic, Inc.) to protect all surfaces except the inner one against attack. Solutions with low transition metal concentrations were used; to achieve this, the nitric acid and sodium sulfate solutions were filtered through chelating ion exchange papers (see Chapter 2.2). Moreover, a blank was made using the same amount of solutions used in the de-scaling process. De-scaling solutions were analyzed using an Atomic Absorption Spectrometer. The flame technique determines with reasonable accuracy the composition of iron, nickel and chromium in the crud. In order to obtain the concentration of other transition metals, such as cobalt, zinc or manganese, which are present in trace amounts, the more sensitive graphite furnace technique should be used. Results of this aspect of the crud analysis will be published in the SM thesis by M. R. Zhang (Z-1).

3.3.2 Results

The specific activities for the first campaign of four runs are recorded in table 3.4.

If we assume that Faraday's law is applicable, and the current efficiency is 100%, 18.1 mg of divalent transition metals per amp.min would be dissolved. In our case, the 15 second anodic step would dissolve a maximum of about 9 mg, since a current of 2 amp is used. Based on the measured specific activities (table 3.4) and the results of the de-scaling process, presented in table 3.5, the following remarks can be made. On average, the correction would represent for Co58 and Co60, respectively, 0.9% and 0.6%: or in other words, a negligible amount. The maximum correction reaches 3.7% for Co58 in slice PH1-8 and 1% for Co60 in slice PH1-8. Since we also know that Faraday's law gives an overestimate of the correction, it was decided not to correct the de-scaling results, and furthermore, no scrap samples need be taken for the spring campaign runs.

Plots of the activity, in nCi/cm^2, for the principal radio-nuclides versus position are shown in Figs. 3.9 through 3.12.

These plots show a relatively linear variation of the activity versus position in the plena. Co 60 is much higher for the PL1 and PBL plena, this tends to confirm what was seen on the Steam Generator traverses: low pH and low boron runs have more crud activity per unit area than the other runs (see chapter 3 section 2). On the other hand, it is difficult to say which pH is the most beneficial. The curves corresponding to pH_{300} 7.0, 7.2

Table 3.4 Specific Activities of base metal for the First Campaign Plena

Run and sample location	Scrap sample weight (mg)	Co58 activity (nCi/mg)	Co60 activity (nCi/mg)	Mn54 activity (nCi/mg)	Zn65 activity (nCi/mg)
PR1-2 ($pH_{300°C}$=7.0)	67.46	/	/	/	/
PR1-5 ($pH_{300°C}$=7.0)	15.91	/	/	/	/
PR1-8 ($pH_{300°C}$=7.0)	33.66	/	/	/	/
PR2-2 ($pH_{300°C}$=7.0)	69.16	0.20 ± 0.06	0.005 ± 0.0014	0.026 ± 0.002	/
PR2-5 ($pH_{300°C}$=7.0)	44.54	0.38 ± 0.07	0.0129 ± 0.0027	0.060 ± 0.006	/
PR2-8 ($pH_{300°C}$=7.0)	74.09	0.92 ± 0.05	0.0177 ± 0.002	0.106 ± 0.004	/
PL1-2 ($pH_{300°C}$=6.5)	85.33	0.17 ± 0.02	0.0019 ± 0.0013	0.023 ± 0.002	0.011 ± 0.003
PL1-5 ($pH_{300°C}$=6.5)	124.97	0.45 ± 0.02	0.0088 ± 0.0011	0.049 ± 0.002	/
PL1-8 ($pH_{300°C}$=6.5)	96.25	0.91 ± 0.03	0.0153 ± 0.0016	0.101 ± 0.003	/
PH1-2 ($pH_{300°C}$=7.5)	62.49	0.25 ± 0.02	0.0060 ± 0.002	0.028 ± 0.003	/
PH1-5 ($pH_{300°C}$=7.5)	95.59	0.52 ± 0.02	0.0107 ± 0.0015	0.051 ± 0.002	/
PH1-8 ($pH_{300°C}$=7.5)	134.84	1.82 ± 0.03	0.0251 ± 0.0015	0.183 ± 0.004	/

/ = not detected

Table 3.5 Plenum De-Scaling (Crud Deposition) Results

	Area (cm^2)	Co58 activity (nCi/cm^2)	Co60 activity (nCi/cm^2)	Mn54 activity (nCi/cm^2)	Zn65 activity (nCi/cm^2)
PR1 (pH=7.0)					
PR1-2	15.96	23.9 ± 1.4	1.61 ± 0.05	1.10 ± 0.05	0.78 ± 0.13
PR1-5	15.56	15.6 ± 1.3	1.05 ± 0.05	0.97 ± 0.05	0.65 ± 0.12
PR1-8	16.36	12.5 ± 1.7	0.78 ± 0.03	0.91 ± 0.04	0.54 ± 0.11
PR2 (pH=7.0)					
PR2-2	15.96	93.0 ± 1.6	2.4 ± 0.06	0.68 ± 0.04	0.65 ± 0.11
PR2-5	15.96	78.9 ± 1.3	2.0 ± 0.05	0.59 ± 0.05	0.45 ± 0.10
PR2-8	23.54	60.8 ± 1.0	1.56 ± 0.04	0.54 ± 0.03	0.58 ± 0.08
PL1 (pH=6.5)					
PL1-2	15.96	72.0 ± 1.1	4.3 ± 0.09	3.01 ± 0.07	1.72 ± 0.15
PL1-5	15.16	57.0 ± 0.7	3.4 ± 0.07	2.7 ± 0.07	1.33 ± 0.13
PL1-8	17.56	47.2 ± 0.8	2.84 ± 0.06	2.6 ± 0.07	1.24 ± 0.11
PH1 (pH=7.5)					
PH1-2	15.56	27.6 ± 0.5	1.45 ± 0.04	0.77 ± 0.03	/
PH1-5	14.76	22.7 ± 0.6	1.16 ± 0.04	0.64 ± 0.04	0.15 ± 0.07
PH1-8	15.96	27.8 ± 0.5	1.36 ± 0.04	0.86 ± 0.04	0.32 ± 0.08
PBR (pH=7.2)					
PBR-2	16.36	30.8 ± 0.4	2.95 ± 0.09	0.96 ± 0.03	0.42 ± 0.07
PBR-5	15.16	24.4 ± 0.3	2.39 ± 0.06	0.83 ± 0.03	0.25 ± 0.07
PBR-8	15.56	21.6 ± 0.3	2.01 ± 0.06	0.90 ± 0.04	0.36 ± 0.06
PBL (pH=7.2) zero Boron					
PBL-2	15.16	40.6 ± 0.4	4.96 ± 0.10	1.0 ± 0.04	0.71 ± 0.07
PBL-5	15.56	34.6 ± 0.3	4.23 ± 0.09	1.0 ± 0.04	0.65 ± 0.07
PBL-8	15.16	26.8 ± 0.2	3.26 ± 0.07	1.0 ± 0.03	0.59 ± 0.06
PNZ (pH=7.2) less zinc					
PNZ-2	15.96	8.68 ± 0.11	2.95 ± 0.07	0.19 ± 0.02	/
PNZ-5	15.56	6.42 ± 0.08	2.29 ± 0.06	0.16 ± 0.02	/
PNZ-8	17.16	5.71 ± 0.07	2.10 ± 0.05	0.17 ± 0.02	/

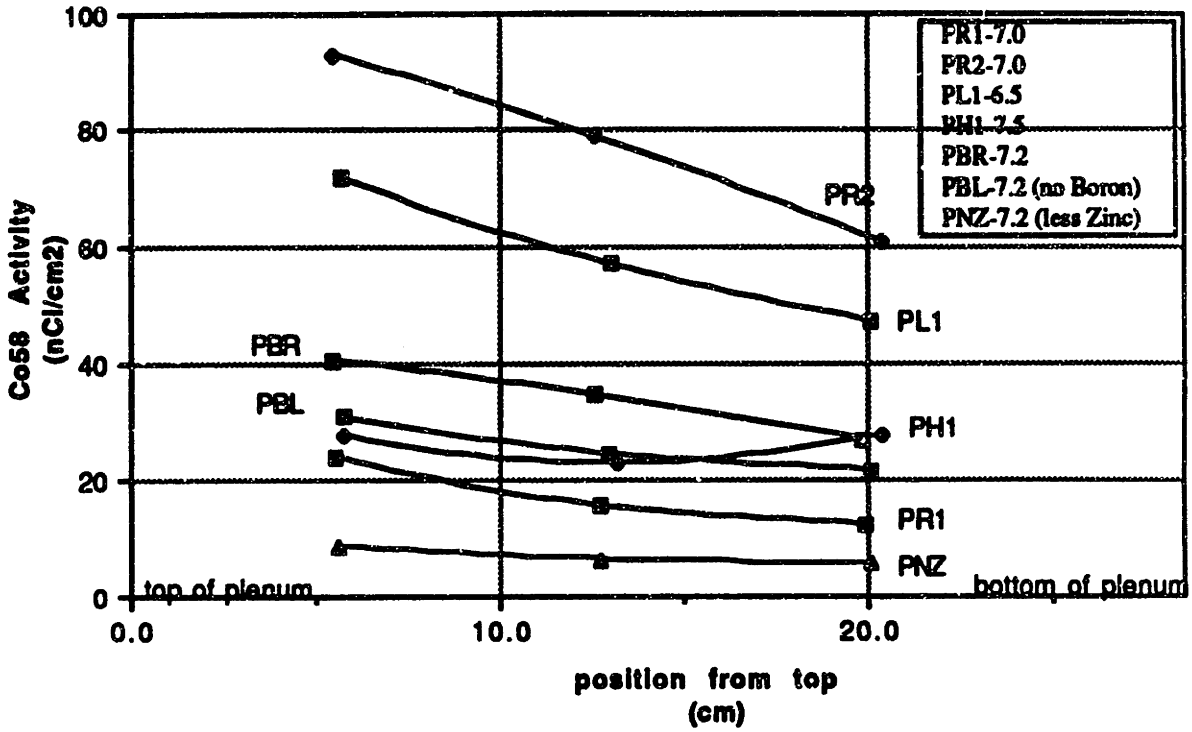

Fig 3.9 Co58 Activity in PCCL Plena

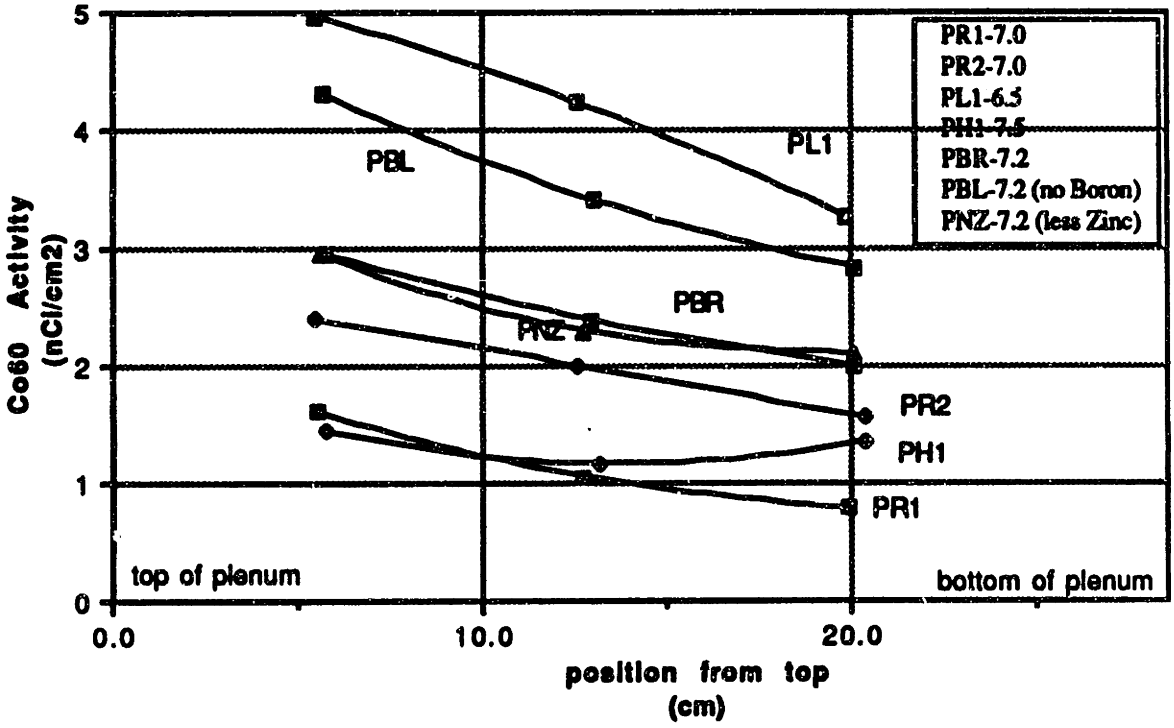

Fig 3.10 Co60 Activity in PCCL Plena

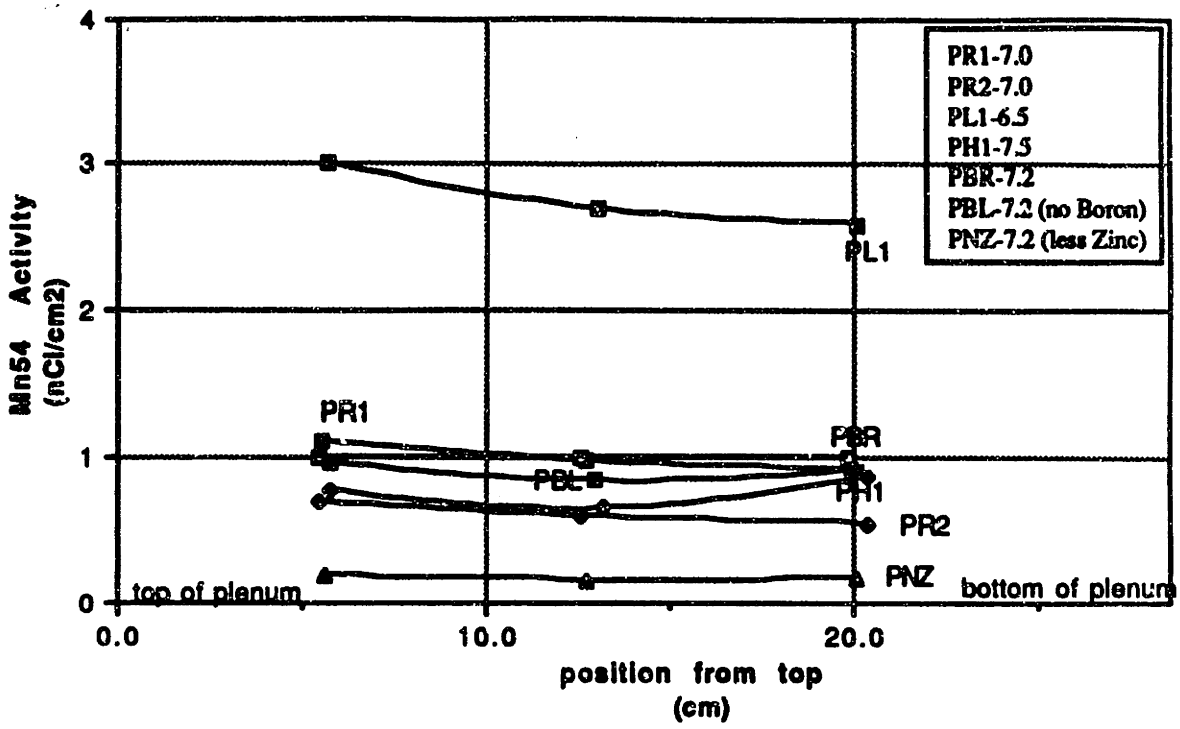

Fig 3.11 Mn54 Activity in PCCL Plena

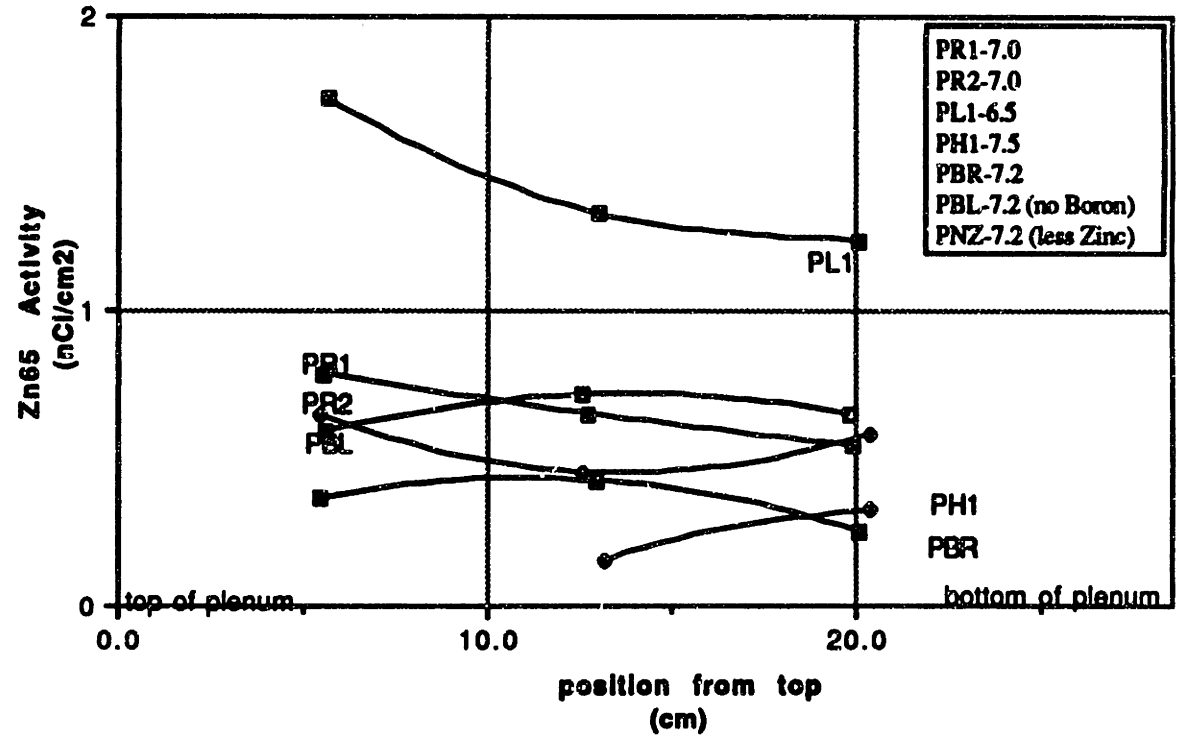

Fig 3.12 Zn65 Activity in PCCL Plena

and 7.5 are grouped and it is difficult to say that one is better than another. However we can remark that PR1 was the longest run and its Co58 and Co60 activities are among the lowest. Also, PR2 Co58 and PNZ Co60 plots may appear higher than one would at first anticipate; however, these results may be due to the fact that these two runs were perturbed by transients due to heater failure,and, moreover, both of them ended in a transient.

Finally, the last plot suggests that PNZ (no Zinc run, pH=7.2) had less zinc than the others, since no zinc was detectable.

3.4 Core Decontamination

3.4.1 Description of the Method

The MIT PCCL core region is made of about 2 meters of 0.794 cm OD, 0.667 cm ID Zircaloy 4 tubing. This tube is bent to form an U and the lower part of the U is inserted in the core. Of the 2 meters, about 1.30 meters of tube is placed in the core. Consequently, the tube, at the end of a PCCL run, is highly activated and for two reasons the crud activity cannot be separated from base metal and oxide activities without being descaled. The first impediment is the very high Zr95 activity which, even when discriminated by the HpGe system (C-1)(S-1), results in a high dead time that does not permit analyzing for low count rate activities from the crud. The second drawback is that

Zircaloy and therefore Zircaloy oxide, has impurities (see table 2.12), such as cobalt and nickel, at non negligible levels. Therefore, decontamination of the tube was necessary.

At the end of each run, The U tube was cut into pieces as shown in Fig. 3.13 (C-1). Segments Z1, Z3, Z5, Z7, Z8, Z10, Z12 and Z14 were analyzed for each run. First, the outside surface of each tube was protected by heat shrinkable tubing to avoid dissolution of activated metal. Each piece was then soaked for 12 hours in aqua regia (2 volumes H_2O + 3 volumes HCl + 1 volume HNO_3) which removed the crud without removing an appreciable amount of base metal. The procedure and its qualification test and results are described in detail in reference C-1. However, it appeared that even if this procedure does not dissolve much of the oxide, it dissolved enough to perturb the measurement of the decontamination solution. In particular, Zr95 was present in large enough quantities to make the determination of the other nuclides of interest impossible. Separation of zirconium was then needed, and was potentially possible by two methods: electrolytic and chemical. The electrolytic technique, on one hand, was aimed at plating the crud nuclides of interest, leaving the Zr95 in solution; however, due to a lack of good plating efficiency (C-1), this method was not applied. On the other hand, the chemical separation method, involving the precipitation of zirconium, leaving the nuclides of interest in solution, was found to be a very efficient method, and was, therefore, adopted. The method is as follows (C-1):

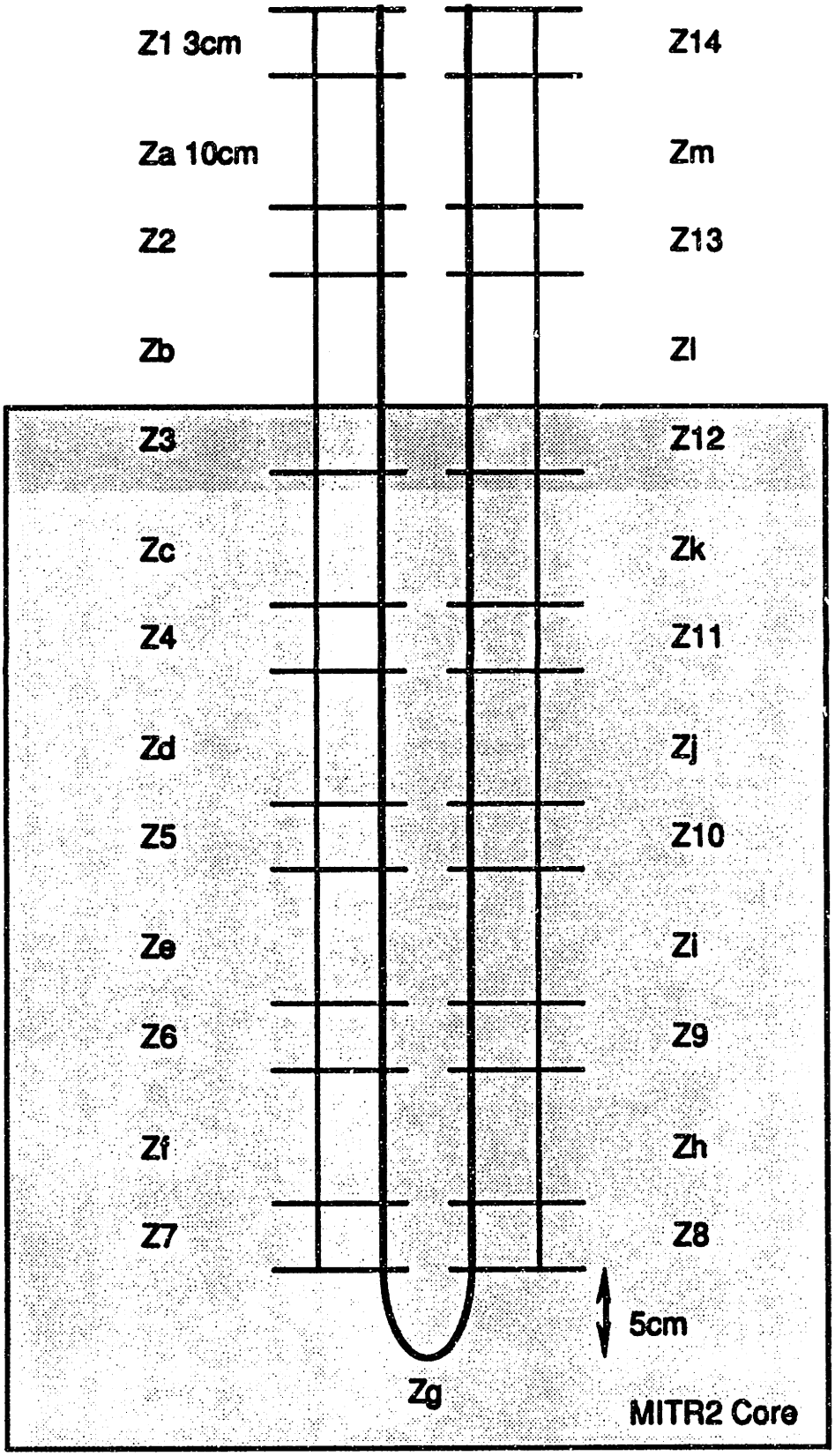

note: All segments are 3 cm or 10 cm, as shown

Fig 3.13 Schematic of Zircaloy Section Segmentation

1- A 1.5 M solution of sodium arsenate was prepared by mixing sodium arsenate in heated water.

2- A wash solution was prepared by diluting 1 ml of the sodium arsenate solution to 100ml using 2.4 N-HCl.

3- A 0.1 M zirconyl chloride ($ZrOCl_2.8H_2O$) solution was prepared by mixing 3.22 gr of $ZrOCl_2.8H_2O$ in 100ml of dionized water at about 80°C.

4- Pipet 20 ml of the sample solution into a 50 ml centrifuge tube and another 20 ml into a 4 oz. bottle, dilute the bottle to 110 ml and count at the gamma counting facility to get baseline measurements.

5- Pipet 2 ml of the zirconium chloride solution into the centrifuge tube, add a small amount (about 200 mg) of cobalt chloride, and mix well.

6- Pipet 2 ml of the sodium arsenate solution into the centrifuge tube, mix by vortex agitation, and wait 30 minutes.

7- Put centrifuge tube into the centrifuge and centrifuge at 3000 rpm for 15 minutes.

8- Decant the resulting solution through a standard 9 cm paper filter paper (Schleicher and Schuell Analytical Paper #595) into a 4 oz. polypropylene bottle.

9- Add 5 ml of wash solution to the centrifuge tube containing the precipitate, mix by agitation, and centrifuge at 3000 rpm for 8 minutes. Pour off liquid into filter, adding to original filtered liquid.

10- Repeat above step twice so that a total of three washes are performed.

11- Dilute liquid in 4 oz. bottle up to 110 ml and count on gamma counting system to determine radionuclide concentration.

Dissolution of a small amount of Zircaloy oxide perturbed the measurement due to the presence of radionuclides produced from alloying elements. Assuming 1μm of bulk metal corrosion, 20 full power days of irradiation, 100% retention in ZrO_2 film and the impurity contents measured by NAA from table 2.12, the activity in the oxide layer was calculated, and results are presented in table 3.6.

3.4.2 Results

The Zircaloy tubes (except PR1-Z1 and PR1-Z3) were all subjected to a 12 hour decontamination soak in aqua regia. The resulting solutions were diluted and counted. Results are presented in table 3.7 (the results were converted from nCi/cc to nCi/cm^2 using 6 cm^2 per tubing segment). Zirconium was then separated following the method described in section 3 of the present chapter and the solutions were counted again. Results are presented in table 3.8. Decontamination of the Zircaloy tubes from the second campaign of runs (PBL, PBR, PNZ) is to be done in the near future.

Table 3.6 Estimated Activity Contribution by 1 μm of Zircaloy to ZrO_2 Corrosion Film

Daughter Radionuclide	Concentration of Parent Element in Zircaloy (ppm)	Projected Activity in ZrO_2 Corrosion Film (nCi/cm^2)
Fe59	2100	6
Mn54	2100	2
Co58	10	0.7
Co60	0.7	0.5
Cr51	1050	800
Zr95	98%	6000

Note: 1μm of bulk metal produces approximately 88 mg/dm^2 of ZrO_2, which (at 90% T. D.) is 1.7μm thick.

Table 3.7 Results of Zircaloy Radionuclide Deposition Measurements (C-1)

Test Piece	Zr-95	Radionuclide Concentrations, nCi/cm^2			
	nCi/cm^2	Co-58	Co-60	Fe-59	Mn-54
PR1-Z1†	-	42	-	-	-
PR1-Z3††	1100 ± 69	79 ± 2.3	98 ± 1.4	440 ± 30	280 ± 1.9
PR1-Z5	530 ± 9.9	190 ± 3.3	44 ± 0.72	-	15 ± 0.32
PR1-Z7	3400 ± 85	45 ± 1.9	16 ± 0.35	-	5.1 ± 0.21
PR1-Z8	5000 ± 130	56 ± 2.1	20 ± 0.38	51 ± 17	5.6 ± 0.22
PR1-Z10	610 ± 7.2	48 ± 1.8	14 ± 0.30	-	3.0 ± 0.17
PR1-Z12	990 ± 18	9.3 ± 2.5	11 ± 0.30	-	0.52 ± 0.1
PR1-Z14	26 ± 2.7	55 ± 1.1	0.73 ± 0.10	-	-
PR2-Z1	33 ± 1.1	1.4 ± 0.39	0.42 ± 0.09	-	-
PR2-Z3	4100 ± 1.2	7.1 ± 0.74	3.4 ± 0.17	8.3 ± 3.9	0.94 ± 0.13
PR2-Z5*	4.6E5 ± 8E4	-	21 ± 7.1	-	110 ± 16
PR2-Z7	6000 ± 220	200 ± 2.3	18 ± 0.44	31 ± 5.3	6.0 ± 0.36
PR2-Z8	1900 ± 39	170 ± 2.9	19 ± 0.36	29 ± 9.3	5.0 ± 0.18
PR2-Z10*	2.1E5 ± 1E4	510 ± 31	44 ± 2.9	-	63 ± 6.2
PR2-Z12	2500 ± 61	15 ± 0.74	5.2 ± 0.17	16 ± 3.7	1.1 ± 0.13
PR2-Z14	17 ± 0.81	1.0 ± 0.39	0.44 ± 0.09	-	0.28 ± 0.12
PL1-Z1	45 ± 1.1	3.3 ± 0.28	0.60 ± 0.10	-	0.51 ± 0.09
PL1-Z3	670 ± 12	11 ± 0.66	8.0 ± 0.25	11 ± 2.2	0.8 ± 0.12
PL1-Z5*	2E5 ± 1.5E4	820 ± 56	140 ± 24	-	-
PL1-Z7	2600 ± 130	1100 ± 12	110 ± 2.5	150 ± 19	45 ± 1.5
PL1-Z8	930 ± 32	920 ± 8.8	87 ± 2.0	31 ± 15	49 ± 13
PL1-Z10	4300 ± 110	270 ± 3.1	51 ± 1.2	82 ± 3.9	31 ± 0.62
PL1-Z12	310 ± 4.9	57 ± 0.94	41 ± 0.67	88 ± 3.6	4.9 ± 0.20
PL1-Z14	13 ± 0.55	6.7 ± 0.34	0.86 ± 0.10	-	0.40 ± 0.08
PH1-Z1	14 ± 1.1	2.2 ± 0.46	0.16 ± 0.09	-	0.31 ± 0.06
PH1-Z3*	2.2E5 ± 9E3	-	9.4 ± 2.9	700 ± 78	-
PH1-Z5*	1.7E5 ± 7E3	390 ± 28	37 ± 3.4	890 ± 69	110 ± 11
PH1-Z7	4700 ± 100	144 ± 1.7	0.75 ± 0.17	-	0.80 ± 0.16
PH1-Z8	9600 ± 290	130 ± 2.2	7.9 ± 0.36	200 ± 7.0	24 ± 0.45
PH1-Z10	8000 ± 210	32 ± 0.91	0.56 ± 0.17	16 ± 2.6	1.5 ± 0.21
PH1-Z12	2200 ± 52	-	-	40 ± 8.4	-
PH1-Z14	71 ± 1.1	0.92 ± 0.32	0.30 ± 0.10	-	0.17 ± 0.07

† PR1-Z1 was counted directly before and after decontamination.

†† PR1-Z3 had no heat shrinkable tube cover, and therefore had lead contamination.

* These pieces require activity correction, see section 2.8.2.

- Indicates that the activity in question was not detected.

Table 3.8 Radionuclides in Core Crud Determined Using Chemical Separation

Test Piece	Zr-95	Transition Metal Radionuclide Concentrations, nCi/cm^2			
	nCi/cm^2	Co-58	Co-60	Fe-59	Mn-54
PR1-Z1†	-	-	-	-	-
PR1-Z3††	-	79 ± 4.9	100 ± 1.6	430 ± 29	280 ± 2.3
PR1-Z5	-	91 ± 2.3	22 ± 0.41	-	11 ± 0.26
PR1-Z7	7.9 ± 1.2	37 ± 1.6	14 ± 0.30	31 ± 9.5	4.8 ± 0.19
PR1-Z8	7.3 ± 1.7	40 ± 1.7	15 ± 0.31	-	4.4 ± 0.19
PR1-Z10	3.2 ± 0.45	25 ± 2.0	9.3 ± 0.23	12 ± 14	2.2 ± 0.15
PR1-Z12	11 ± 2.1	5.0 ± 1.3	6.3 ± 0.19	<17	0.49 ± 0.14
PR1-Z14	7.5 ± 2.0	4.3 ± 1.2	0.63 ± 0.09	<14	0.29 ± 0.09
PR2-Z1	-	1.3 ± 0.54	0.31 ± 0.09	-	0.14 ± 0.08
PR2-Z3	14 ± 1.5	4.1 ± 0.49	2.9 ± 0.13	12 ± 3.1	0.60 ± 0.10
PR2-Z5*	-	380 ± 5.5	54 ± 1.1	440 ± 15	110 ± 1.9
PR2-Z7	14 ± 1.0	200 ± 2.0	17 ± 0.36	33 ± 4.1	5.9 ± 0.18
PR2-Z8	5.2 ± 0.46	160 ± 2.0	19 ± 0.37	26 ± 4.2	4.9 ± 0.17
PR2-Z10*	1200 ± 160	560 ± 5.4	44 ± 0.80	240 ± 18	77 ± 0.77
PR2-Z12	6.1 ± 0.76	16 ± 0.66	4.8 ± 0.16	14 ± 0.33	1.1 ± 0.10
PR2-Z14	-	-	0.21 ± 0.09	-	0.09 ± 0.08
PL1-Z1	1.9 ± 0.30	1.7 ± 0.27	0.50 ± 0.09		0.27 ± 0.07
PL1-Z3	2.0 ± 0.74	5.5 ± 0.80	6.2 ± 0.20	8.9 ± 2.3	0.74 ± 0.09
PL1-Z5*	1200 ± 250	1300 ± 14	200 ± 4.0	930 ± 23	310 ± 2.9
PL1-Z7	15 ± 3.7	1100 ± 12	110 ± 2.5	180 ± 19	45 ± 1.5
PL1-Z8	4.2 ± 0.7	910 ± 1.	79 ± 3.4	34 ± 13	48 ± 1.3
PL1-Z10	53 ± 2.8	620 ± 5.8	120 ± 2.1	180 ± 7.9	60 ± 1.0
PL1-Z12†††	-	-	-	-	-
PL1-Z14	2.0 ± 0.39	2.3 ± 0.27	0.45 ± 0.09	-	0.30 ± 0.07
PH1-Z1	1.8 ± 0.36	2.1 ± 0.24	0.24 ± 0.12	15 ± 1.4	1.5 ± 0.14
PH1-Z3*	280 ± 24	45 ± 1.3	17 ± 0.41	800 ± 14	19 ± 0.33
PH1-Z5*	19 ± .19	410 ± 5.6	35 ± 0.89	910 ± 26	120 ± 2.4
PH1-Z7	20 ± 1.9	150 ± 1.5	0.84 ± 0.14	6.8 ± 1.4	0.96 ± 0.09
PH1-Z8	45 ± 3.5	140 ± 1.7	7.7 ± 0.29	220 ± 5.0	26 ± 0.35
PH1-Z10	63 ± 1.9	37 ± 0.63	0.53 ± 0.12	14 ± 1.4	1.6 ± 0.13
PH1-Z12	100 ± 3.2	2.2 ± 0.27	1.8 ± 0.12	93 ± 3.8	1.4 ± 0.10
PH1-Z14	1.3 ± 0.33	0.62 ± 0.17	0.2 ± 0.09	<0.8	0.05 ± 0.05

† PR1-Z1 was counted directly with no prior separation done

†† PR1-Z3 had no shrink tube, and therefore had lead contamination

††† PL1-Z12 separation solution was lost in an accidental spill

* These pieces require an activity correction, see section 2.8.2

- Indicates that the activity in question was not detected.

Table 3.7 and 3.8 allow estimation of in-core average and total Co58 and Co60 activities (C-1).

For the first reference run (PR1), it was found that the in-core average Co58 and Co60 activities were 68 and 31 nCi/cm^2 respectively. On the other hand, the second reference run yielded 210 and 18 nCi/cm^2 of Co58 and Co60, respectively. Thus these two reference runs did not show the same activities per unit area, even after correction for differences in neutron fluence and decay; these differences can be attributed to transients that occured during the run (see table 1.1).

PL1, the low pH run shows 650 and 91 nCi/cm^2 for the in-core average Co58 and Co60 activities, respectively.

Finally, 120 and 9.6 nCi/cm^2 for Co58 and Co60 were observed for pH1 (high pH).

The estimated total activities for Co58 and Co60 on the in-core Zircaloy for each run are documented in table 3.9 and 3.10: these values were computed by multiplying the average deposition by the total in-core tubing area.

3.5 Chapter Summary

In this chapter the various methods used in the PCCL experimental program to assay the radionuclide inventory per unit area in the different loop regions have been described. Ultrasound in 5% nitric acid was adequately effective to descale the Inconel tubing region, except for the PL1 hot leg, which

appeared to be more resistant when treated with ultrasound. A combination of cathodic and anodic electrolysis in sodium sulfate, followed by ultrasound in 5% nitric acid, was qualified to decontaminate the plenum Stainless Steel. Finally, aqua regia was used to descale the highly activated Zircaloy tubes.

Results are summarized in table 3.9 and table 3.10, where Co58 and Co60 total activity are shown for the regions of interest (ie Stainless Steel plenum, hot leg and cold leg of the Inconel cooled section, and Zircaloy core region). The differences in deposition show the significant benefit of operating in the $pH_{300°C}$=7.2 to 7.5 range, as opposed to lower pH. Furthermore, the presence of boron appears to lower deposition for a fixed pH.

Table 3.9 Co58 Activity Deposited in Loop Components (nCi)

Run ID	Zircaloy Core	Stainless Steel Plenum	Inconel Steam Generator Hot Leg	Cold Leg
PR1(pH 7.0)	17000	3044	4488	3646
PR2(pH 7.0)	53000	15394	6767	6381
PL1(pH 6.5)	160000	11121	38040	4663
PH1(pH 7.5)	30000	4429	2489	3681
PBR(pH 7.2)	TBD	4760	912	1613
PBL(pH 7.2, no B)	TBD	6751	3015	2209
PNZ(pH 7.2, less Zn)	TBD	1253	1718	2805

TBD = To Be Determined

Table 3.10 Co60 Activity Deposited in Loop Components (nCi)

Run ID	Zircaloy Core	Stainless Steel Plenum	Inconel Steam Generator Hot Leg	Cold Leg
PR1(pH 7.0)	7800	205	603	557
PR2(pH 7.0)	4500	390	473	344
PL1(pH 6.5)	23000	663	2388	386
PH1(pH 7.5)	2400	226	84	137
PBR(pH 7.2)	TBD	446	105	165
PBL(pH 7.2, no B)	TBD	825	463	284
PNZ(pH 7.2, less Zn)	TBD	447	508	891

TBD = To Be Determined

4 SHUTDOWN CHEMISTRY EFFECTS STUDY

4.1 Introduction

Shutdown, in a power plant, can be divided into three main phases (A-1):

1-immediately after the reduction in power

2-cooling phase and boration

3-oxygenation (after injection of H_2O_2 or after opening to air)

During phase 1, mostly particles are reported to be released because of control rod movements and modification of the thermal stresses. A high increase in the Co58 and Co60 activities, as well as a high increase of the Ni concentration, in the water are characteristic of phase two. By looking at the ratios Co58/Ni, Co60/Co and Co58/Co60, phase 2 can be subdivided into two steps. During the first one, when T>150°C, the Co58/Co60 ratio in the water is the same as in the core deposits, which tends to make one think that the core deposits are dissolving. However, the transfer of activity during this step is low compared to the out-of-core activity. This is followed by a second step, when T<150°C, during which the Co60/Co and Co58/Ni ratios are larger than the corresponding values during the first step. In-core structural material seem to be dissolving during this step. Finally, during phase three, when oxygen appears in the circuit, the Co58/Co60 ratio in the water, as well as the nickel concentration, continue to rise because of the dissolution of (what are postulated to be)

metallic nickel deposits in the core. In reference A-2, it is reported that about 90% of the activity released is released during phase three, and it is emphasized that, in France, there has never been seen any reduction in out-of-core activities during shutdown, which seems to rule out any important release from the steam generator, as early anticipated in reference H-1. This is also supported by large activity releases in spent fuel pools (W-2).

Around the world, the primary objective, during shutdown, is to solubilize activated corrosion products, and then remove them by coolant purification, when this approach constitutes a real or efficient way of reducing out-of-core contamination. The first point of difference is whether LiOH is added to reduce dissolution of core crud. This approach is used in Japan, even though concerns exist elsewhere that this may just postpone the core crud dissolution until the assemblies are in the spent fuel pool. Also of concern are the detrimental effects of lithium at high concentrations on both Zircaloy and Inconel. The second point of difference is whether hydrogen peroxide is added in the last stage of the cooldown. H_2O_2 addition has the advantage of scavenging the remaining hydrogen in solution, however, it is warned in several references against premature establishment of oxygenating conditions as a time saver, and it is recommended that addition be made only when the temperature is below 90°C (A-2). In Japan, where plant operators have in the past relied upon H_2O_2 created in-situ by gamma radiation, injection of hydrogen peroxide during shutdown has recently been adopted (H-2).

An earlier MIT review concerning hydrogen peroxide addition during shutdown is included as Appendix B; it presents an analysis of peroxide behavior, as well as parametric computer studies of H_2O_2 formation under shutdown conditions.

4.2 Description of the Experimental Work

The first part of this work was done by Cabello (C-1) and was aimed at determining the effect of cooldown chemistry conditions on tubes from the PCCL steam generator sections. Eight tubes from the reference runs ($pH_{300°C}$=7.0) were subjected to various conditions. Table 4.1 shows the test matrix used for each of the eight tubes. All the experiments were carried out in open-to-air containers (see ref. (C-1) for a complete description of the procedures).

The second part of this work was aimed at determining the effect of cooldown chemistry conditions on tubes from the core section. Two 5 cm tubes, Zc and Zk (see Fig. 3.13) from the PBR (800ppm Boron, 3.0ppm Lithium, $pH_{300°C}$=7.2) core section, were cut in half in the hot cell. One half of each tube was descaled using aqua regia at room temperature for 12 hours (see chapter 3 section 4). The resulting solutions were counted using the projects' HpGe detector (C-1) (S-1) and an estimated inventory for the crud on these tubes was deduced. The second half of each tube underwent three sequential steps which are described in

Table 4.1 Test Matrix for shutdown Experiments on Inconel Tubing Sections and Results (from Ref (C-1))

Case	Temperature (°C)	Boron (ppm)	Lithium (ppm)	$pH_{300°C}$	Oxidant	Result (Decon Factor)*
1	90	800	1.84	7.0	aerated	1.1
2	90	2000	1.84	6.6	aerated	1.0
3	90	2000	5.15	7.0	aerated	1.1
4	90	2000	5.15	7.0	aerated+ 10ppm H_2O_2	1.1
5	22	800	1.84	7.0	aerated	1.1
6	22	2000	1.84	6.6	aerated	1.0
7	22	2000	5.15	7.0	aerated	1.1
8	22	2000	5.15	7.0	aerated+ 10ppm H_2O_2	1.0

* Decon Factor = activity on tube before / activity on tube after

Table 4.2 Results of Shutdown Chemistry Tests on Core Zircaloy Tubing Sections

Tube ID	Treatement	removed Co58 (nCi/cm^2)	removed Co60 (nCi/cm^2)	removed Mn54 (nCi/cm^2)	removed Zn65 (nCi/cm^2)	removed Zr95 (nCi/cm^2)
PBR-Zc	Aqua Regia 12h	110	110	27	16	2270
PBR-Zc	DI water, 12 hr, 90°C, aerated	19.2	26.8	13.3	5.0	5.6
	3000ppm B, 3ppm Li 12h, 90°C, aerated	2.5	3.4	0.3	1.3	4.8
	3000ppm B, 3ppm Li, 10ppm H_2O_2, 12h, 90°C, aerated	0.6	0.5	0.1	0.2	0.9
PBR-Zk	Aqua Regia 12 h	18	6.6	4.4	/	1670
PBR-Zk	DI water, 12 hr, 90°C, aerated	14.6	2.1	0.3	0.5	/
	3000ppm B, 3ppm Li 12h, 90°C, aerated	4.8	0.7	0.1	0.2	0.7
	3000ppm B, 3ppm Li, 10ppm H_2O_2, 12h, 90°C, aerated	1.0	0.2	/	0.1	/

/ = not detected

table 4.2. Temperature was controlled using a conventional hot plate and an oil bath. First, the outside of the tube was protected with heat-shrinkable tubing to avoid contamination from the outside activated surface. Then the tubes were dropped in separate 4 oz. polypropylene bottles containing 50 ml of the desired solution. After 12 hours, each tube was removed and placed in the next solution. Finally, the solutions were counted using the counting facility (C-1) (S-1).

Finally, when the PCCL is shut down, the reactor is first shut down, then the heater power is reduced in steps (see complete procedure in ref. (S-2)). During this process, for the PBL run, in order to check for the water activity, samples from the outlet of the discharging line, after passing through a 0.45μm Millipore filter, were taken every 30 minutes (see table 4.3).

4.3 Results

The results of the experiments on the Inconel and Zircaloy tubes are presented in tables 4.1 and 4.2.

Table 4.1 shows that none of the treatments have an important effect on the crud from the Inconel section. Less than 2 nCi/cm^2 were removed from each tube, and, furthermore, even this can be due to statistical variation in the counting process. Since enormous amounts of water-borne radionuclides are seen in a plant cooldown during shutdown (several orders of magnitude higher than under operating conditions), these results suggest that

the radionuclides released in a plant cooldown do not come from the steam generator walls.

Table 4.2 suggests that a large amount of the core crud can be remove somewhat easily. The large removal by aerated DI water suggests that either aerated DI water is a more aggressive environment than regular aerated chemistry, or that the crud layer is loose, or has been made loose because of the post-run treatment of these tubes. Another possibility is that the outer crud layer is very easily solubilized. In any case, these results do not rule out the possibility that all the released crud during plant shutdown is from the core.

Worth noting is the fact that all these experiments have been performed with stagnant solutions, thus the representive nature of these experiments is open to question. Also, it should be emphasized that these tubes had all undergone a loop shutdown (ie cooldown and aeration). After PBR shutdown and aeration, the loop remained filled for 10 days at room temperature; it was then drained into two 4 oz. polypropylene bottles which were counted using the PCCL counting facility. The results are as follows:

- Co58=0.759 nCi/ml
- Co60=0.081 nCi/ml
- Cr51=1.87 nCi/ml
- Fe59=0.16 nCi/ml
- Mn54=0.064 nCi/ml
- Zn65=0.008 nCi/ml
- Zr95=0.060 nCi/ml

Even if the ratio Co58/Co60 does not allow one to draw conclusions on the origin of these radionuclides, the high Cr51 suggests that the Zircaloy oxide from the core could participate substantially in the process. Also, it should be noted that these activities per unit volume, measured in the post-shutdown aerated coolant chemistry are comparable to the levels seen in the 50 ml collected after step 2 of the shutdown experiment on the Zircaloy sections (see table 4.2).

Finally, the volumetric activities measured during PBL shutdown are presented in table 4.3. The observed decrease in activity during shutdown is not surprising because PBL was a zero boron run, and the solubility, in that case, does not vary much with temperature (see Fig 4.1 (K-1)). More tests of the same kind are planned during the NUPEC run cooldowns

4.4 Chapter summary

This chapter summarizes and analyzes all the data obtained during shutdown experiments. The main purpose was to find out where the radionuclides observed during shutdown were coming from. Work done on the steam generator section shows very little release from Inconel tubes under shutdown conditions. On the other hand, high release was observed when shutdown conditions were applied to Zircaloy sections. However, it must be pointed out that these tests followed an actual shutdown where release had already occured, and they were performed using stagnant solutions, thus the representive nature of such tests is

Table 4.3 Discharge Water Activity (μCi/ml) at Various Times During PBL Cool Down

Isotope	Before	Beginning	End	After
Co58	1.63 E-5	8.47 E-7	1.10 E-6	6.81 E-7
Co60	2.69 E-5	1.08 E-6	1.02 E-6	9.37 E-7

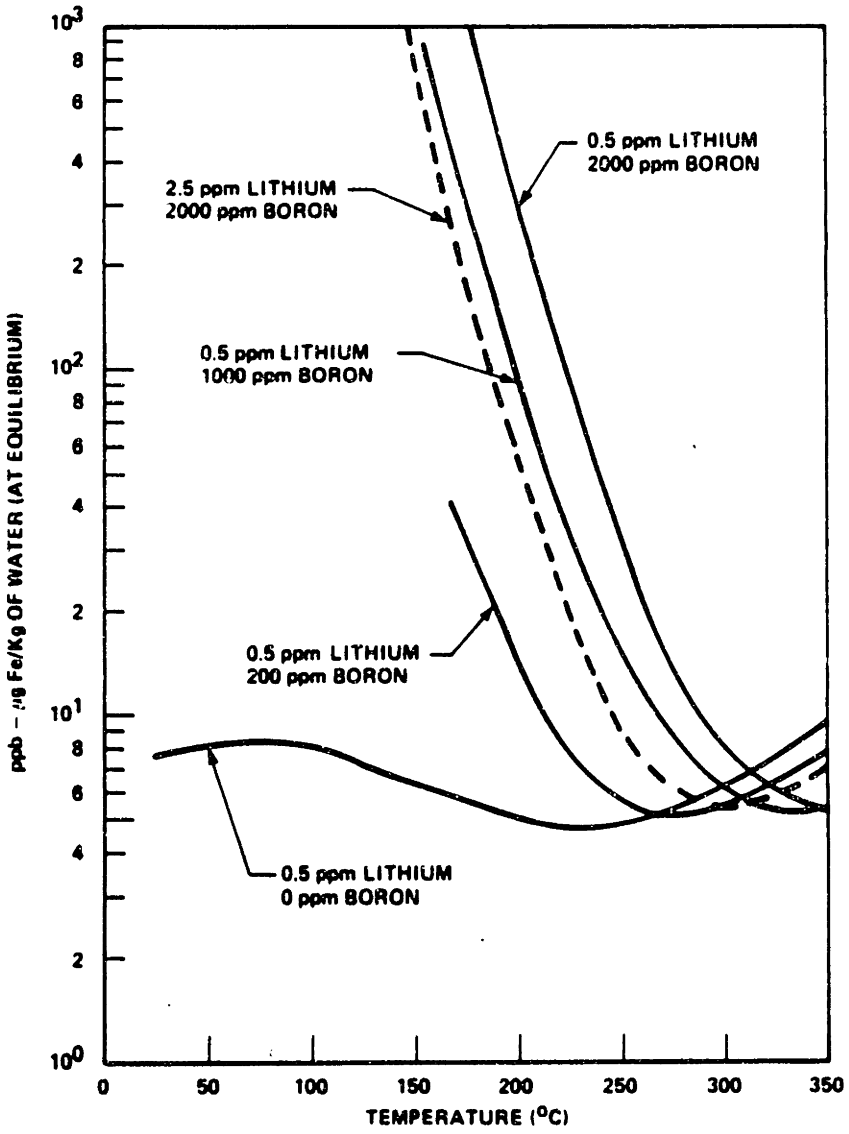

Fig 4.1 Magnetite Solubility for Various Coolant Chemistry Conditions Versus Coolant Temperature (from Ref. (K-1))

questionable. Clearly, more tests are needed in the future. If possible, a test loop should be used to simulate an actual plant shut down under unaerated conditions.

5 DETERMINATION OF INITIAL INVENTORIES

5.1 Introduction

The loops studied in the present work were prefilmed together for one month out-of-pile using PWR reference chemistry (1.41 ppm Li, 600 ppm Boron) and then preconditioned separately for another month under chemistry identical to that used in the subsequent following month-long in-pile run. The chemistry for the seven in pile runs is as follows:

PR1: 1.84 ppm Li, 800 ppm B	$pH_{300°C}$=7.0
PR2: 1.84 ppm Li, 800 ppm B	$pH_{300°C}$=7.0
PH1: 6.26 ppm Li, 800 ppm B	$pH_{300°C}$=7.5
PL1: 0.56 ppm Li, 800 ppm B	$pH_{300°C}$=6.5
PBR: 3.00 ppm Li, 800 ppm B	$pH_{300°C}$=7.2
PBL: 0.46 ppm Li, 0 ppm B	$pH_{300°C}$=7.2
PNZ: 3.00 ppm Li, 800 ppm B, "less Zinc"	$pH_{300°C}$=7.2

In the preconditioning, along with the PCCL sections pieces of extra prefilmed Inconel and Zircaloy tubes were inserted, as well as prefilmed Stainless Steel coupons. All these pieces were representative of the corresponding sections of the PCCL: by that is meant that they were made of the exact same material and had the same initial surface conditions. At the end of each preconditioning, these pieces were removed and stored in plastic bags.

It was necessary especially from a modelling point of view, for each run, to measure the initial inventory of transition metal

oxide species on the loop surfaces. The preconditioned tubes and coupons to be descaled were presumed to have low concentrations of metal oxide deposits, and thus special methods had to be developed for this particular application. Since work had already been done on descaling the inventory at the end of the in-pile run (see chapter 3), the methods used were adapted from the ones described in chapter 3, and are described in detail in the following section.

5.2 Description of the methods

For each case (ie Inconel tube, Zircaloy tube and Stainless Steel coupons), a descaling method was adapted from the ones used in chapter 3. These methods are described in detail in the following paragraphs:

•Stainless Steel Coupons

The coupons, 2.6 cm by 2.8 cm, of Stainless Steel 316, were made from the same pipe as the plenum, and received the same preparation as the plenum surface. Consequently, they were considered as representative of the plenum surface. After a month of prefilming and a month of preconditioning they were removed, and expected to have the same surface oxide inventory as the plenum itself. Since about 0.1 mg/cm^2 of crud plus oxide were expected, the method applied to decontaminate the plenum appeared to be suitable to descale the coupons, and was thought to dissolve less base metal than would perturb the measurement.

Consequently the following three step procedure was adopted and applied to one coupon from all the runs except PR1 (missing). All the solutions were first filtered through a chelating paper (see chapter 2 section 6) to remove all the contaminants and thereby facilitate post-descaling analyses. Since only the inner surface was representative of the plenum surface, the outer surface was protected with microstop paint (see chapter 3 section 2). As in the plenum descaling, a graphite electrode was used.

1st step: Cathodic electrolysis, 30 ml of Na_2SO_4 (saturated solution), 0.8 Amp., 3min.

2nd step: Anodic electrolysis, same 30 ml of Na_2SO_4 (saturated solution)as first step, 0.8 Amp., 15 seconds.

3rd step: Ultrasound, 20 ml of 5% HNO_3, 2 min.

This three step process removed the original black oxide surface of the coupon and left a shiny metallic surface. The solutions were mixed and a 50 ml mixture containing the initial inventory from the coupons resulted. All the solutions were analyzed for iron, nickel and chromium using Atomic Absorption (flame method). A blank made of the solutions used was analyzed to correct for species already present in the solutions.

• Inconel De-scaling

The Inconel tubing segments, provided to study the Inconel surface condition after the preconditioning, were about 15 cm in length and were made from the same batch as the Inconel used in the in-pile run. They were removed at the end of the

preconditioning and stored. One 2.5 cm piece was cut from each segment and descaled following the procedure described below. All the solutions were first filtered through a chelating paper (see chapter 2 section 6) to remove all contaminants, to ease post-descaling analyses. All the outside surfaces were protected using clear microstop paint (see chapter 3 section 2) to avoid dissolution of the base metal from these surfaces and therefore the attendant contamination. The same setup as for the decontamination of the activated Inconel region was used (see Fig. 3.2) except that a graphite electrode was used in this case.

1st step: Cathodic electrolysis, 70 ml of Na_2SO_4 (saturated solution), 0.4 Amp., 3min.

2nd step: Anodic electrolysis, same 70 ml of Na_2SO_4 (saturated solution)as first step, 0.4 Amp., 10 seconds.

3rd step: Ultrasound, 20 ml of 5% HNO_3, 4 min.

The rest of the procedure was the same as for the Stainless Steel coupons; the solutions were mixed and a 90 ml mixture was obtained and analyzed for iron, nickel and chromium using AA. A blank correction was again performed.

• Zircaloy De-scaling:

The major difference between the Zircaloy and the other elements of the PCCL is that the Zircaloy was not inserted during the prefilming, and consequently underwent the preconditioning only. Therefore it was thought to have much cleaner surfaces to begin with than the Inconel or the Stainless

Steel. The descaling procedure was adapted from the post-irradiation Zircaloy decontamination procedure (see chapter 3 section 3). First a 2.5 cm piece of tube was cut, using a tubing cutter, from the 15 cm Zircaloy tube that was present in the preconditioning, and its outside surface was protected using shrink wrap tubing (see chapter 3 section 3). Finally it was placed in 20 ml of aqua regia at room temperature for 12 hours. In order to make aqua regia, Mallinckrodt Analytical Reagents were used, having specified limits of 29 ppb and 30 ppb iron for HCl and HNO_3, respectively. Once again the aqua regia was circulated through chelating papers to minimize the amount of contaminants from the solution. Furthermore a blank of aqua regia was made for analyses. Since aqua regia is very strong, analysis by AA was not possible, because the solutions dissolved the AA injection system, and consequently perturbed the measurements. As a result, NAA was performed. Seven aqua regia samples from the seven runs and one blank aqua regia sample were first dried in an oven at about 90°C and then irradiated in the 1PH4 facility of the MIT Reactor (approximatively 7.35 10^{12} n/cm^2sec when the reactor is at 4.5 MW) for 4 hours. Samples were counted using one of the high efficiency, high resolution GeLi detectors in the NRL Radiochemistry Laboratory operated by Dr Ilhan Olmez. Iron, cobalt, and chromium could be measured with this technique.

5.2 Results

• Stainless Steel Coupons

Results from the analyses of the descaling solutions were corrected for contamination from the solutions and then transformed to surface concentration based on a 7.28 cm^2 coupon surface area. Furthermore, assuming a $(Fe,Ni,Cr)_2O_3$ type crud and oxide, the initial weight of initial oxide could be deduced. Results are presented in table 5.1.

• Inconel De-Scaling

Similarly to the Stainless Steel coupons, results from the descaling solutions were corrected and processed; they are presented in table 5.2.

• Zircaloy De-Scaling

Results from the NAA are presented in table 5.3. Since nickel represents an important component of the crud, and was not determined, it was not possible to get the initial "crud" weight per unit area assuming a $(Fe,Ni,Cr)_2O_3$ type crud.

It can be seen from table 5.4 (P-1) that the crud composition results presented in table 5.1, 5.2 and 5.3 are representative of full scale PWRs. A larger inventory on the plenum surfaces than on the Inconel was expected; however, they are comparable, probably because the flow velocity (hence

Table 5.1 Results of De-Scaling of the Preconditioned Stainless Steel Coupons

	Area (cm^2)	Fe (mg/cm^2)	Ni (mg/cm^2)	Cr (mg/cm^2)	Fe (%)	Ni (%)	Cr (%)	Areal weight $(Fe,Ni,Cr)_2O_3$ (mg/cm^2)
316 SS base metal					67.6	11.6	16.3	
PR2 (pH=7.0)	7.28	0.13 ± 0.02	0.056 ± 0.005	0.065 ± 0.005	51.8 ± 8	22.3 ± 2	25.9 ± 2	0.36
PL1 (pH=6.5)	7.28	0.09 ± 0.01	0.025 ± 0.003	0.051 ± 0.003	54.2 ± 6	15.1 ± 2	30.7 ± 2	0.24
PH1 (pH=7.5)	7.28	0.08 ± 0.01	0.015 ± 0.003	0.047 ± 0.003	56.3 ± 7	10.6 ± 2	33.1 ± 2	0.20
PBR (pH=7.2)	7.28	0.11 ± 0.02	0.023 ± 0.003	0.058 ± 0.003	57.6 ± 10	12.0 ± 2	30.4 ± 2	0.27
PBL (pH=7.2 no B)	7.28	0.11 ± 0.02	0.023 ± 0.003	0.058 ± 0.003	57.6 ± 10	12.0 ± 2	30.4 ± 2	0.27
PNZ (pH=7.2 less Zn)	7.28	0.07 ± 0.01	0.011 ± 0.003	0.018 ± 0.003	70.7 ± 10	11.1 ± 3	18.2 ± 3	0.14

Table 5.2 Results of De-scaling of Preconditioned Inconel Tubing

	Area (cm^2)	Fe (mg/cm^2)	Ni (mg/cm^2)	Cr (mg/cm^2)	Fe (%)	Ni (%)	Cr (%)	Areal weight $(Fe,Ni,Cr)_2O_3$ (mg/cm^2)
Inconel base metal					8.7	74.6	15.8	
PR1 (pH=7.0)	4.87	0.14 ± 0.02	0.20 ± 0.02	0.06 ± 0.01	35 ± 5	50 ± 5	15 ± 3	0.57
PR2 (pH=7.0)	4.87	0.044 ± 0.01	0.13 ± 0.02	0.05 ± 0.01	20 ± 5	58 ± 10	22 ± 5	0.32
PL1 (pH=6.5)	4.87	0.07 ± 0.01	0.31 ± 0.02	0.07 ± 0.01	16 ± 3	69 ± 5	16 ± 3	0.64
PH1 (pH=7.5)	4.87	0.13 ± 0.02	0.55 ± 0.02	0.13 ± 0.02	16 ± 3	68 ± 3	16 ± 3	1.15
PBR (pH=7.2)	4.87	0.08 ± 0.02	0.39 ± 0.02	0.06 ± 0.01	15 ± 2	74 ± 4	11 ± 2	0.75
PBL (pH=7.2 no B)	4.87	0.06 ± 0.02	0.30 ± 0.02	0.06 ± 0.01	14 ± 3	71 ± 5	14 ± 3	0.60
PNZ (pH=7.2 less Zn)	4.87	0.33 ± 0.02	1.07 ± 0.2	0.57 ± 0.2	17 ± 1	54 ± 1	29 ± 1	2.8

Table 5.3 Results of De-scaling of Preconditioned Zircaloy Tubing

	Fe (mg/cm^2)	Cr (mg/cm^2)	Co (mg/cm^2)
PR1 (pH=7.0)	0.0078 ± 0.0025	8.9 e-4 ± 1.7 e-4	5.8 e-5 ± 4 e-6
PR2 (pH=7.0)	< 0.0072	5.3 e-4 ± 2.6 e-4	/
PL1 (pH=6.5)	< 0.0047	3.3 e-4 ± 2.5 e-4	4. e-5 ± 1.2 e-5
PH1 (pH=7.5)	0.013 ± 0.005	5.3 e-4 ± 2.6 e-4	1.5 e-4 ± 1.5 e-5
PBR (pH=7.2)	< 0.013	5. e-4 ± 1.5 e-4	9. e-5 ± 8. e-6
PBL (pH=7.2 no B)	< 0.0078	2.9 e-4 ± 8.7 e-5	9.3 e-5 ± 6.5 e-6
PNZ (pH=7.2 less Zn)	0.05 ± 0.01	0.011 ± 0.003	4. e-5 ± 7.e-6

Reynolds number) in the plenum is very low compared to that in the Inconel sections (17 times lower), or because of different initial surface roughness.

From table 5.1 it can be observed that the iron is depleted in the oxide on Stainless Steel; this can be explained by an hypothetical preferential corrosion release of iron from the steel, and could explain the higher iron concentrations on the Inconel and Zircaloy.

Also of interest are the high chromium values on the Stainless Steel and Inconel compared to the the initial base metal concentrations. Because chromium is very insoluble, it could concentrate in the oxides rather than being released. A low chromium concentration on the Zircaloy appears to support this hypothesis, especially if one notes that Zircaloy also contains chromium as an alloying element.

5.3 Chapter Summary

In this chapter, representative pieces of the loop as they existed before the in-pile run were studied. Special methods were developed to descale what were presumed to be thin oxide deposits with low concentrations of metal. Dissolution of base metal was minimized to avoid contamination.

The results show that the initial inventory, in amounts and composition, on the PCCL surfaces is representative, if compared to the typical values observed in a Westinghouse PWR (P-1). Moreover, the observed inventories are fairly consistent from run

to run, with the exception of PNZ, which had a larger inventory to start with; this may be due to the high O_2 concentration (~100ppb) observed during PNZ preconditioning (to be compared to <1 ppb O_2 for the other runs). In view of the large differences later observed in activity deposition for PL1 and PH1, it is interesting to note that their pre-irradiation inventories are comparable.

If further work is planned in this area, SEM pictures of the surface before an in-pile run should be taken; differences in the initial oxide/crud layer structure may explain some of the differences observed at the end of the in-pile runs.

6 COMPUTER CODE STUDIES

6.1 Introduction

It was of considerable benefit in the planning and the interpretation of PCCL experiments to have analytical predictions of activity deposition on the loop surfaces using state-of-the-art computer models. Three codes were made available to MIT: CRUDSIM from its developer Dr. W.T. Lindsay (formerly of Westinghouse), PACTOLE from the CEA (Commisariat à l'Energie Atomique) and, more recently, CORA from Westinghouse. Separate efforts, mostly parametric studies, using CRUDSIM and PACTOLE are reported in refs. (L-1) and (B-1), respectively. An earlier review of crud transport modelling as it applies to the PCCL is contained in the thesis by Morillon (M-2). In the present work, the three codes have been used to model the MIT PCCL, to predict activity deposition at the end of each run. However, code specialists have cautioned against the use of the codes (PACTOLE, in particular) for simulation of periods less than a month, and therefore, it was prefered to run the codes for a one year period and then scale back the results. Code runs were 1 year at 100% reactor capacity factor, hence fluences are approximatively 20 times those of a typical loop run (30 days at 60% reactor capacity factor).

To help future researchers to run the codes, input instructions and typical PCCL input data are documented in appendix C.

6.2 Description of the codes available at MIT

6.2.1 CRUDSIM (B-5)

The approach that was chosen in the development of this model is very simple, and is illustrated in Fig 6.1 (B-5). As shown in the figure, CRUDSIM is a two node model, one being the in-pile part of the primary system (hot) and the other one being the entire out-of-pile of the loop (cold). Corrosion products are added at a constant, or pH dependent, rate R; tanks are mixed to achieve equilibrium between solids and solution at the conditions of each tank; solids are filtered in each tank and an empirical fraction βF of the flow goes to the core tank and is equilibrated with the hot tank contents. It should be noted that transport of iron is done only by dissolved species. The basic equations used in the CRUDSIM model are as follows:

$$\Delta I_h=\beta F(S_c-S_h)\,\Delta\theta \tag{6.1}$$

$$\Delta I_c=[R-\beta F(S_c-S_h)]\Delta\theta \tag{6.2}$$

$$\Delta A_c=[-\beta F(\frac{S_c A_c}{I_c}-\frac{S_h A_h}{I_h})-\lambda A_c]\Delta\theta \tag{6.3}$$

$$\Delta A_h=[\alpha P I_h+\beta F(\frac{S_c A_c}{I_c}-\frac{S_h A_h}{I_h})-\lambda A_h]\Delta\theta \tag{6.4}$$

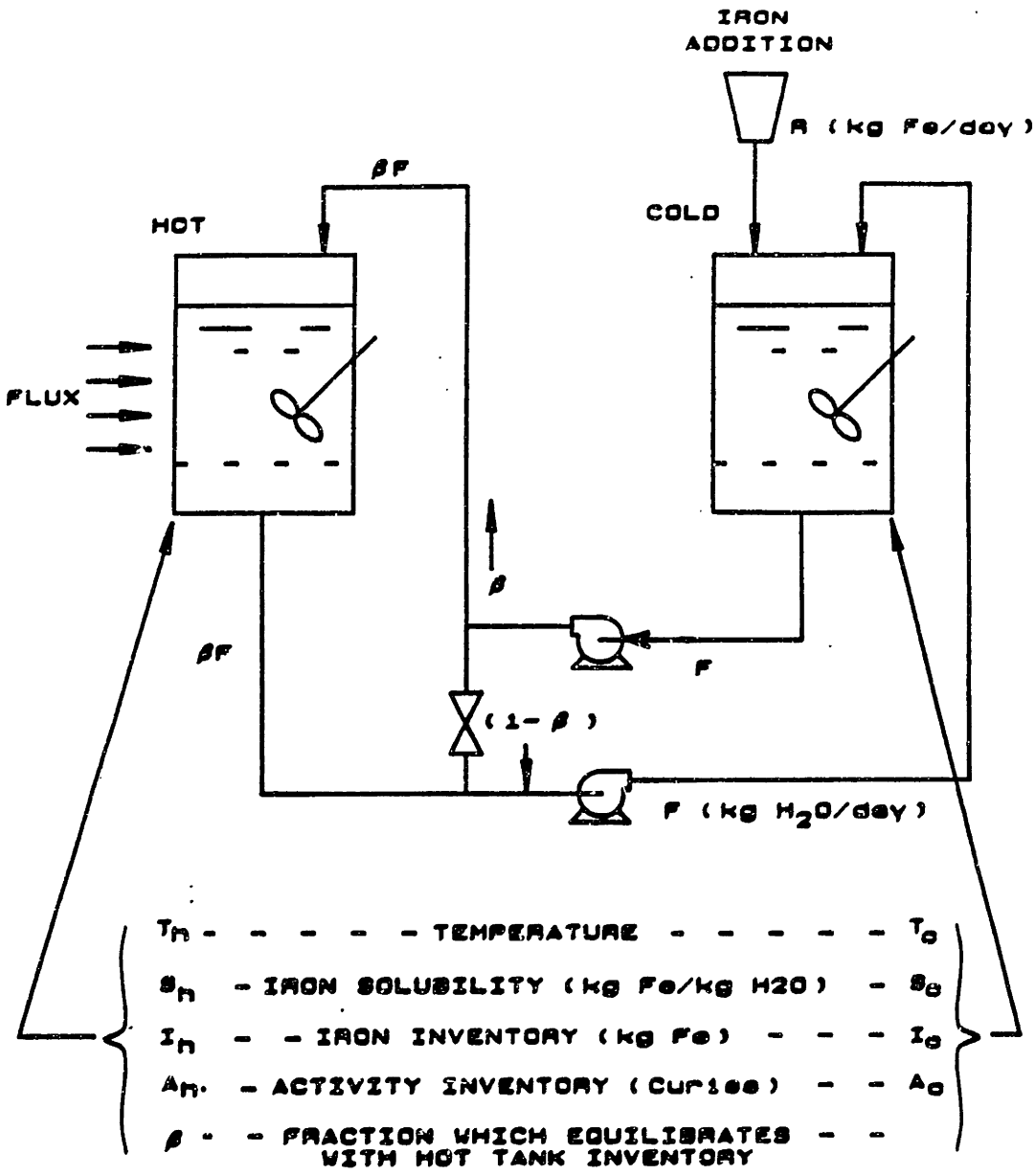

Fig 6.1 Schematic Representation of CRUDSIM "Slurry Tank" Model (B-5)

where,

I_h = iron inventory in the hot tank (kg-Fe)

I_c = iron inventory in the cold tank (kg-Fe)

S_h = iron solubility in the hot tank (kg-Fe/kg-H_2O)

S_c = iron solubility in the cold tank (kg-Fe/kg-H_2O)

A_h = activity inventory in the hot tank (Co58 or Co60)

A_c = activity inventory in the cold tank (Co58 or Co60)

R = iron input into the cold tank (kg-Fe/day)

λ = decay constant (day^{-1})

α = neutron activation factor (Ci/kg-Fe % power day

β = empirical transport factor for the crud and activity

F = primary system flow rate (kg-H_2O/day)

P = percent of full power (% power)

C. B. Lee has studied the CRUDSIM model in great detail, and has elaborated upon the basic code (L-4). He has shown that its approach is fully compatible with the surface-to-bulk mass transfer models used in CORA and PACTOLE.

6.2.2 CORA

CORA, uses some of the same basic ideas as CRUDSIM, but is a much more comprehensive code. The model is semiempirical. It is based on a theoretical understanding of the physical processes involved in radiation field buildup, but also uses experimental

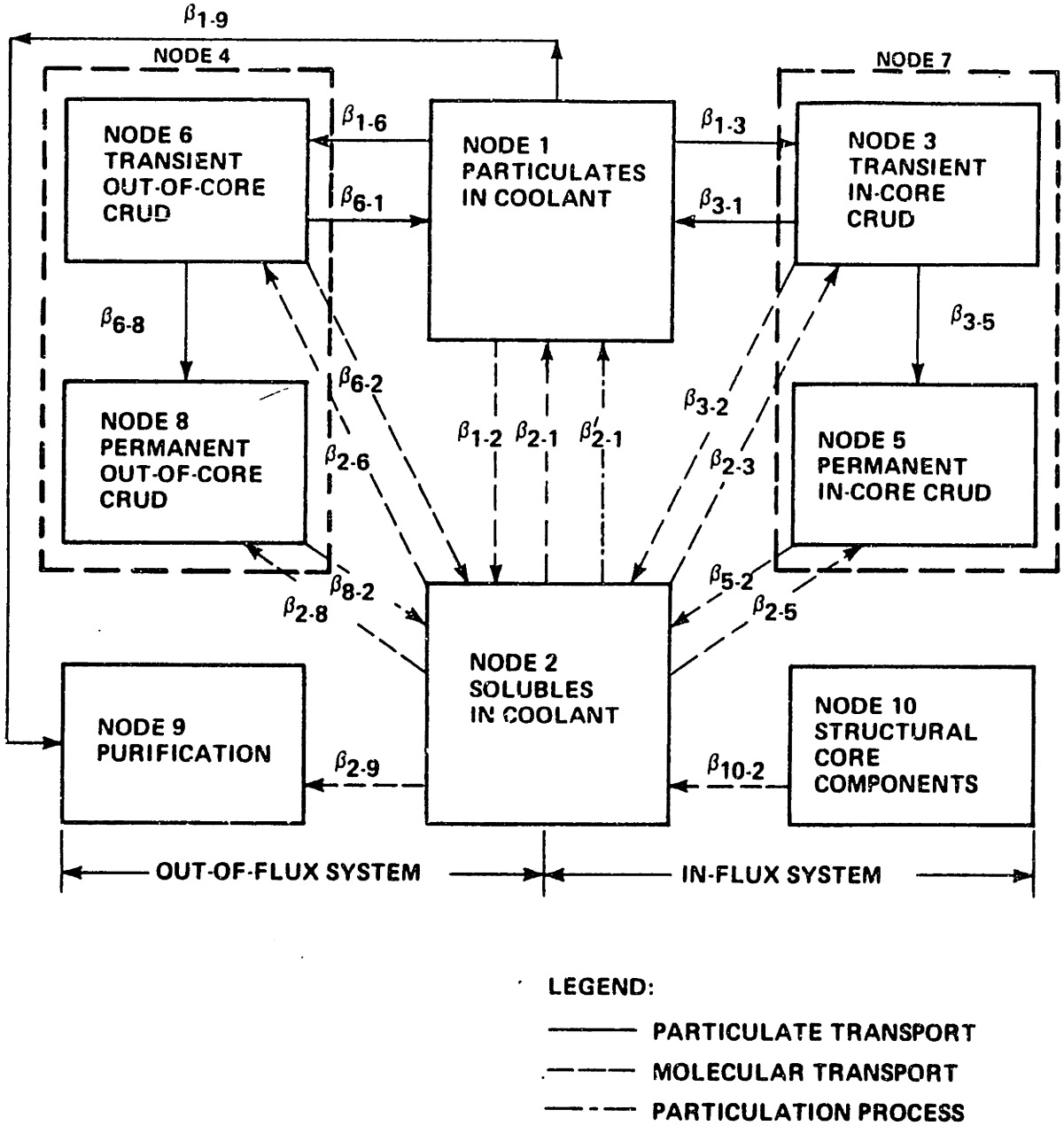

Fig 6.2 CORA Code Nodal Diagram (from Ref K-1)

data from plants. Therefore it is primarily useful for evaluating the effect on radiation level and crud characteristics for system or chemistry changes.

The model is a multinodal one, as shown in Fig 6.2, in which crud characteristics and transfer paths are indicated. Various theories, as well as data from plants were used to define an analytical approach consistent with observation. Basic mass and radionuclide balances are used to describe exchanges between nodes. For example, the transport between node 1 and node 2 is given by (L-4):

$$\beta_{2\text{-}1} - \beta_{1\text{-}2} = kA_{12}(C_2 - C_1) \qquad (6.5)$$

where,

$\beta_{2\text{-}1}$ = amount of material passing from node 1 to 2

$\beta_{1\text{-}2}$ = amount of material passing from node 2 to 1

k = first order transfer coefficient for material, m, passing from nodes 1 and 2

A_{12} = interfacing surface area between nodes 1 and 2

C_2 = effective concentration in node 2

C_1 = effective concentration in node 1

Furthermore, CORA considers most of the effects of coolant chemistry and other transport mechanisms, such as recoil release or erosion. However, it is noted in ref (K-1) that the corrosion input from auxiliary systems such as the Chemical and Volume Control System (CVCS) is not included. Nevertheless, CORA is

considered as one of the most comprehensive codes available worldwide for corrosion product transport in PWRs.

6.2.3 PACTOLE

Pactole , developed in France, is able to handle as many zones as neccessary to describe a circuit. Each zone is characterized by its average temperature, its wall temperature, its dimensions, the fluid velocity, the composition of surface material and other physico-chemical variables.

Fig 6.3 (B-2) summarizes the exchange modes used in PACTOLE.

If one considers a region at a point y in a system (B-6), the concentration of ions of element j is given by:

$$\frac{\partial C_{j,y}}{\partial t} + V_y \frac{\partial C_{j,y}}{\partial y} = \frac{hX}{A} \qquad (6.6)$$

with,

$X=P$ if $C_{j,y} > S_{j,p}$ (precipitation)

and $X=A_s M_{j,y} + RP$ if $C_{j,y} < S_{j,p}$ (dissolution and release)

where,

h = mass transfer coefficient ($cm.sec^{-1}$)

P = wetted perimeter (cm)

S = wetted surface area (cm^2)

A = cross sectional area (cm^2)

$C_{j,y}$ = ion concentration in the bulk of the fluid

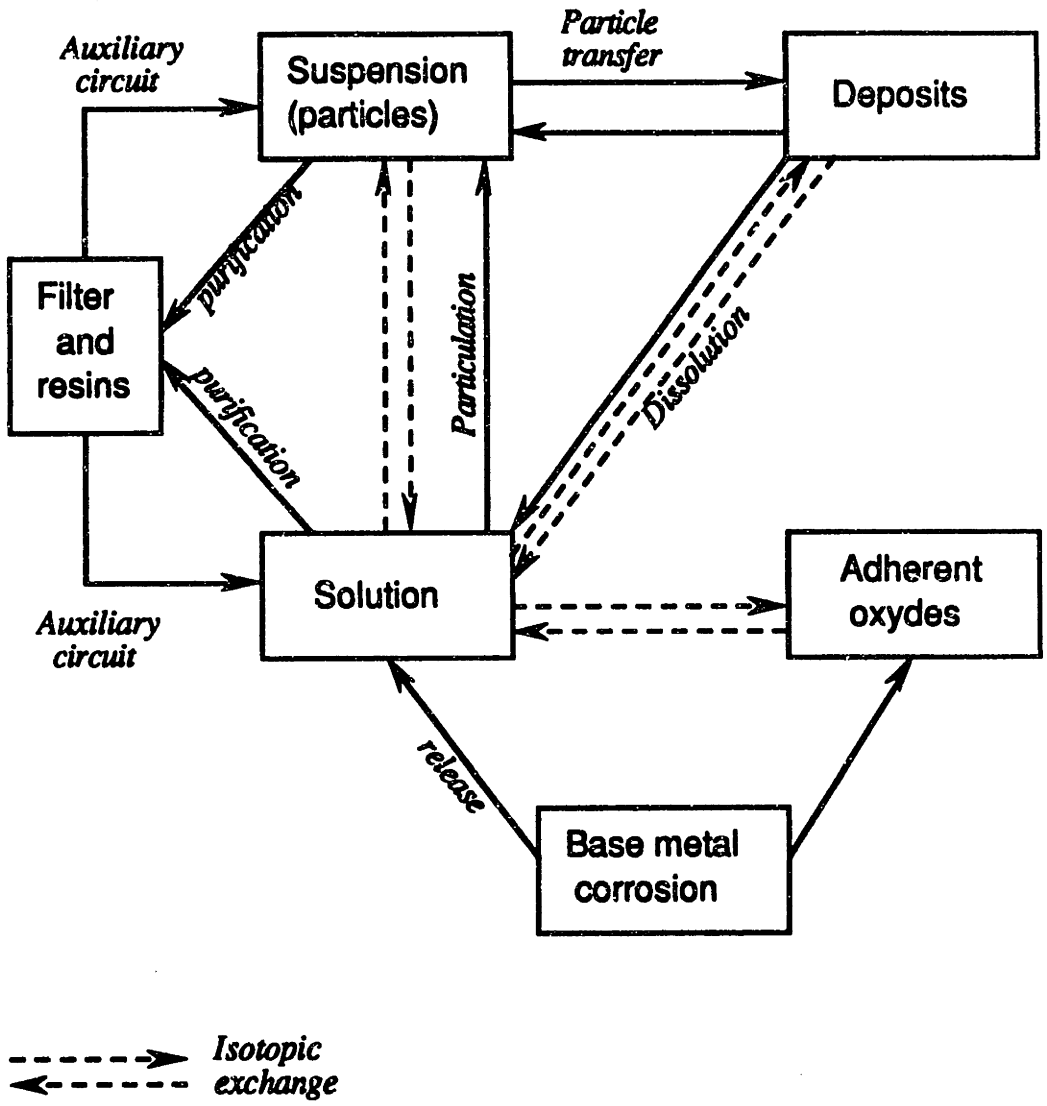

Fig 6.3 Exchange Modes Used in PACTOLE (B-2)

$S_{j,p}$ = Solubility (ion concentration at the surface of the wall)

A_s = specific area of the deposits ($cm^2.g^{-1}$)

V_y = Fluid velocity ($cm.sec^{-1}$)

$M_{j,y}$ = element mass per unit area (g/cm^2)

R = parameter defining the kinetics of the release

The concentration of element j in the <u>particulate</u> form is given by:

$$\frac{\partial N_{j,y}}{\partial t}+V_y\frac{\partial N_{j,y}}{\partial y}=\frac{hP}{A}(S_{j,p}-C_{j,y})-\frac{h'_pP}{A}N_{j,y}+\frac{\alpha_yP}{A}M_{j,y} \qquad (6.7)$$

precipitation deposition erosion

(if $C_{j,y}<S_{j,p}$)

where,

h'_p = mass transfer coefficient of the particles ($cm.sec^{-1}$)

α_y = erosion constant

• and the <u>deposit</u> mass per unit area ($M_{j,y}$):

$$\frac{dM_{j,y}}{dt}=h'_pN_{j,y}+hA_sM_{j,y}(C_{j,y}-S_{j,y})-\alpha_yM_{j,y} \qquad (6.8)$$

(if $C_{j,y}<S_{j,p}$)

The equations above (B-6) represent the basic equations. To these basic equations, representing the basic phenomena, are added equations which simulate state-of-the-art mechanisms and phenomena. Table 6.1 lists the phenomena which are treated by the code, as well as their link with various variables. However, it

the code, as well as their link with various variables. However, it should be noted that, like the other codes, PACTOLE is not adequate to study transients, or even runs shorter than a month or so, due in part to dependence on initial conditions which are unfortunately very often not well known.

6.3 Code predictions

Activities per unit area predicted by CRUDSIM, CORA and PACTOLE, for a one year run using PCCL characteristics are presented in Figs. 6.4, 6.5 and 6.6, respectively. It can be noted that all three codes exhibit the same qualitative trends; low pH produces a high radionuclide inventory in the core as well as in the steam generator, and high pH (ie higher than 7.1) reduces significantly the deposits on surfaces. In that key respect, the codes are in agreement with experimental results.

Since PACTOLE allows one to model a loop region by region, it was possible to separately model the cold leg and hot leg of the PCCL steam generator. It can be seen from Fig. 6.6 that the Co58 and Co60 activities are higher in the hot leg than in the cold leg for PACTOLE runs for which the pH was 7.0 and less; on the other hand, for pH=7.2 and 7.5 the activities are higher in the cold leg than in the hot leg. With these predictions in mind, if one looks at the experimental results (Figs. 3.4 and 3.5), it can be seen that the observed trends in the PCCL are similar.

Table 6.1 Main Phenomena and Mechanisms Involved in Corrosion Product Contamination (B-6)

Mechanisms and Phenomena	Dependent on or Governed by	Treated by PACTOLE
Nuclide Formation	Neutron Flux	Yes
Neutron Capture	Power	Yes
Atomic Ejection	Time	Yes
Decay	Time	Yes
Molecular Diffusion	Temperature	Yes
(isotopic exchange)	Time	
Filtration	Temperature	Yes
Purification	Time	empirical
Gamma Attenuation	Flow Rate	Yes
(dose rate calculation	Resin Efficiency	
Convection	Fluid Velocity	Yes
Particulation	Thermohydraulics	Yes
Brownian Diffusion	Particle size	Yes
Turbulent Inertial Projection	Reynolds & Schmidt numbers	Yes
Gravity	Temperature	Yes
Thermophoresis	Geometry, etc..	Yes
Lift Force	Hydraulics & wall roughness	Yes
Surface Charge	Temp. pH, etc..	No
Sticking Probability	Surface charge?	empirical
Dissociation of soluble products:		
H_2O, LiOH, H_3BO_3, H_2,..	Chemistry	Yes
Solubility of Metallic Ferrites	Chemistry	Yes
Passivation	Operation	empirical
Oxide Formation+ Elemental Release	Material comp., chemistry	Yes
Wear Release	Material comp., chemistry	empirical
Deposit Dissolution	Chemistry	Yes
Precipitation (Co)	Chemistry	Yes
Interaction Between Elements	Chemistry	Yes
Shutdown	Chemistry, Time	empirical

note: "empirical" implies that the user can not affect the phenomenon by external data input

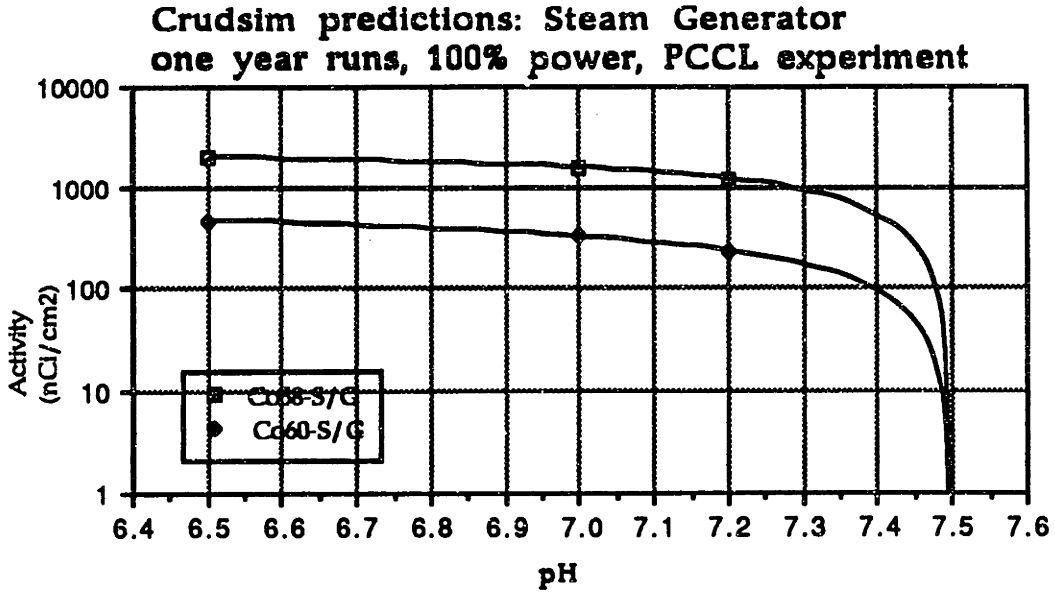

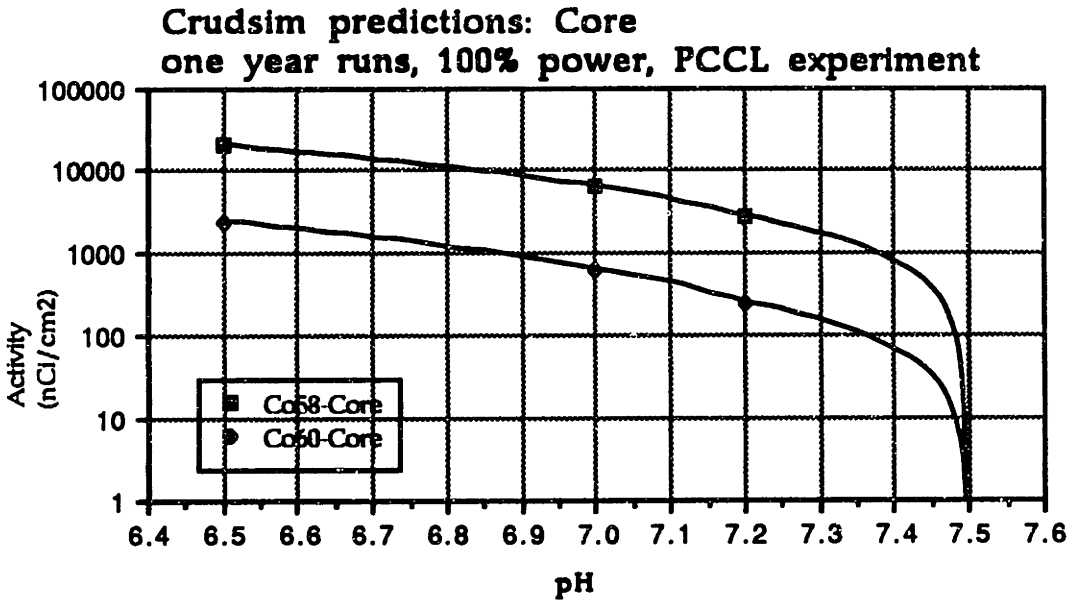

Fig 6.4 PCCL: CRUDSIM Predictions for Experiments

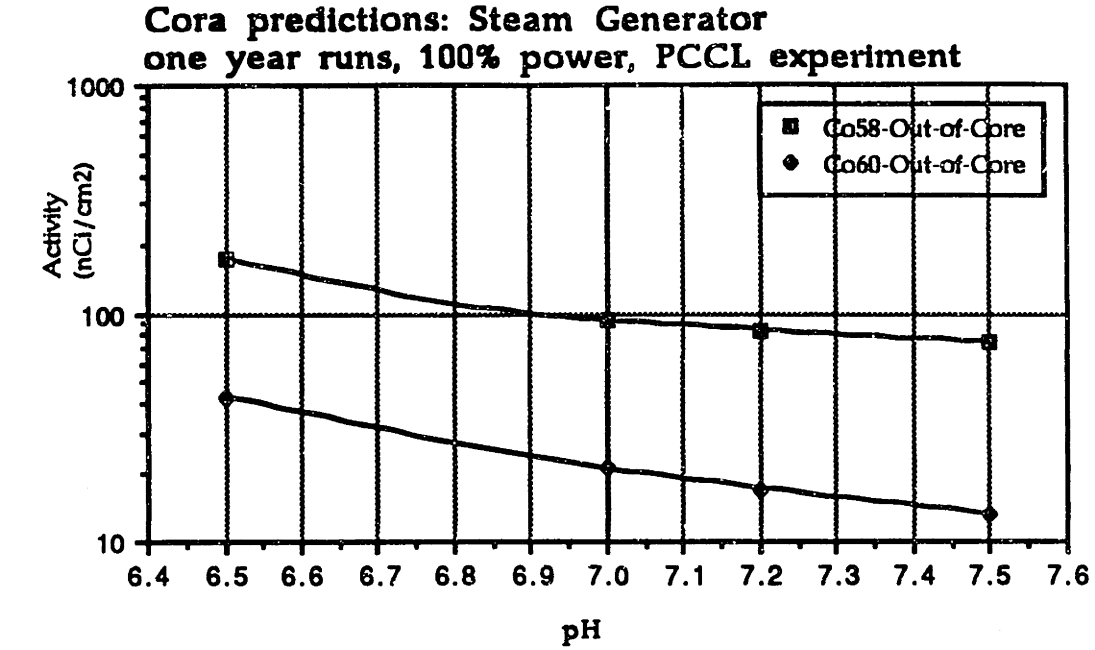

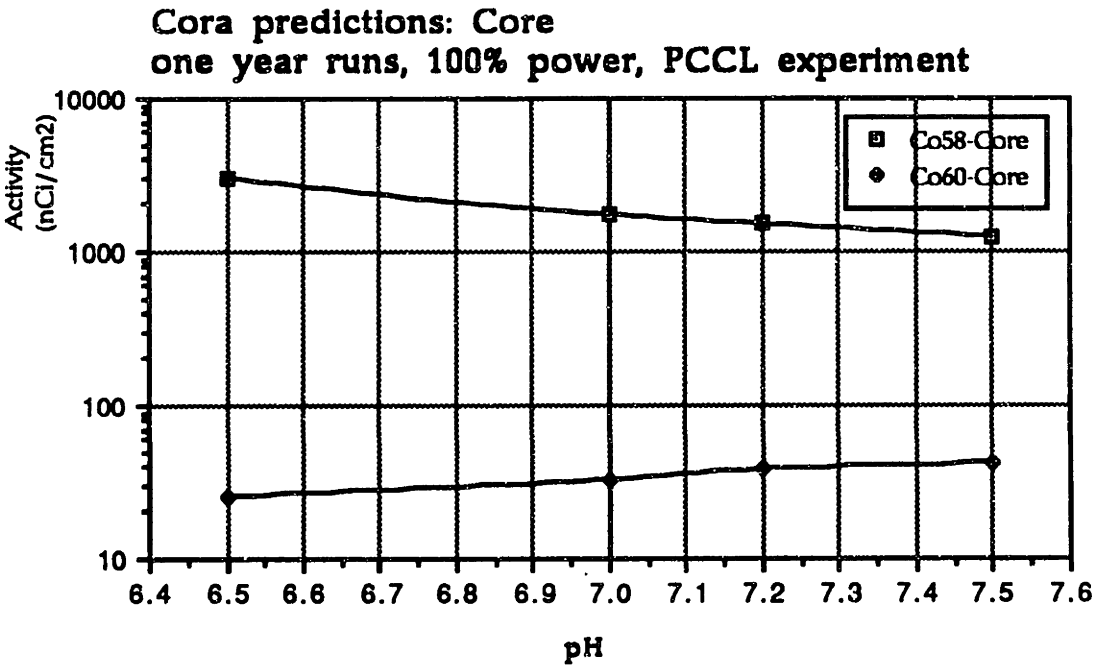

Fig 6.5 PCCL: CORA Predictions for Experiments

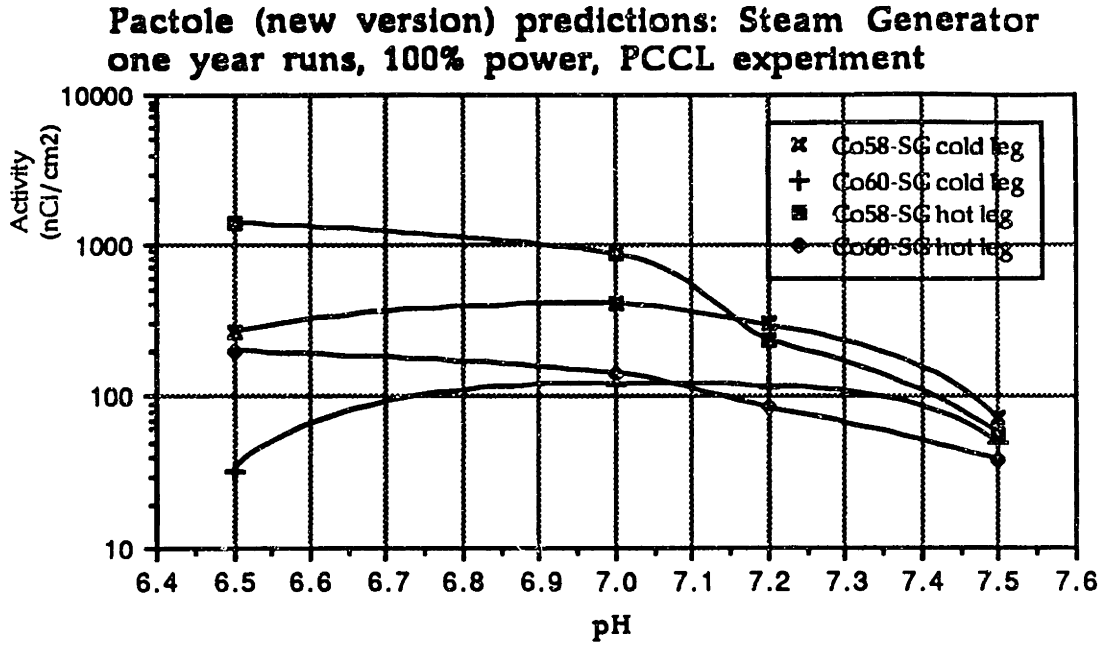

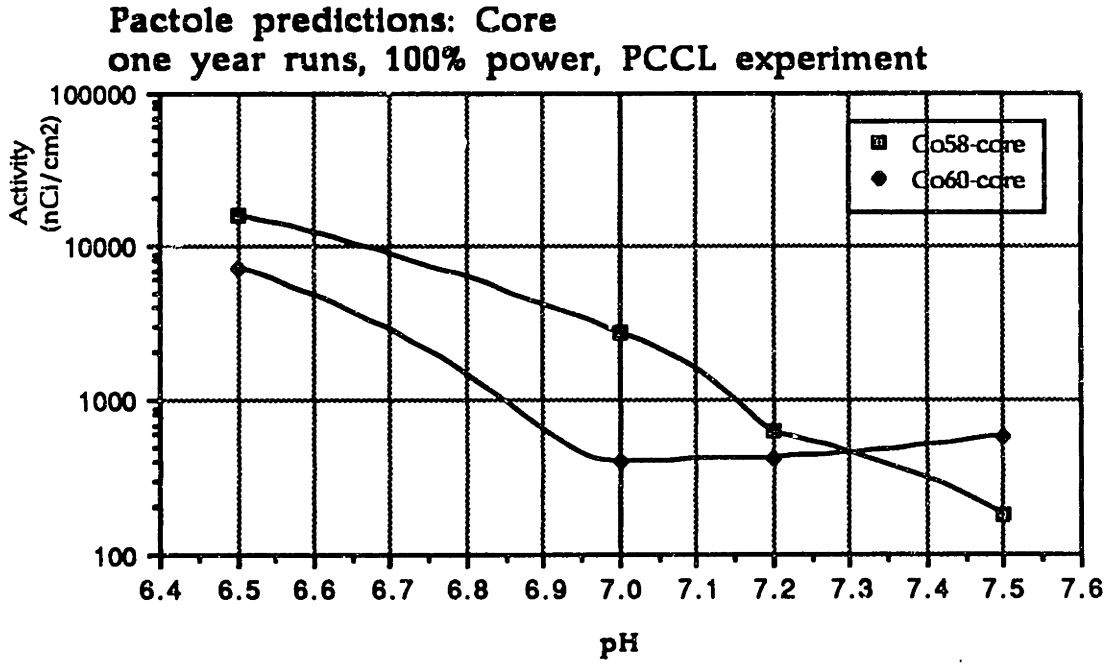

Fig 6.6 PCCL: PACTOLE Predictions for Experiments

Worth noting is the fact that PACTOLE predicts a substantial participation of the CVCS in metal release in real PWRs as well as in the PCCL.

Finally, none of the codes model the phenomenon observed at the interface of cooled region of the steam generator and the adjacent adiabatic region (see chapter 3 section 2.2). Furthermore, this phenomenon is not explained with classical solubility driven mass transfer analysis; this suggests a phenomenon not taken into account in the computer models. SEM pictures of the crud layer in these regions will be taken in the near future and reported in (Z-1).

6.4 Chapter Summary

This chapter has presented the predictions of CRUDSIM, CORA and PACTOLE when applied to the PCCL. Because these codes were designed to simulate full-scale PWR units for long cycles, they were applied to the PCCL for a one year period (instead of the actual month-long runs). Similar trends, and more particularly low radionuclide deposition at high pH ($pH_{300°C}>7.1$), were observed both in the predictions and the experimental results, which confirm, at least, at a qualitative level the ability of these codes to predict the effect of conditions and chemistry changes on activity deposition in plants.

Extensive work in the computer code area is planned in the 1991 and 1992 time frame. In particular, comparison between the three codes is planned using French and US plant data, as well as PCCL data. Moreover, work will be performed to improve the models. This work is to be funded by Framatome.

7 SUMMARY, CONCLUSIONS AND RECOMMENDATIONS

7.1 Summary and Conclusions

In an effort to understand, and ultimately reduce radiation field build-up, a research group at the Nuclear Reactor Laboratory of MIT has designed and built a small in-pile loop to simulate a PWR primary system, to study chemistry effects on corrosion product behavior. The first two campaigns of runs were aimed at the optimization of coordinated $LiOH/H_3BO_3$ (pH) chemistry to minimize radionuclide deposition on out-of-core surfaces. The success of the subject experiments depends on the ability to determine, both before and afterwards, the inventory of deposited corrosion products and their associated radionuclides. This task was the principal focus of the present work, to include both methods development and their application.

Because the entire PCCL is placed in the MIT Reactor core tank, some of its components become activated, which makes direct assay of radionuclide deposition impossible. In the present work, descaling methods were developed from plant decontamination techniques in order to acquire data from end of run loop surfaces. Ultrasound and electrolysis were shown to be very effective to decontaminate Inconel and Stainless Steel tubing with a minimum of base metal dissolution. Aqua Regia was used to descale the core Zircaloy tubing. Results from the Inconel, Stainless Steel and Zircaloy surfaces show clearly the advantage of runing at high pH (e. g. above $pH_{300°C}$=7.1) compared to low pH

($pH_{300°C}$=6.5). A summary of the results obtained from the Inconel steam generator tubing is shown in Fig 7.1, where radionuclide inventory is plotted versus pH. The similarity with PACTOLE predictions is impressive. CRUDSIM and CORA show a reasonable, but more qualitative, agreement in the deposition trends.

In the present work, charging water chemistry analyses have been carried out to evaluate the importance of impurities introduced from the PCCL charging system. Different methods, such as NAA, AA, ion chromatography and colorimetry have been used. Globally, the PCCL chemistry is clean and within the EPRI guideline specifications. On the other hand, the charging system may consitute a non negligeable source of transition metals. Materials used to build the loop components were analyzed using NAA; they were found to be within specification and representative of full scale PWRs, for the EPRI/ESEERCO as well as for the NUPEC loops.

Work was performed to assay the initial surface inventory on loop surfaces prior to the in-pile run, and post-preconditioning. This work was done mainly because this data is required in computer models of crud transport, and in some cases, such as CRUDSIM, the final predictions are very sensitive to the initial inventory (L-4). Descaling methods were developed, using the process developed to decontaminate activated PCCL components as a basis. Ultrasound, electrolysis and aqua regia were used to solubilize the initial crud and oxide layers; AA (flame technique)

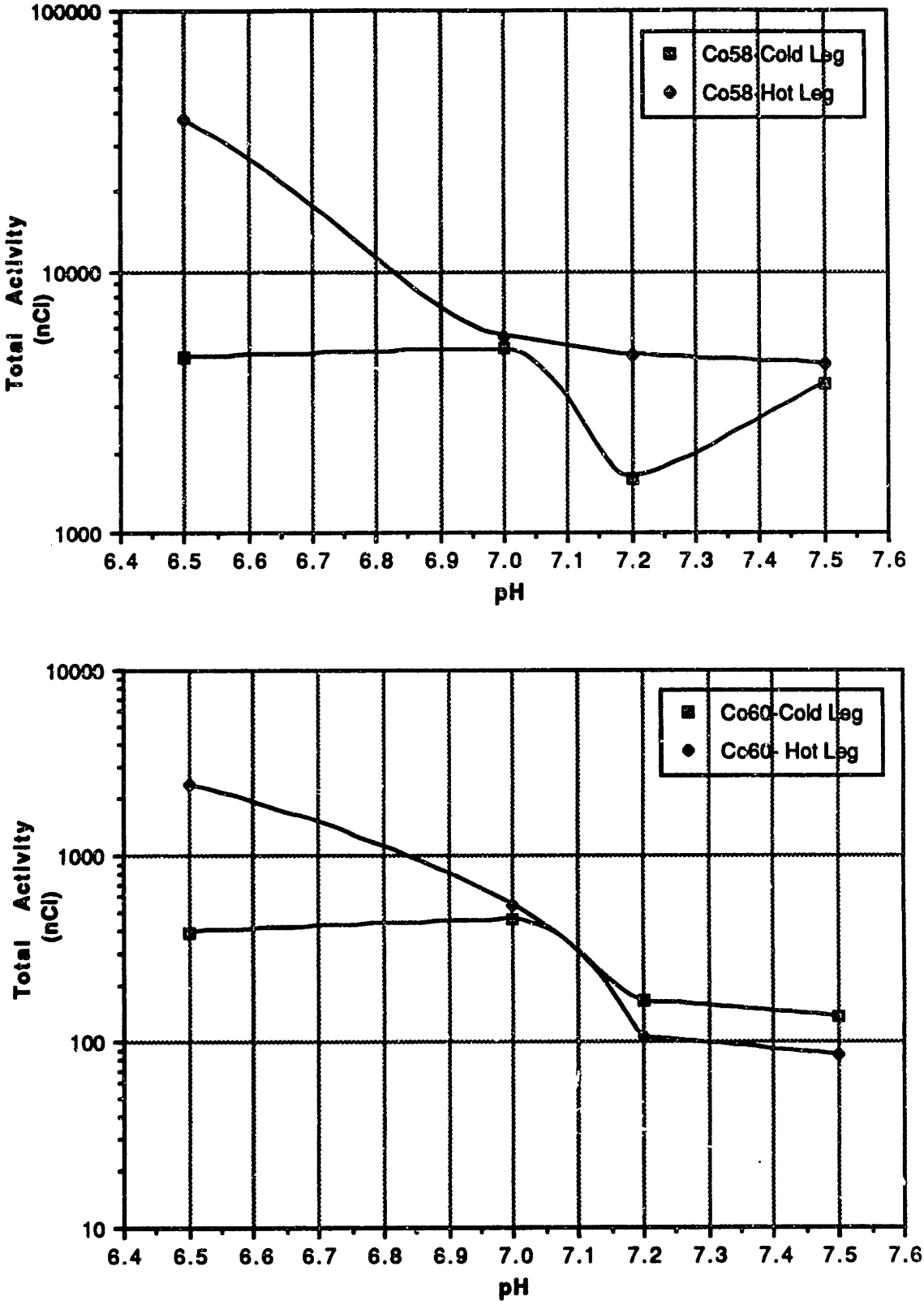

Fig 7.1 Measured Co58 and Co60 Steam Generator Tubing Deposition Versus pH from PCCL runs

and NAA were performed to assay the composition. The PCCL initial crud inventory was found to be representative of the inventory seen in Westinghouse plants.

Table 7.1 presents a summary of the work reported in this thesis, as well as findings and representative results.

The success of the descaling techniques as well as the success of water and material analyses techniques, is encouraging for the NUPEC PCCL campaign. Good performance of the computer code models, particularly PACTOLE, suggests that more work using the model should be done and used in decision making and interpretation of the results.

7.4 Recommendations for Future Work

It is recommended that further work be done on the impact of the input of metals from the charging system on final radionuclide inventory. Samples should be analyzed using graphite furnace AA whenever possible. Furthermore, crud composition in the different PCCL components should be analyzed and compared with typical crud compositions seen in plants. This would be another important step in the qualification of the computer models. SEM pictures should be taken in order to explain the behavior of radionuclide deposition observed at the interface of the cooled region of the steam generator and the adiabatic region (see chapter 3 section 2.2). SEM pictures of the

Table 7.1 Summary of Principal Findings

	Measurement	Principal Findings Representative Results
CORE	•initial metal inventory •final radionuclide inventory	~0.008 mg/cm^2 Fe more than 10 times higher than in the S/G PL1>>PR1&2>PH1 (Co60) (6.5>>7.0&7.0>7.5)
PLENUM	•initial metal inventory •final radionuclide inventory	~0.1 mg/cm^2 Fe ~twice that in the S/G PL1>PR1&2, PBR, PH1 (Co60) (6.5>7.0&7.0, 7.2, 7.5)
S/G (hot leg)	•initial metal inventory •final radionuclide inventory	~0.09 mg/cm^2 Fe ~8 nCi/cm^2 Co60 for PL1 ~1 nCi/cm^2 Co60 for PR1&2, PBL ~0.3 nCi/cm^2 Co60 for PBR, PH1 PL1>>PR1&2, PBL>PH1, PBR (Co60) (6.5>>7.0&7.0,7.2$_{no\ B}$>7.5, 7.2)
S/G (cold leg)	•initial metal inventory •final radionuclide inventory	~0.09 mg/cm^2 Fe ~ 0.5 nCi/cm^2 Co60 for PH1, PBR ~ 1 nCi/cm^2 Co60 for all other runs
CONSTRUCTION MATERIALS	•elemental composition by NAA	~0.7 ppm Co in PCCL Zir-4 ~400 ppm Co in PCCL Inconel 600 ~800 ppm Co in PCCL SS316
MAKEUP WATER	•elemental composition	non negligible transition metal input from the makeup water
SHUTDOWN	•radionuclide release under different conditions	important release from core surfaces when exposed to DI or borated aerated water
CODES (CRUDSIM, CORA, PACTOLE)	•Predictions for PCCL runs	qualitative agreement with experimental results for deposition vs pH. PACTOLE predicts activity deposition in SG hot leg/cold leg with very good accuracy

post-preconditioning surfaces would also be useful to help optimize the preconditioning conditions in plants.

Since discrepancies have been observed in the results from the aqua regia treatment, better methods to decontaminate the in-core Zircaloy section should be developed. More particularly, ultrasonic descaling should be tried.

Evaluation of shut-down condition effects on radionuclide release could be improved using a small loop in order to better simulate PWR conditions.

Finally, the computer codes, and more particularly PACTOLE, should be used more intensively in the data analysis process.

REFERENCES

(A-1) Al-Jobori, S.M. "Determination of Impurities in Zircaloy Clad By Means of Neutron Activation Analysis". Journal of Radioanalytical and Nuclear Chemistry, January 1988, Vol. 120, p. 145.

(A-2) S. Anthoni, P. Ridoux, and C. Chevalier, "Evaluation of Corrosion Products in a Pressurized Water Reactor During Shutdown," Water Chemistry of Nuclear Reactor Systems 5, Vol. 2, BNES, London, 1989.

(B-1) P. Borys et al, "Parametric Studies of the MIT PWR Coolant Chemistry Loop Using the PACTOLE Code, MITNRL-034, September 29, 1989.

(B-2) P. Beslu, et al, "A Computer Code PACTOLE to Predict Activation of Corrosion Products in PWRs", Proceedings of International Conference on Water Chem. of Nucl. React. Syst., Bournemouth, BNES, London, 1978.

(B-3) P. Beslu, "Mechanisms and Driving Forces in Corrosion Product Transport and Build-up: PACTOLE Code", IAEA Specialist Meeting, San Miniato, Italy, October, 1981.

(B-4) P. Beslu and A. Lalet, "Computer Prediction in Radiation Exposure Reduction", JAIF Int. Conf. on Water Chem. in Nucl. Power Plants, Tokyo, Japan, 1988.

(B-5) C. A. Bergmann and W. T. Lindsay, et al., "The Role of Coolant Chemistry in PWR Radiation Field Buildup", EPRI NP-4247, 1985

(B-6) P. Beslu, G. Frejaville, "Modèles Décrivant la Formation et le Transport des Produits de Corrosion Dans les Réacteurs à Eau Sous Pression", IAEA-SM-264/34, International Atomic Energy Agency, Vienna, 1983.

(C-1) E. D. Cabello, "Decontamination Studies of Simulated PWR Primary Coolant System Components," M. S. Thesis, Dept of Nucl. Eng., MIT, 1990.

(C-2) Cole Parmer Catalogue 1989-1990

(D-1) M. J. Driscoll, et al., "In-Pile Loop Studies of the Effect of PWR Coolant pH on Corrosion Product Radionuclide Deposition", EPRI Report, Dec 1990 (estimate).

(F-1) M. Fukuda, fax from MHI to Y. Hemmi, MHI/MIT, May,31,1990.

(H-1) F. W. Hartley, "Coolant Activity Experiences at Connecticut Yankee," ANS Conference on Power Reactor Systems and

Components, Supplement to Vol. 13, Trans. Am. Nucl. Soc., September 1970.

(H-2) Y. Hemmi, "The MHI Radiation Exposure Reduction Program", proceedings of the REM Seminar, Oct.30, 1990, Pittsburgh.

(I-1) Y. Izumida et al., "Electrolytic Decontamination of Surface-contaminated metal Alternating Electrolysis Using Square-Wave Current In Neutral Salt Electrolyte," Nuclear Technology, Vol.70, August 1985.

(I-2) Instra-tech inc., Colorimeter, model T-600, manual, Theory, Operation, and Laboratory Experiments.

(K-1) S. Kang, J. Sejvar, "The Cora II Model of PWR Corrosion Product Transport", EPRI Report NP-4246, September 1985.

(L-1) N. R. Large, D. R. Woodwark, "Effect of Coolant Chemistry on PWR Radiation Transport Processes". EPRI Report NP-6657, December 1989, Vol.1, p.4-10

(L-2) S. Lindsay, High Performance Liquid Chromatography, Wiley, 1987.

(L-3) J. L. Linsley-Hood, "The Effect of Ultrasonic Agitation on Surface Decontamination Rates," UKAEA, R&DB(W)TN-113, 1958.

(L-4) C. B. Lee, "Modeling of Corrosion Product Transport In PWR Primary Coolant," PhD Thesis, Dept. of Nucl. Eng., MIT, 1989.

(M-1) E. Metcalfe, Atomic Absorption and Emission Spectroscopy, Wiley, 1987.

(M-2) A. M. Morrillon, "Computer Modeling of Corrosion Product Radionuclide Transport in a Simulated PWR Environment", S.M. MIT Nuclear Engineering Departement. August 1987.

(O-1) J. Outwater, P. Borys, E. Cabello, M. Driscoll, I. Olmez, "Cobalt in Nuclear Service Zircaloy", Trans. Am. Nucl. Society, November 1990.

(P-1) Perkin-Elmer, Instructions-Model 306 Atomic Absorption Spectrophotometer, May 1971.

(P-2) M. Polley and M. Pick, "Iron, Nickel and Chromium Mass Balances in Westinghouse PWR Primary Circuits", Proceedings of International Conference on Water Chem. of Nucl. React. Syst., Bournemouth, 4 BNES, London, 1986.

(R-1) J. F. Remark, "Plant Decontamination Methods Review", EPRI Report, NP-1168, May 1981.

(S-1) G. R. Solares, "An Automated Computer Controlled Counting System for Radionuclide Analysis of Corrosion Products in LWR Coolant Systems," Nucl. Eng. Thesis, Dept of Nucl. Eng., MIT, 1988.

(S-2) R. G. Sanchez, "Construction and Operation of an In-Pile Loop for PWR Dose Reduction Experiments," PhD Thesis, Dept. of Nucl. Eng., MIT, 1990

(T-1) Tubesales, Manufacturer Material Certificate, Cranbury, NJ.

(W-1) C. J. Wood (EPRI), "Seminar on PWR Water Chemistry and Radiation Field Control", Proceedings, Berkeley, California, March 1986.

(W-2) H. Weitze et al.,"Dose Rate Build-Up Investigations and Modelling for Goesgen and Neckarwestheim," Water Chemistry of Nuclear Reactor Systems 4, Vol. 2, BNES, London (1986).

(Z-1) M. R. Zhang, "Measurement and Interpretation of Chemical and Radiochemical Data from PWR In-Pile Loop Runs," SM Thesis, MIT Nuclear Engineering Department, December 1990 (est.)

APPENDICES

Appendix A: Manufacturers Material and Chemical Specifications

The appendix consists of:

1- Manufacturer certificate for EPRI Inconel

2- Manufacturer certificate for EPRI Plenum Stainless Steel

3- Manufacturer certificate for EPRI Stainless Steel

4- Manufacturer certificate for NUPEC Titanium

5- Manufacturer certificate for NUPEC Stainless Steel

6- Manufacturer certificate for NUPEC Inconel

7- Manufacturer certificate for AE Pump Stainless Steel

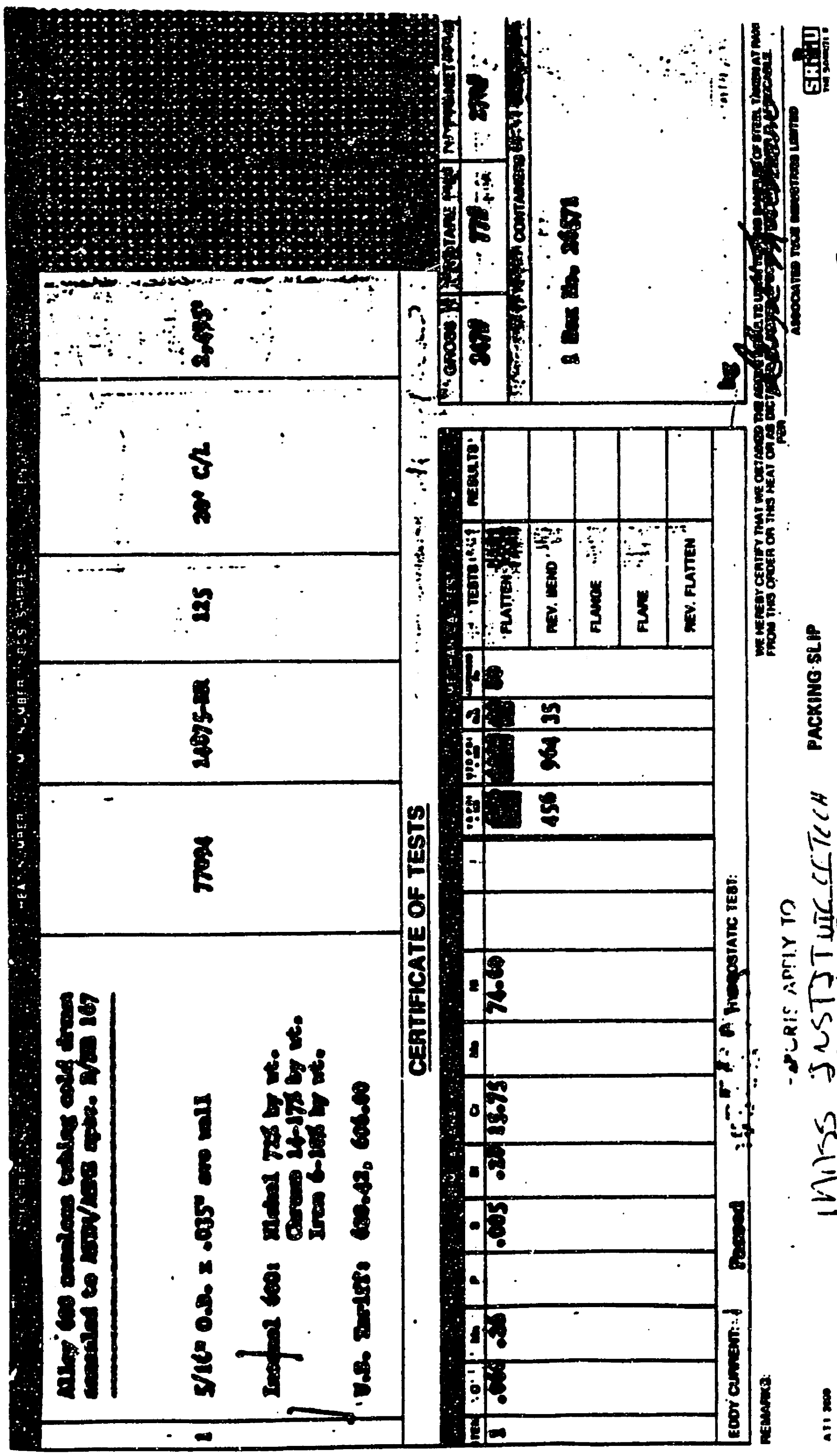

Alloy 600 seamless tubing cold drawn annealed to ASTM/ASME spec. B/SB 167

	Description	Heat Number	Number	Pcs Shipped	Length	
1	5/16" O.D. x .035" ave wall	77094	14875-RR	125	20' C/L	2,495'

Inconel 600: Nickel 72% by wt. Chrome 14-17% by wt. Iron 6-10% by wt.

U.S. Tariff: 610.42, 606.00

CERTIFICATE OF TESTS

Item	C	Mn	P	S	Si	Cr	Mo	Ni							Tests	Results
1	.066	.26		.005	.28	15.75		74.40			456	964	35	80	FLATTEN	
															REV. BEND	
															FLANGE	
															FLARE	
															REV. FLATTEN	

EDDY CURRENT: Passed HYDROSTATIC TEST:

REMARKS:

Gross	Tare	Net
3470	770	2700

1 Box No. 26571

WE HEREBY CERTIFY THAT WE OBTAINED THE ABOVE RESULTS ... FROM THIS ORDER OR THIS HEAT ...

ASSOCIATED TUBE INDUSTRIES LIMITED

REPORTS APPLY TO

MASS INSTITUTE OF TECH

CGC 911184

791616

240'0" 12/28/87

PACKING SLIP

A T I 3000

Fig A.1 Manufacturer certificate for EPRI Inconel

TUBULAR PRODUCTS IN CARBON STEEL, ALLOY STEEL, STAINLESS STEEL, ALUMINUM, NICKEL AND HASTELLOY

TUBESALES.

MATERIAL CERTIFICATE
PROSPECT PLAINS ROAD
CRANBURY, NJ
08512

MASS INSTITUTE OF TECH
P O BOX 69
CAMBRIDGE MA
02139

CUSTOMER ORDER NO. 99 R 806571 SHIPPER NO. 4740756 DATE 10/28/97

ITEM NO. 1 QUANTITY 21'0"

SPECIFICATION ASTM A511-85 GRADE SMLS 316

SIZE 1-3/4 OD X .375 WALL MANUFACTURER SANDVIK

HEAT NUMBER 476139 LOT NUMBER

MELTER GRAIN SIZE

CHEMICAL ANALYSIS

C	MN	P	S	SI	NI	CR	MO	CU
.012	1.680	.021	.021	.540	11.560	16.330	2.050	.160

MECHANICAL PROPERTIES

ULTIMATE STRENGTH P.S.I.	YIELD POINT P.S.I.	% ELONGATION	ROCKWELL HARDNESS	BRINELL	HARDENABILITY	FREQ.	SEVERITY

THE FOLLOWING TESTS HAVE BEEN PERFORMED SATISFACTORILY:

7-30457

I CERTIFY THE ABOVE TEST INFORMATION TO BE CORRECTLY REPORTED FROM ACTUAL MILL TEST REPORTS AS CONTAINED IN THE RECORDS OF TUBESALES.

TUBESALES.

BY AUTHORIZED TEST DEPARTMENT CLERK

Fig A.2 Manufacturer certificate for EPRI Plenum Stainless Steel

No. FU-19-87/5

MILL CERTIFICATE

TSK

TOKYO SEIMITSUKAN CO.,LTD.
HEAD OFFICE & FACTORY
No. 1298 JINBO YOSHIIMACHI TANO-GUN GUNMA-PREF.
PHONE: 0273—87—3131

Messrs. TUBE SALES.

Article. Seamless Stainless Steel Tubes, Cold Drawn, Annealed & Pickled.

Spec. ASTM A269/A213 ASME SA213 AVE.WALL TP304 Date. July 21.1987.

Order No. CHI7-11162

Item No.	Size	Quantity: Number of Pieces	Quantity: Total Length ft Meter	Quantity: Total Weight Kg	Heat No.	Chemical Composition (%): C MAX. 0.08	Si MAX. 0.75	Mn MAX. 2.00	P MAX. 0.040	S MAX. 0.030	Ni 8.00 11.0	Cr 18.0 20.0
	5/16" X 0.035" X 20'	78	1,560	75	802466	0.05	0.42	1.10	0.034	0.010	9.16	18.24

Item No.	Hydrostatic Test 1,000 PSI	Surface & Dimensions	Tension Test: Yield Strength MIN. 30,000 PSI	Tension Test: Tensile Strength MIN. 75,000 PSI	Tension Test: Elongation MIN. 35 %	Flattening Test	Flaring Test	Hardness Test MAX. HRB 90	Eddy Current Inspection	Remarks
	Good.	Good.	34,270	82,620	58	Good.	Good.	77		

TUBE SALES
THESE TEST REPORTS APPLY TO
P.O. NO. 992-70942 6
T/S NO. 4150026
FOOTAGE [illegible] DATE [illegible]
HEAT NO. 1 MARK NO. 1

IT IS HEREWITH CERTIFIED THAT THE ABOVE MATERIALS ARE SATISFACTORY IN COMPLIANCE WITH THE REQUIREMENTS SPECIFIED IN THE CONTRACT.

TOKYO SEIMITSUKAN CO., LTD.

Chief of Inspection Section

Fig A.3 Manufacturer certificate for EPRI Stainless Steel

TICO TITANIUM, INC.
24581 Crestview Court • Farmington Hills. Michigan 48331
(800) 521-4392 • (313) 478-4700 • FAX (313) 478-0223

TO: MAIND
M. I. T.
P.O. BOX 69
CAMBRIDGE, MA 02139

DATE: 7/05/90

CUSTOMER PO: GGR-125280 CERTIFICATION OF TESTS

S.O. No: 011863

HEAT NO. 6LE
SPECIFICATION: ASTM B-338-83 GRADE 2

DESCRIPTION: SMLS TUBE 1/8 OD X .032 WALL X 100'0" - 100FT

CHEMISTRY

IRON	.035	
OXYGEN	.09	
NITROGEN	.005	
CARBON	.015	
HYDROGEN	.0006	FINAL PRODUCT
RESIDUAL ELEMENTS (EACH)	LESS THAN .10	
RESIDUAL ELEMENTS (TOTAL)	LESS THAN .40	
TITANIUM REMAINDER		

TENSILE DATA	TEST 1	TEST 2	TEST 3	TEST 4
TENSILE PSI	73900	69500		
YIELD 0.2 OFFSET	53300	46300		
EL %	27.0	34.0		
FLATTENING TEST	C			
HYDROSTATIC TEST	C			
FLARING TEST	P			
EDDY CURRENT TEST	P			

MATERIAL FREE OF MERCURY CONTAMINATION.

BONNIE BREY\CERTIFICATION CLERK

Signature: Bonnie Brey

Fig A.4 Manufacturer certificate for NUPEC Titanium

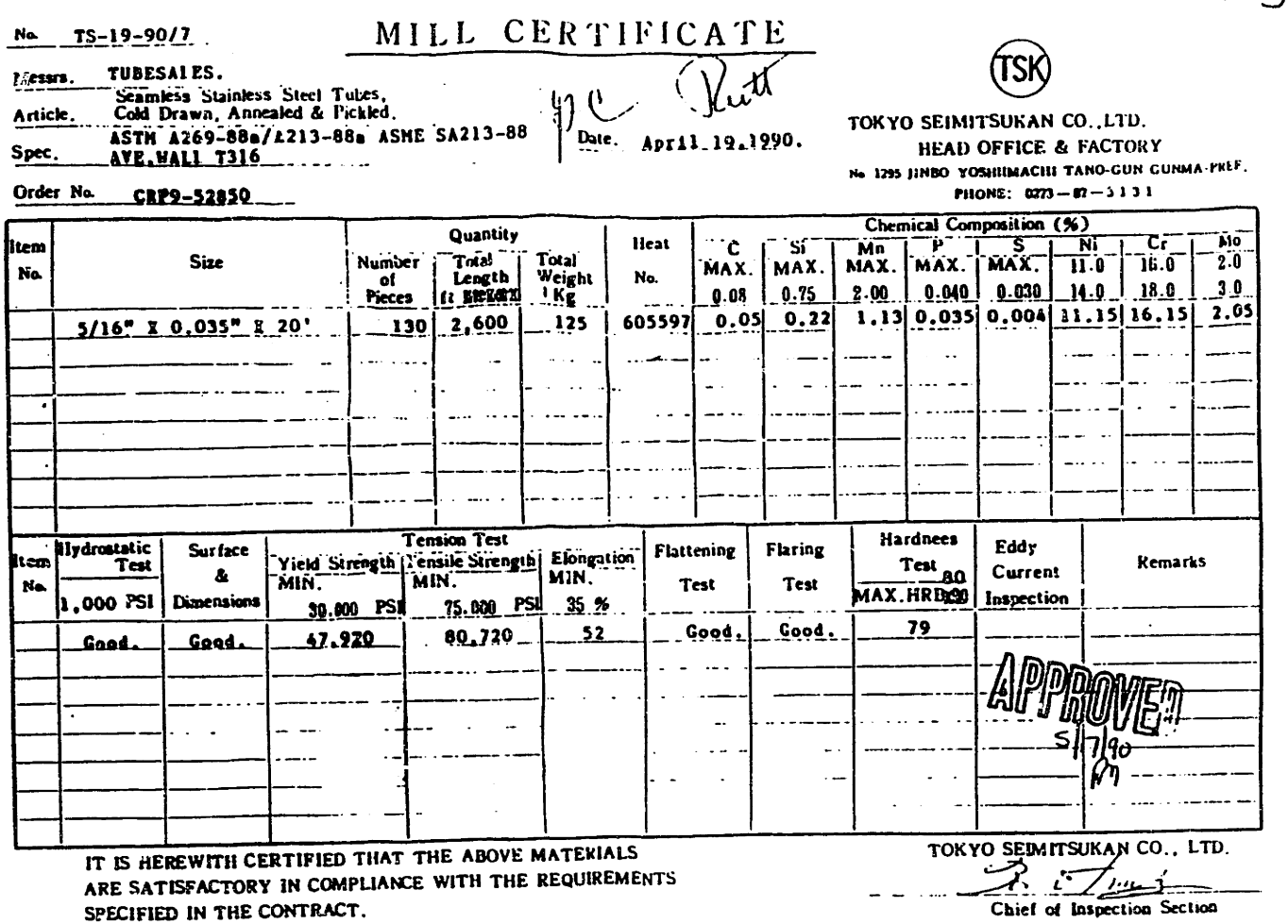

No. TS-19-90/7

MILL CERTIFICATE

Messrs. TUBESALES.

Article. Seamless Stainless Steel Tubes, Cold Drawn, Annealed & Pickled.

Spec. ASTM A269-88a/A213-88a ASME SA213-88 GR.TP316

Order No. CRP9-52850

Date. April 19,1990.

TSK

TOKYO SEIMITSUKAN CO.,LTD.
HEAD OFFICE & FACTORY
No 1295 JINBO YOSHIIMACHI TANO-GUN GUNMA-PREF.
PHONE: 0273-87-3131

Item No.	Size	Quantity: Number of Pieces	Quantity: Total Length ft	Quantity: Total Weight Kg	Heat No.	Chemical Composition (%): C	Si	Mn	P	S	Ni	Cr	Mo
						MAX.	MAX.	MAX.	MAX.	MAX.	11.0	16.0	2.0
						0.08	0.75	2.00	0.040	0.030	14.0	18.0	3.0
	5/16" X 0.035" X 20'	130	2,600	125	605597	0.05	0.22	1.13	0.035	0.004	11.15	16.15	2.05

Item No.	Hydrostatic Test 1,000 PSI	Surface & Dimensions	Tension Test: Yield Strength MIN. 30,000 PSI	Tension Test: Tensile Strength MIN. 75,000 PSI	Tension Test: Elongation MIN. 35 %	Flattening Test	Flaring Test	Hardness Test MAX. HRB 80	Eddy Current Inspection	Remarks
	Good.	Good.	47,920	80,720	52	Good.	Good.	79		

APPROVED
5/7/90

IT IS HEREWITH CERTIFIED THAT THE ABOVE MATERIALS ARE SATISFACTORY IN COMPLIANCE WITH THE REQUIREMENTS SPECIFIED IN THE CONTRACT.

TOKYO SEIMITSUKAN CO., LTD.

Chief of Inspection Section

Fig A.5 Manufacturer certificate for NUPEC Stainless Steel

SUPERIOR TUBE COMPANY

Wapakoneta, Ohio 45895

Customer TUBESALES, CRANBURY,N.J.
Customer Order No. CMJ 0-80518-SD
Ship To: MASS. INST. OF TECHNOLOGY
144 ALBANY, BLDG NW13
CAMBRIDGE, MASS 02139

Date 8-31-90
Superior Order No. D-5259
Check Sheet No. W-131388 291 ft.
Quantity

ORDER #GGR 122504 CH TS

This is to certify that the part, parts or product listed on this report were manufactured and inspected in conformance with applicable purchase orders, drawings, specifications and process requirements. Reports governing this material are on file, subject to examination, and indicate conformance to the specification unless otherwise noted under remarks and/or attachments.

NOTE: "FABRICATION OF THIS PRODUCT RESULTING IN FUMES, DUST OR SOLUTIONS MAY BE INJURIOUS TO YOUR HEALTH"

Certificate of Test [X] Certificate of Compliance [ ] Certificate of Chemical Analysis [ ]

Description of Material Shipped	Applicable Specifications
SMLS ALLOY 600 .3125" OD X .035" WALL	

Chemical Analysis:

Heat No.	C	Mn	P	S	Si	Ni	Cr	Mo	Cb+Ta	Ti	Cu	Fe
NX7160 INCO	.04	.23		.001	.21	77.05	15.17				.20	7.10

Mechanical Properties:

3 Tests were Performed at Room Temperature

Yield (Psi)	Ultimate (Psi)	% Elong. 2 in.	Hardness
	105,000	38	
	104,100	39	
	104,800	39	

Micro-Inch Finish:

O. D.	I. D.

Additional Tests Made		Applicable Specifications
Embrittlement		
Micro		
Grain Size		
Flatten		
Flare		
Hydrostatic		
Bend		
Flange		
Reverse Flatten		
Pressure		
Reverse Bend		
Macro Etch		
Surface Condition		
Passivity		
White Cloth		
Dye Penetrant		
Ultrasonic 100%		
Eddy Current 100%		

Dimensions:

O. D.	I. D.	Wall	Length

Remarks:

LAB SUPERVISOR - R.L. CLARK

AUTHORIZED SIGNATURE
QUALITY ASSURANCE DEPT.

Fig A.6 Manufacturer certificate for NUPEC Inconel

Crucible Specialty Metals
A Division of Crucible Materials Corporation
PO Box 977
Syracuse New York
13201-0977

CERTIFICATE OF TEST

SOLD TO	SHIP TO	OUR ORDER NO
Autoclave Engineers Inc., 2930 West 22nd., Street Erie, Pennsylvania 16512	Autoclave Engineers Inc., 2930 West 22nd., Street Erie, Pennsylvania 16512	32-05584 DATE 5/1/87

CUSTOMER ORDER # & DATE	CUSTOMER REQ. #	DISTRICT	SHIPPED FROM
70-7407		Cleveland	Cleveland, Ohio

DESCRIPTION OF MATERIAL

ru 316 RTA Autoclave SA-182 (3)
A/E Code #MS17-015

ITEM NO.	SIZE	QUANTITY	HEAT NO.	PHYSICAL PROPERTIES YIELD PSI	TENSILE PSI	% ELONG IN.	% RED AREA	HARD-NESS	IMPACT
	9" Rd.	2979#	A17735	44,000	81,800	58.0%	74.5%	BHN 143	

Material is Free From Mercury Radiation and Alfa Radiation at Time of Shipment."

HEAT NO.	CHEMICAL PROPERTIES C	MN	P	S	SI	NI	CR	V	W	MO	CU	CO	AL
													N
.17735	.039	1.75	.024	.026	.54	10.28	16.44			2.11			.074

AUTOCLAVE ENGINEERS
U.S. APPROVED
BY
DATE 5-6-87

D 10-1401

SWORN TO AND SUBSCRIBED BEFORE ME THIS
_____ DAY OF _____, 19
NOTARY PUBLIC

THE TEST RESULTS SHOWN IN THIS REPORT ARE CORRECT TO THE BEST OF OUR KNOWLEDGE AND BELIEF
CERTIFIED COLT INDUSTRIES CRUCIBLE INC
BY REPRESENTATIVE

Fig A.7 Manufacturer certificate for AE Pump Stainless Steel

Appendix B: Hydrogen Peroxide Addition During Shutdown

1. Introduction

The purpose of this note is to update progress and plans on our investigations of this subject. Prior results are reported in Refs. (1) and (2).

A bibliography of the literature on this subject compiled to date is appended.

The sections which follow address a number of issues raised by evaluation of the literature, before reviewing the status of our studies. The following topics are covered:

- background perspective
- comments on PWR practice, with Japanese procedures as a specific example
- concurrent LiOH dosage
- peroxide decomposition
- computer model predictions
- MIT benchtop studies

---

(1) Quarterly Progress Report for January–March 1990 Coolant Technology Research in Support of LWR Operations, MIT Electric Utility Program, April 16, 1990.

(2) E. D. Cabello, "Decontamination Studies of Simulated PWR Primary Coolant System Components," SM Thesis, MIT Nuclear Engineering Department, May 1990.

2. Parameters Defining the Problem

Activity inventories vary significantly from plant to plant, but a mature PWR can be expected to contain the following quantities of Co-58, the nuclide of principal concern in a shutdown transient:

On Surfaces:

	$\mu Ci/cm^2$	cm^2	Total Ci
Core	25	6×10^7	1500
S/G	8	2×10^8	1600

In Coolant:

	$\mu Ci/cc$	Total Ci
Normal	4×10^{-4}	0.12
Shutdown Peak	0.4	120

Thus either the core or the steam generators contain enough Co-58 to account for the large observed increase in the coolant inventory: solubilization of as little as 10% of their crud will suffice. Early speculation implicated the steam generators (H-1), but more recent evidence indicates that most of the activity release originates in the core. This includes crud specific activity measurements (Ci Co-58 / g Ni), and is supported by incidents of large activity releases in spent fuel pools (W-1).

It should be noted that the total peak waterborne Co-58 inventory cited above is much less than the total inventory removed from the coolant by purification over the entire course of the shutdown, which amounts to several hundred curies, and frequently in the kilocurie range.

3. PWR Practice

The general consensus worldwide is that intervention to solubilize transportable Co-58 (and other nuclides), which can then be removed by coolant purification, is called for. The major point of difference is whether hydrogen peroxide is added in the latter stages of cooldown, or whether aerated water (e.g., O_2) is added when the main coolant loops are no longer in use and solid.

One advantage of early H_2O_2 addition is that the final 5 cc/kg or so of dissolved H_2 can be scavenged: the 0.45 ppm H_2 reacts with 7.6 ppm H_2O_2 on a stoichiometric basis - hence the rule of thumb that adding 10 ppm H_2O_2 will scavenge H_2 and leave a 2 ppm H_2O_2 residual (E-1). On the other hand, several references warn against the premature establishment of oxygenating conditions; waiting until cooldown reaches ~ 90°C (194°F) is recommended in Ref. (A-1).

While it might appear that H_2O_2 addition during cooldown has the potential for speeding up the shutdown schedule, the operators of the Farley unit indicate that waiting until partial draindown to add H_2O_2 is a time saver (M-1).

Finally, as already noted, aeration creates H_2O_2 in situ. Hence the French and Japanese do not separately add H_2O_2. Figures 1 and 2 illustrate the Japanese (Mitsubishi) procedure.

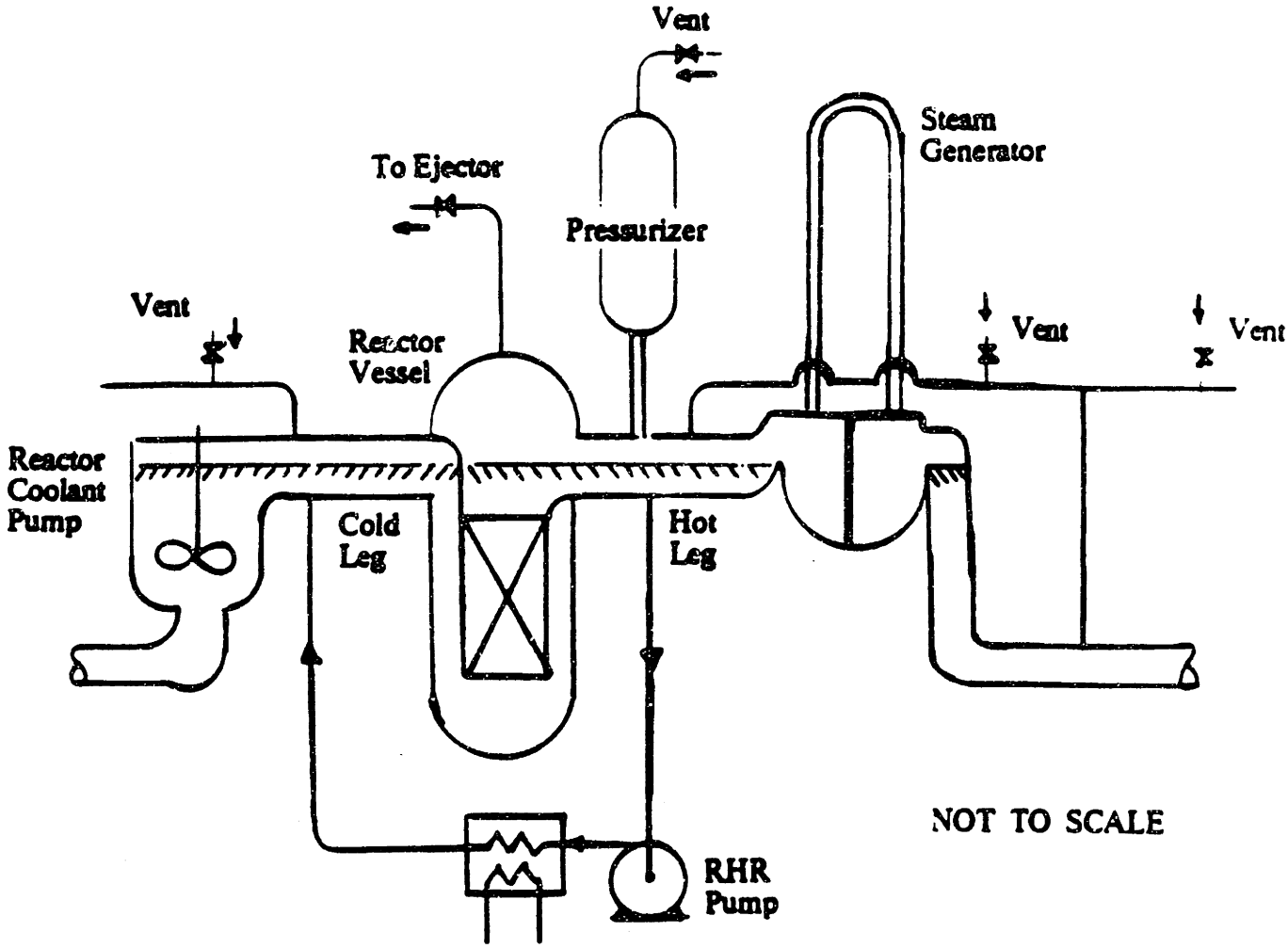

Fig B.1 Plant Status During Aeration of Primary Coolant

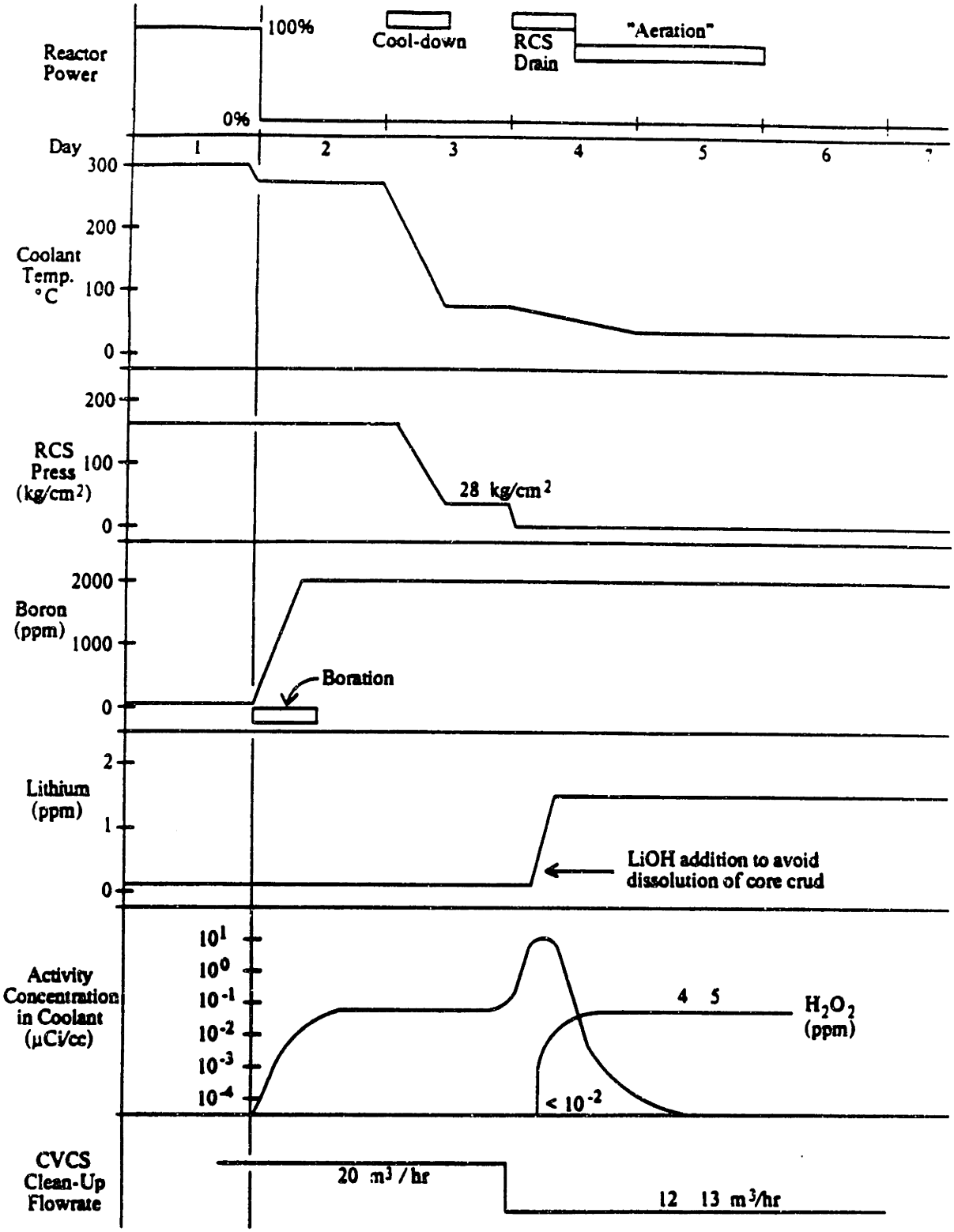

Fig B.2 Plant Cool-Down Sequence for MHI Plants

4. Other Approaches

There is one discussion in the literature of post-shutdown pH adjustment through addition of LiOH to inhibit crud dissolution (B-1). The principle is straightforward: if one considers the solubility product of the hydroxides of transition metal ions, a one unit increase in pH will decrease divalent ion solubility by a factor of 100, and that of trivalent ions by a factor of 1000. Thus an increase of 1-2 pH units can compensate for, and hence counteract, the increase in solubility due to cooldown. There are some potential problems with this approach, the most worrisome being that crud dissolution might merely be postponed until the fuel is in the spent fuel pool, unless it is also chemically treated. However, an appropriate chemical treatment may be difficult to devise: an alkaline pool open to the air will absorb CO_2 (which lowers pH), O_2 (which forms H_2O_2 in the presence of gamma irradiation), and N_2 (which with O_2, in the presence of gamma irradiation, forms nitric acid).

Another problem is that high lithium concentrations are currently thought to be detrimental to both Zircaloy and Inconel at operational temperatures (~ 300°C), and there might be concern that local oxide film concentrations of lithium could remain high, even after readjustment of bulk chemistry conditions during plant post-refueling startup.

Nevertheless, the Japanese add LiOH at the outset of aeration (see Fig. 2) to avoid dissolution of core crud, with no apparent detrimental effects.

5. Peroxide Behavior

A curve fit to measurements at GE and MIT gives the following approximate prescription for the chemical (thermal decomposition) half-life of H_2O_2 in pure high temperature water:

$$T_{1/2} = e^{\left[\frac{6274}{T°K} - 13.8\right]} \text{ min.}$$

Hence,

at 298°K = 25°C = 77°F, $T_{1/2}$ ≈ 24 hrs.,

at 351°K = 78°C = 172°F, $T_{1/2}$ ≈ 1 hr,

at 454°K = 181°C = 359°F, $T_{1/2}$ ≈ 1 min.

These values can be reduced by an order of magnitude or more by contact with metal surfaces above ~140°C, or by transition metal ions in solution.

In addition, of course, H_2O_2 is consumed by oxidation-reduction reactions.

In acid media: $H_2O_2 + 2H^+ + 2e^- \rightarrow 2H_2O$

In basic media: $H_2O_2 + 2e^- \rightarrow 2OH^-$

Hence, to change Fe (or other transition metals) by one valence state, roughly 0.5 kg of H_2O_2 will be consumed per kg of metal ions reacted; 0.5 kg H_2O_2 corresponds to 2 ppm H_2O_2 in 250,000 kg of coolant, while 1 kg of metal represents about 10% of the crud deposited on a representative LWR core.

6. Parametric Computer Studies

J. Chun's computer program, RADICAL 1.0, has been used to study peroxide formation following oxygen (air) addition to the PWR system described in Table 1. In the reference case, pure H_2O containing 8.6 ppm O_2 yielded 3.68 ppm at equilibrium, as reported in Ref. (1).

Parametric variations and sensitivity studies have now been carried out, with the results summarized in Table 2. As can be seen, the equilibrium concentration of H_2O_2 is sensitive to O_2 concentration, and insensitive to temperature (in the range 40°C - 130°C), gamma dose rate (in the range 10^6 - 10^7 R/hr), or flow velocity (varied by factor of 4).

It should be noted that these computations do not consider the following phenomena: surface-induced decomposition, boric acid (if any), or reactions involving N_2 (also introduced in air).

A much cruder calculation will yield results within a few percent of the computer model. Assume that the following reaction is gamma catalyzed:

$$O_2 + 2\,H_2O \underset{\gamma}{\rightleftharpoons} 2\,H_2O_2$$

Then 2.125 ppm of H_2O_2 should be created for every ppm of O_2 consumed. This prescription, when applied to RADICAL 1.0 output, gives peroxide levels only 3-6% lower. Of course, the computer model is still required to compute the equilibrium state: under the conditions studied here, only about one-fifth of the initial O_2 reacts to form H_2O_2. This suggests that final ppm H_2O_2 ≈ 0.4 initial ppm O_2.

RADICAL 1.0 computes composition as a function of time, hence also indicates the time to reach equilibrium: for the runs of Table 2, this ranged between 20 and 80 minutes (i.e., ~100 cycles = system volume: recirculation rate; but note that the precise correspondence between computational and flow cycles has not been confirmed).

Table B.1 Model of Shutdown PWR for Radiolysis Computations

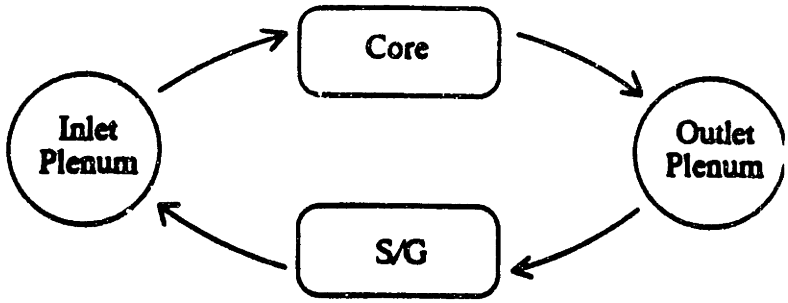

Plant Characteristics:

	Volume (m^3)	Hydraulic Dia. (cm)	Velocity (m/sec)
Inlet Plenum	133		
Core	23	1.2	5.1
Outlet Plenum	49		
S/G	79	2.1	5.2
Total	284		

Coolant Flow Rate: 24 m^3/sec

Water Properties:

Temperature: 90°C Density: 963 kg/m^3

Added H_2: zero

Air Saturated at 20°C { O_2 = 6 cc/kg = 8.6 ppm; N_2 = 12 cc/kg = 15 ppm

Dose Rate:

γ dose rate in core = 10^7 R/hr

n dose rate in core = 0

Table B.2 Parametric Studies of H_2O_2 Formation

	Case	Equilibrium ppm H_2O_2
1.	Original Reference 10^7 R/hr 90°C 8.6 ppm O_2 24 m^3/s flow rate	3.68
2,	Revised reference 10^6 R/hr 40°C 4.3 ppm O_2 6 m^3/s	1.76
3.	Same as 2 but 130°C	1.76
4.	Same as 2 but 10^7 R/hr	1.886
5.	Same as 2 but 8.6 ppm O_2	3.81

7. MIT Benchtop Studies

As reported in Ref (2), cited earlier, we have tested the effect of H_2O_2 and H_3BO_3 on Inconel tubing cut from the simulated steam generator tubing from one of our EPRI/ESEERCO PCCL runs. Room temperature and 90° C exposures were evaluated. Essentially none of the deposited radionuclides (Co-58, Co-60, Fe-59, Mn-54, Cr-51) were removed. This is consistent with the contention that the core (Zircaloy) region is the source of large Co-58 releases in PWR units. The tubing in question had experienced loop cooldown (at constant LiOH and H_3BO_3 concentration and without aeration prior to draining), with subsequent exposure to the atmosphere (in the absence of significant ambient radiation) prior to and during the subject tests. During cooldown we see the first phase of enhanced radionuclide release to loop coolant associated with the increased solubility of transition metals.

The next step in the investigation is to perform similar tests on in-core Zircaloy segments. If we can simulate plant Co-58 releases, then PCCL in-core tubing can be used in the final phase of this work to evaluate ex-core re-deposition behavior of such crud releases.

Measurements of H_2O_2 and NO_3^- are also being made in the MITR-II spent fuel pool, which simulates conditions of interest: aerated water exposed to high gamma fluxes. The nitrate values are of interest because air addition (as opposed to O_2 or H_2O_2 addition) raises the possibility of nitric acid synthesis from the dissolved N_2 -which might in turn lead to significantly different radionuclide release characteristics. At present, J. Chun's code does not handle N_2 reactions (which are to be added), hence experimental evidence is of particular interest.

Bibliography on PWR Shutdown Chemistry

(A-1) S. Anthoni, P. Ridoux, and C. Chevalier, "Evaluation of Corrosion Products in a Pressurized Water Reactor During Shutdown," Water Chemistry of Nuclear Reactor Systems 5, Vol. 2, BNES, London, 1989. *(Also see discussion of paper on p. 44, 45.)*

(B-1) J. P. Berthet, "Overview of Cold Shutdown Procedure in EDF Nuclear Power Plants," EPRI Seminar on PWR Water Chemistry and Radiation Field Control, March 1986.

(B-2) E. J. Bird et al., "Cobalt Measurements on the DOEL Reactors," Water Chemistry of Nuclear Reactor Systems 4, Vol. 1, BNES, London, 1986.

(D-1) P. DeRegge, K. Dinov, K. DeRanter, "Radioactivity and Corrosion Product Concentration During the Normal Operation and Revision Shut-Down of a 900 MWe PWR-DOEL 3," Proceedings JAIF International Conference on Water Chemistry in Nuclear Power Plants, Tokyo, April 1988.

(E-1) EPRI NP-859, "Shutdown Operational Techniques for Radiation Control in PWR Plants," May 1981.

(E-2) EPRI NP-3245, "The Effects of Cold Shutdown Chemistry on PWR Radiation Control," September 1983.

(E-3) EPRI NP-4762-SR, "PWR Primary Water Chemistry Guidelines, Appendix: PWR Shutdown Chemistry," September 1986.

(F-1) K. Fink, J. W. Kormuth, and J. Roesmer, "Peroxide Reactions in Cold Shutdown Chemistry," EPRI Seminar on PWR Water Chemistry and Radiation Field Control, March 1986.

(H-1) F. W. Hartley, "Coolant Activity Experiences at Connecticut Yankee," ANS Conference on Power Reactor Systems and Components, Supplement to Vol 13, Trans. Am. Nucl. Soc., September 1970.

(H-2) F. W. Hartley, "Coolant Activity at Connecticut Yankee, Cores I and II," ANS Conference on Reactor Operating Experience, Supplement No. 2 to Vol. 14, Trans. Am. Nucl. Soc., August 1971.

(K-1) J. W. Kormuth, "The Control of Co-58 Dissolution During Refueling Shutdowns of Pressurized Water Reactors Using a Hydrogen Peroxide Addition," Nucl. Technol., 37, 99, February 1978.

(K-2) J. W. Kormuth, "The Control of ^{58}Co Dissolution During Refueling Shutdowns of PWRs Using Hydrogen Peroxide Addition," Trans. Am. Nucl. Soc., Vol. 26, pp. 426, June 1977.

(M-1) D. N. Morey, T. H. Esteve, J. A. Rumancik, "Innovative Technology to Reduce Outage Time," Trans. Am. Nucl. Soc., Supplement No. 1 to Vol. 54, 1987.

(R-1) J. Rozenberg et al., "Activated Corrosion Products Released By Thermal Shocks in Reactor Primary Circuits," Water Chemistry of Nuclear Reactor Systems, BNES, London (1978).

(S-1) W. R. Stagg, "Pressurized Water Reactor Radiation Control: A Summary," EPRI Seminar on PWR Water Chemistry and Radiation Field Control, March 1986.

(V-1) R. Vanbrabant and P. de Regge, "Characterization of the Corrosion Products in Primary Reactor Water of PWR During Normal Operation and Transient Phases," Water Chemistry of Nuclear Reactor Systems 2, BNES, London (1981).

(W-1) H. Weitze et al., "Dose Rate Build-Up Investigations and Modelling for Goesgen and Neckarwestheim," Water Chemistry of Nuclear Reactor Systems 4, Vol. 2, BNES, London (1986).

Appendix C: Code Instructions and Typical PCCL Input Data

The purpose of this appendix is to give to future researchers, interested in running the CRUDSIM, CORA or PACTOLE codes, enough basic information to do so.

For each code, the configuration of input data, description of input variables and an input data file for a sample problem are given. The sample problem corresponds to a one year PCCL run at 100% power and 800 ppm Boron, 1.84 ppm Lithium ($pH_{300°C}$=7.0)

The following references are useful:

CRUDSIM:

(1)-C. B. Lee, "Modeling of Corrosion Product Transport In PWR Primary Coolant," PhD Thesis, Dept. of Nucl. Eng., MIT, 1989.

(2)-C. A. Bergmann and W. T. Lindsay, et al., "The Role of Coolant Chemistry in PWR Radiation Field Buildup", EPRI NP-4247, 1985

CORA:

(3)-S. Kang, J. Sejvar, "The Cora II Model of PWR Corrosion Product Transport", EPRI Report NP-4246, September 1985.

(4)-"Cora II Code Description and User Manual", Westinghouse.

PACTOLE:

(5)-P. Beslu, et al, "A Computer Code PACTOLE to Predict Activation of Corrosion Products in PWRs", Proceedings of International Conference on Water Chem. of Nucl. React. Syst., Bournemouth, BNES, London, 1978.

(6)-P. Beslu, "Mechanisms and Driving Forces in Corrosion Product Transport and Build-up: PACTOLE Code", IAEA Specialist Meeting, San Miniato, Italy, October, 1981.

(7)-P. Beslu and A. Lalet, "Computer Prediction in Radiation Exposure Reduction", JAIF Int. Conf. on Water Chem. in Nucl. Power Plants, Tokyo, Japan, 1988.

(8)-P. Borys et al, "Parametric Studies of the MIT PWR Coolant Chemistry Loop Using the PACTOLE Code, MITNRL-034, September 29, 1989.

(9)-P. Beslu, F. Joyer, "Transfer of the Pactole Code: Accompanying Memorandum", Note Technique SCOS/LCC/89-047, March 1989.

Table C.1 Description of PACTOLE Input Variables (ref (9))

No.	Variable	Description
1	TITLE	
2	ILECT	=1...read data of a previous cycle =0...cycle 1, start-up initialization
3	IPERF	=1...end cycle data output =0...no data output
4	INDIC	=0 and IPERF=1...deposit and oxide activity at the end of a real cycle used as data for the following cycle are not corrected for decay time between these 2 cycles =1 and IPERF=1...correction for decay time performed INDIC is not used if IPERF=0
5	NELEM	number of chemical elements processed (maximum 5) Fe-Ni-Co-Cr-Mn-
6	NREAC	number of reactions processed (maximum 8) -Fe59-Mn54-Co58-Ni59-Ni63-Co60-Cr51-Mn56-
7	IFEM	=1...activity calculation on the "FILT" area (=filter, see REPART) =0...no calculation
8	KD	declogging of the "FILT" area every KD days
9	EFD	declogging efficiency of "FILT" (0<EFD<1)
10	COEF	coefficient of particle trapping on "FILT"
11	IOPT	=1..calculation of operating pH at TOPT and comparison with optimum pH (DpH=operating pH - optimum pH)
12	PHOPT	optimum pH at TOPT
13	TOPT	optimum temperature for the calculation DpH=operating pH - optimum pH (if IOPT=1) (°C)
14	NPROL	=1 if the cycle is prolonged (with modification of TMY - cf. TMYPRO) =0 no prolongation of cycle
15	TMOY	mean temperature of the fluid at nominal power (°C)
16	TMY	mean temperature of the fluid at zero power (°C)
17	VOLU	total primary circuit volume excluding pressurizer and auxiliaries (m^3)
18	DB	nominal mass flow rate of the primary circuit ($kg.s^{-1}$)
19	DELTA	maximum time step (s)
20	DELMX	minimum time step (s)
21	TPI	minimum wall temperature (°C)
22	TPB	maximum wall temperature (°C)
23	TMYPRO	if NPROL=1, enter TYMPRO=mean fluid temperature at zero power during prolongation (°C) if NPROL=0, enter no value and go to ELEM
24	ELEM	write chemical elements to be processed from among: Fe, Ni, Co, Cr, Mn (maximum 5, one element per PCB)
25	EROS	erosion rate of the elements (NELEM values, ELEM order) ($mg.s^{-1}$)
26	ROP	oxide density ($g.cm^{-3}$)
27	DA	diameter of the atom (m)

28	PC	probability of agglomeration
29	DG	geometric diameter = mean diameter by number for passage of 50% of the particles (m)
30	SI	standard deviation corresponding to DG
31	NB	number of particle size areas
32	PAS1	step of particle size areas (m)
33	TOBO10	B10 reaction rate (n, alpha)Li7 (s^{-1})
34	CAPLI	reaction rate of Li7 capture (s^{-1})
35	REAC	write reactions to be processed from among Fe59, Mn54, Co58, Ni59, Ni63, Co60, Cr51, Mn56 (maximum 8 - one reaction per PCB)
36	TOREAC	reaction rate (NREAC values, REAC order); represents the product n*sigma*phi and integrates the isotopic abundance (s^{-1})
37	EJEC	ejection rate (NREAC values, REAC order); represents the elastic shocks of the neutrons on the atoms (s^{-1})
38	CAPT	capture rate (NREAC values, REAC order); represents the disappearance of the final nuclide (s^{-1})
39	PARC	recoil range (NREAC values, REAC order) ($g.cm^{-2}$)
40	DO	frequency factor for calculating the diffusion coefficient $D=D_0*\exp(-QACT / RT)$ ($cm^2.s^{-1}$)
41	QUACT	activation energy (see D_0) ($cal.mole^{-1}$)

CIRCUIT MODELIZATION

1-general

42	NREG	total number of circuit areas (maximum 58)
43	NRCP	number of the last area of the main circuit
44	NRCA	number of the last area of the main circuit + bypass circuits except those in which the temperature is not between TPI and TPB (normally the CVCS)
45	NCAT	total number of bypass circuits (maximum 10)
46	NCD	number of sites for which a dose rate calculation is required (maximum 9)
47	REPART	write areas (4 characters per area). If a REPART=FILT...area is modelized, then IFEM=1 and the area must be characterized by KD, COEF, EFD. If, in addition, this area is in a bypass circuit, enter FS=0.,only FP can be different from 0.

2-definition of bypass circuit

48	NR1	area number of the primary circuit from which the bypass circuit is to leave
49	NR2	area number of the primary circuit at which the bypass circuit is to arrive
50	NUCAT	number of the first area of the bypass circuit
51	NF	area number of the bypass circuit on which purification takes place
52	NX	number of areas of bypass circuit
53	FS	efficiency of resins for purification of the bypass circuit (0<FS<1)
54	FP	efficiency of filters for purification of the bypass circuit (0<FP<1)

repeat parameters NR1 to FP NCAT times
caution: the bypass circuits processed last are those in which the temperature is not between TPI and TPB (normally the CVCS). The numbers of these areas are higher than NRCA.

3-characteristics of each area

55	SMAT	wetted surface of the area (m^2)
56	COR	ratio of surface of open pores to the geometric surface
57	TERCO	characterizes the distribution of axial power TERCO=0 over out-of-core areas
58	RUGO	surface roughness of the area (m)
59	IDECH	=1...unload area =0...no unloading of area
60	FDEB	fraction of nominal main flow rate (DB) in the area 0<FDEB<1
61	COM	composition by weight of chemical elements constituting the material in the area (NELEM values, ELEM order)
62	VIT	speed of fluid at nominal power calculated at mean temperature of the fluid in the area ($m.s^{-1}$)
63	DIAM	equivalent hydraulic diameter of the area (m)
64	TE	mean temperature of the fluid in the area (°C)
65	TPA	temperature of walls at area outlet (°C)
66	REL	relaxation length of the area
67	GRAV	coefficient of gravity of the area (horizontal=1, vertial=0, =5e-5 for lower part of the core)

remarks: parameters SMAT to FDEB on a single PCB
parameters COM on a single PCB
parameters VIT to GRAV on a single PCB
and repeat this group of 3 PCBs NREG times

68	CPKi with i from 1 to 4	cefficients for calculating the concentration of dissolved H_2. The code calculates: H_2 concentration =(FAC/17.7)*(CPK1+CPK2*T+CPK3*T^2+CPK4*T^3) with FAC in $cm^3.kg^{-1}$ TPN (see FAC), 17.7:$cm^3.kg^{-1}$TPN at 1 bar and 25°C, operating temperature in °C
69	OALKW	write selected log(K_w) of water. 3 possibilities: 1) FT3...formulation by temperature; in this case, go to ALKWi 2)MESM...Mesmer's formula;in this case, go to DELTAGi,j 3)MARS...Marshall's formula; in this case, go to DELTAGi,j
70	ALKWi with i from 1 to 4	coefficient for calculating log (K_w) of water using a polynomial which is a function of the temperature, as follows: ALKW1+ALKW2*T+ALKW3*T^2+ALKW4*T^3
71	DELTAGi,j with 1<i<4 and 1<j<20	coefficients for calculating Gibb's free energy of reaction expressed in $cal.mol^{-1}$. DG(-T)j= DELTAG1+DELTAG2*T+DELTAG3*T^2+DELTAG4*T^3 with T in °C

remarks: Enter the coefficients of DELTAG1 to DELTAG4 for each reaction, processing one reaction per PCB (total 20 reactions) in the following order:

Fe_3O_4....Fe^{++},....$Fe(OH)^+$,....$HFeO_2^-$,....$Fe(OH)_2$

$NiFe_2O_4$....Ni^{++},....$Ni(OH)^+$,....$HNiO_2^-$

$CoFe_2O_4$....Co^{++},....$Co(OH)^+$,....$HCoO_2^-$

$MnFe_2O_4$....Mn^{++},....$Mn(OH)^+$,....$HMnO_2^-$

Cr_2O_4....$Cr(OH)^{++}$,....$Cr(OH)_2^+$,....CrO_2^-

Ni under a different form than ferrite....Ni++,....Ni(OH)+,....HNiO2-

NiFe2O4....Ni(OH)2

It is possible to enter 0 for reaction 17, 18 and 19; the other reactions must at least have a coefficient not equal to 0.

72	DISFLUi,j with 1<i<4 and 1<j<4	coefficients of dissociation constants of the j reactions: K=10.**(DISFLU1+DISFLU2*T+DISFLU3*T^2+DISFLU4*T^3) with T in °C

enter coefficients DISFLU1 to DISFLU4, processing one reaction per PCB in the following order:

1- LiOH....Li^+ + OH^-

2- $B(OH)_3$ + OH^- ....$B(OH)_4^-$

3- $2B(OH)_3$+ OH^- ....$B(OH)_7^-$

4- $3B(OH)_3$+ OH^- ....$B(OH)_{10}^-$

OPERATION

1-general

73	NFONC	number of calculation operations (maximum 200)
74	NCYCLE	number of calculation cycles (maximum 200)
75	DT	total duration of the calculation (days)
76	DTPROL	time during which the reactor is in cycle prolongation (DTPROL<DT, if NPROL =0....no prolongation, enter DTPROL =0.) (days)
77	PBO	step of boron concentration (ppm)
78	PLI	step of lithium concentration (ppm)
79	NARRET	number of intermediate pauses during an operating and modelization cycle. If NARRET =0 go to DEC2
80	NRELA	number of releasing areas
81	NUMREL	reference numbers of releasing areas

2-characteristics of the cycles

82	DEC2	duration of one "NCYCLE" cycle (sum of DEC2 =DTs) (days)
83	REC2	duration of pauses between 2 "NCYCLE" cycle (days)
84	BOR2	initial boron concentration of one "NCYCLE" cycle (ppm)
85	BR2	disappearance rate of boron during one "NCYCLE" cycle (days)
86	FREC	fraction of fuel unloaded at the end of each NCYCLE cycle if FREC =-1....intermediate cold shutdown....XRELA else, return to DEC2 at the end of the NCYCLE cycles (or one fuel cycle, 0<FREC<1)
87	XRELA	release fraction, multiplied by NRELA, for previously defined NUMRELs ($mg.cm^{-1}$)

remarks: parameters DEC2 to FREC on a single PCB, repeat this PCB NCYCLE times, interpolating XRELA PCB if necessary

3-characteristics of the operations

88	TFONC	duration of operation (cumulative from start-up....last value of TFONC =DT) (days)
89	CL1	minimum concentration of lithium during operation (ppm)
90	XLI	initial concentration of lithium during operation (ppm)
91	CL2	maximum concentration of lithium during operation (ppm)
92	FAC	dissolved hydrogen content during operation ($cm^3.kg^{-1}$ TNP)
93	FL	fraction of nominal power during operation
94	DFU	circuit leak rate during operation ($g.s^{-1}$)
95	NIMPR	number of intermediate entries during TFONC operation (if NIMPR =0, no TIMPR PCB....process TFONC+1 operation)
96	TIMPR	days for which intermediate printouts are required (included in TFONC-1 and TFONC times, NIMPR values)

remarks: parameters TFONC to NIMPR on a single PCB and repeat this PCB NFONC times

caution: if NIMPR is different from 0, interpolate the TIMPR PCB between TFONC and TFONC+1 operations

DOSE RATE

97	RDDD	name of area for which a dose rate calculation is required (maximum 9)
98	ICD	number of areas included in the dose of the RDDD area
99	IR	reference number of area included in the dose
100	COED	dose rate coefficient compatible with activities in $GBq.m^{-2}$ (NREAC values, REAC order)

remarks: COED parameters on a single PCB
and repeat the IR-COED group of PCBs ICD times
then repeat the RDDD-IR-COED groups of PCBs NCD times

INITIALIZATION OF THE CALCULATION

1-cycle 1 scenario:

101	ETA	composition by weight of chemical elements constituting the deposits at the end of precritical hot tests (NELEM values, ELEM order)
102	ESURF	initial mass release for each area on reactor start up (NREG values, REPART order) $(mg.cm^{-2})$

go to 117 (ADENT)

2- >1 cycles scenario:

103	TCAL	total operating time of previous cycle (s)
104	ESURF	thickness limit at end of previous cycle (NREG values, REPART order) (cm)
105	RPR	release at end of previous cycle (NREG values, REPART order) (mg)
106	MASDEP	mass of "surface +deep" deposits at end of previous cycle (NREG values, REPART order) and repeat NELEM times in ELEM order (mg)
107	MASINT	mass of "deep" deposits at end of previous cycle (NREG values, REPART order) and repeat NELEM times in ELEM order (mg)
108	MASINT	mass of oxides at end of previous cycle (NREG values, REPART order) and repeat NELEM times in ELEM order (mg)
109	ETA	composition by weight of crud at end of previous cycle (NELEM values, ELEM order)
110	MASS1	mass in suspension in the fluid at end of previous cycle (NELEM values, ELEM order) (mg)
111	MASS2	mass in solution in the fluid at end of previous cycle (NELEM values, ELEM order) (mg)
112	Y1 and Y2	number of active atoms in suspension and solution in the fluid at end of previous cycle (NELEM values, ELEM order)
113	YDS	number of active atoms in the "surface" deposit at end of previous cycle (NREG values, REPART order) and repeat NELEM times in ELEM order

114	YDI	number of active atoms in the "deep" deposit at end of previous cycle (NREG values, REPART order) and repeat NELEM times in ELEM order
115	YOXY	number of active atoms in the oxide at end of previous cycle (NREG values, REPART order) and repeat NELEM times in ELEM order
116	ASP	number of base metal atoms in flux of daughter nuclide per gram of parent element at end of previous cycle (NREG values, REPART order) and repeat NELEM times in ELEM order

117	ADENT	wtite FIN in columns 1, 2 and 3

```
TITLE
ILECT        PERF          NELEM         NREAC
IFEM    KD      EFD     COEF    IOPT    PHOPT   TOPT    NPROL
TMOY    TMY     VOLU    DB      DELTA   DELMX   TPI     TPB
if NPROL ≠ 0 ... TMYPRO then go to ELEM
if NPROL = 0 ... go to ELEM

ELEM (1 element per PCB)
EROS (NELEM times)
ROP     DA      PC      DG      SI      NB      PAS1
TOB010  CAPLI
REAC (1 nuclide per PCB)
TOREAC (NREAC times)
EJEC (NREAC times)
CAPT (NREAC times)
PARC (NREAC times)
DO      QACT
NREG    NRCP    NRCA    NCAT    NCD
REPART (to 18A4)
NR1     NR2     NUCAT   NF      NX      FS      FP      (NCAT times this PCB)

SMAT    COR     TERCO   RW      IDECH   FDEB    | (NREG times
COR (NELEM times)                               | this group
VIT     DIAM    TE      TPA     REL     GRAV    | of 3 PCBs)

CPKi (i from 1 to 4)
OALKW (to 1A4: choice between FT3-MESM-MARS)
if FT3...go to ALKWi
else...go to DELTAGi,j

ALKWi (i from 1 to 4)
DELTAGi (i from 1 to 4) (20 times this PCB)
DISFLUi (i from 1 to 4) (4 times this PCB)

NFONC   NCYCLE  DT      DTPROL  PBO     PLI     NARRET
if NARRET = 0, go to DEC2

NRELA   NUMREL (NRELA times)

DEC2    REC2    BOR2    BR2     FREC
if FREC = -1...XRELA (NRELA times, NUMREL order)
if FREC ≠ -1...go back to DEC2 and repeat NCYCLE times

TFONC   CL1     XLI     CL2     FAC     FL      DFU     NIMPR
if NIMPR ≠ 0...TIMPR (NIMPR times)
if NIMPR = 0...go back to TFONC and repeat NFONC times

RDDD                                            | NCD times
ICD                                             | this group
IR                      | ICD times these       | of 4
COED (NREAC times)      | 2 PCBs                | PCBs

if cycle 1:     ETA (NELEM times)
                ESURF (NREG times), and go to ADENT
if cycle>1:     introduce the set of PCBs from the end of previous cycle
ADENT
```

Fig C.1 Diagram of PACTOLE Input Data (ref (9))

```
MIT pH7  run1 NEW COMPOSITIONS+AVERAGE FLUX

          0           0          1          5          5
   0     0    0    0      1     7   300   0
   296.6  270.0  7.94E-4 6.84E-2  86400.0 3600.   272.4         336.4
FE
NI
CO
CR
MN
 0.      0.      0.   0.        0.
 4.0  5.0E-10  1.0 2.0E-07  2.00   10  10.e-7
            9.2E-8   4.7E-12
FE59
MN54
CO58
CO60
CR51
         9.26E-14  1.94e-13    3.40E-12   9.62-10   1.14E-11
         3.95E-12   1.37e-11  1.37e-11  3.95-12   3.95e-12
         0.0          0.0             9.2-08    0.0            0.0
  0.0         8.3E-06   9.1E-06   0.0         0.0
 1.48e-2        4.500E+04
   22  19  19  1  1
out1SG1 SG2 INC1PLENSTSTZIR1ZIR2ZIR3ZIR4ZIR5ZIR6ZIR7ZIR8INC2SG3 SG4 OUT2
PUMPCVC1CVC2CVC3
                              1 18  20  20  3  .999  .999
  0.053  0.01 0.0 2.5E-6  0  1.
  0.09  0.746  3.7E-4  0.1575  0.0026
  3.13  6.159E-3 296.1 290.2  0.  1.
                  0.0185   .01  0.  2.5E-6  0  1.
                  .09  .746    3.7E-4  0.1575  0.0026
                  3.09  6.159E-3  291.4  281.3   0.  0.
      0.0185   .01  0.  2.5E-6  0  1.
      .09  .746   3.7E-4  0.1575         0.0026
      3.02  6.159E-3  282.5   272.4   0.  0.
                  5.2E-3   .01   0.  2.5E-6  0  1.
                  .09  .746   3.7E-4   .1575   0.0026
                  2.97  6.159E-3  277.8  277.5 0.  0.
      0.0195   .04  4.E-5  2.5E-6  0  1.
      .677  .116     5.E-4  .163    .0168
      .177  .0244  277.3  277.  0.122   0.
                  3.71E-3  0.04 6.E-4  2.5E-6  0  1.
                  .677  .116    5.E-4  0.163   0.0168
                  2.96  6.159E-3  277.  277.  0. 0.
         6.4E-3  1.E-4  0.3 2.5E-6  0  1.
         2.E-3   1.0E-5  0.7E-6  1.E-3 5.E-5
         2.68  6.52e-3  278.4  303.0 0.0  0.
                  3.22e-3  1.e-4  1.0  2.5E-6  0  1.
```

Fig C.2 Diagram of PACTOLE Input Data for MITPCCL (1 year run, $pH_{300°C}$=7.0)

```
MIT pH7.2run1 NEW COMPOSITIONS+AVERAGE FLUX

          0           0           1           5           5
   0     0    0    0      1     7   300   0
   296.6  270.0  7.94E-4 6.84E-2  86400.0 3600.   272.4         336.4
FE
NI
CO
CR
MN
 0.      0.      0.   0.        0.
 4.0  5.0E-10  1.0 2.0E-07  2.00   10  10.e-7
            9.2E-8   4.7E-12
FE59
MN54
CO58
CO60
CR51
         9.26E-14  1.94e-13    3.40E-12   9.62-10   1.14E-11
         3.95E-12   1.37e-11  1.37e-11  3.95-12   3.95e-12
         0.0         0.0             9.2-08    0.0            0.0
  0.0         8.3E-06   9.1E-06   0.0         0.0
 1.48e-2        4.500E+04
   22  19  19  1  1
out1SG1 SG2 INC1PLENSTSTZIR1Z/R2ZIR3ZIR4ZIR5ZIR6ZIR7ZIR8INC2SG3 SG4 OUT2
PUMPCVC1CVC2CVC3
                                1 18  20  20  3  .999  .999
  0.053  0.01 0.0 2.5E-6  0  1.
  0.09  0.746  3.7E-4  0.1575  0.0026
  3.13  6.159E-3 296.1 290.2  0.  1.
                  0.0185   .01  0.  2.5E-6  0  1.
                  .09  .746    3.7E-4  0.1575  0.0026
                  3.09  6.159E-3  291.4  281.3   0.  0.
      0.0185   .01  0.  2.5E-6  0  1.
      .09  .746   3.7E-4  0.1575         0.0026
      3.02  6.159E-3  282.5   272.4   0.  0.
                  5.2E-3   .01   0.  2.5E-6  0  1.
                  .09  .746   3.7E-4   .1575   0.0026
                  2.97  6.159E-3  277.8  277.5 0.  0.
      0.0195   .04  4.E-5  2.5E-6  0  1.
      .677  .116     5.E-4  .163    .0168
      .177  .0244  277.3  277.  0.122   0.
                  3.71E-3  0.04 6.E-4  2.5E-6  0  1.
                  .677  .116    5.E-4  0.163   0.0168
                  2.96  6.159E-3  277.  277.  0. 0.
         6.4E-3  1.E-4  0.3 2.5E-6  0  1.
         2.E-3   1.0E-5  0.7E-6  1.E-3 5.E-5
         2.68  6.52e-3  278.4  303.0 0.0  0.
                  3.22e-3  1.e-4  1.0  2.5E-6  0  1.
```

Fig C.2 Diagram of PACTOLE Input Data for MITPCCL (1 year run, $pH_{300°C}$=7.0)

```
                2.e-3    1.0E-5  0.7e-6  1.e-3  5.e-5
                2.74  6.52e-3  282.6  308.6  0.0   0.
        3.22E-3   1.e-4    1.0    2.5E-6    0    1.
        2.E-3   1.0E-5    0.7E-6   1.e-3   5.E-5
        2.77   6.52e-3  288.2  314.1 0.0   0.0
                3.22E-3   1.e-4  1.  2.5e-6   0  1.
                2.E-3 1.0e-5   0.7e-6  1.e-3  5.e-5
                2.82   6.52E-3  293.7  319.7    0.0 0.0
 3.22e-3 1.E-4  1.  2.5E-6  0  1.
  2.E-3 1.0E-5  0.7e-6 1.e-3  5.E-5
 2.87  6.52e-3   299.3  325.3  0.  0.
                    3.22e-3 1.e-4  1. 2.5E-6  0   1.
                    2.e-3   1.0E-5  0.7e-6  1.e-3  5.e-5
                    2.92 6.52E-3  304.9  330.8  0.00  0.000
        3.22e-3 1.E-4  1.0   2.5E-6  0  1.
        2.0E-3  1.0E-5  0.7e-6 1.E-3 5.E-5
         2.96  6.52E-3  310.4  336.4   0.  0.
 6.43e-3  1.e-4 0.3  2.5e-6  0  1.
 2.e-3  1.0e-5 0.7e-6  1.e-3  5.e-5
 3.04  6.52e-3  314.6  316.0  0.   0.
         1.38e-2  0.01  2.7e-4   2.5E-6  0  1.
         .09  0.746   3.69E-4   0.1575  0.0026
          3.35  6.159e-3  315.5  309.4  0.    0.
                    .0185  0.01  2.e-6   2.5E-6  0   1.
                    0.09  0.746   3.69e-4   0.1575  0.0026
                    3.26 6.159E-3 310.6  300.5   0  0.
  0.0185  0.01  0.  2.5E-6  0  1.
  0.09  0.746   3.69e-4   0.1575   0.0026
  3.16  6.159E-3  301.7  291.7  0.    0.
         0.0490  .01  0.0     2.5E-6  0  1.
         0.09  0.746   3.69e-4   0.1575   0.0026
         3.15  6.159e-3  297.1  296.8  0.0 1.
  2.25e-2  0.04 0.   2.5e-6  0 1.
  0.677  0.116         5.0e-4  0.163   0.0168
  0.24  0.0226 296.6  296.6  0. 0.
         9.6e-3  0.01  0.  2.5e-6  0  8.8e-4
         0.063  0.76  3.69e-4   0.15   0.01
         0.020  2.16e-3  240.  200. 0. 1.
                   0.065  0.02  0. 2.5e-6  0 8.8e-4
                   0.50  0.1     5.e-4  0.1    0.02
                  2.6e-3  5.33e-3  21.  65.  0.  1.
  5.8e-2 0.01 0.  2.5E-6  0  8.8e-4
  0.063  0.76   3.69e-4   0.15   0.01
  1.6e-2  2.16e-3  21.  65.  0. 0.
  1.07288933        .138710998E-02  -.350908958E-04   .678307970E-07
FT3
 -14.613  3.13376e-2  -8.85994e-5  6.95324e-8
  -47600.0000        85.592689         .389512181E-1    -.10603985E-3
  -11778.0000        64.1680000        .270332098E-1    -.975000001E-4
```

```
  79335.00000      -43.8900000      1.01237774       -.154120000E-2
  31620.3594        22.4742279       .349869072      -.514469575E-3
 -45710.0000        74.820282        .691640973E-1   -.158460476E-3
 -10630.0000        67.5000000       .247350931E-1   -.116000000E-3
  78673.0000       -50.8023987      1.04607964       -.150000000E-2
 -45000.0000        72.7433777       .75489521E-1    -.143232144E-3
 -10350.0000        81.7584686       .198225975E-1   -.101300000E-3
  79850.00         -33.1825409       .952556789      -.143150000E-2
 -46157.9531        69.4519806       .151711345      -.326872570E-3
 -8668.37891        61.3527527       .425853133E-1   -.117140939E-3
  84095.125        -46.7049103      1.02793026       -.159883196E-2
 -14174.25          73.7179871       .132757008      -.706932333E-4
  3016.58447        59.4344482       .12481159       -.650002476E-4
  54760.2734       -45.2883911       .738931239      -.927461078E-3
  -15000.           41.00           -9.36e-4         -6.6E-5
  -6000.            49.0             -0.0380         -3.00e-5
  22700.            1.53             0.327           -4.54E-4
  37707.3594        16.5611267       .361570954      -.535933301E-3
 -.821699977       -.310000009E-02   .0               .0
  5.32417965       -.258145109E-01   .635595643E-04  -.555539685E-07
  5.35170555       -.231129117E-01   .561919878E-04  -.549930093E-07
  6.94832230       -.393063612E-01   .788164762E-04  -.749785727E-07
        1      1    365  0.     1.0   0.001   0
365.  0.  800.  0.  0.
365  1.84  1.84  1.84   24.  1.0      0.      0
365.
1
1

6
3  1.5  1.5  6.7  7.5e-3
0.00700   0.0023     4.E-06  5.e-04  2.e-04

0.05  0.05  0.05  0.05  0.1  0.1 5.e-3  5.e-3  5.E-3  5.E-3
5.E-3  5.E-3
5.e-3  5.e-3  0.05  0.05  0.05  0.05  0.05  0.05  0.05  0.05
FIN
```

Table C.2 Description of CORA-II release 2.0 Input Variables (ref (4))

No.	Variable	Description
1	TITLE	Any alphabetic or numeric information
2	K	number of isotopes (max. of 10)
3	NMAT	number of materials (max. of 10)
4	NP	number of parent elements of K isotopes
5	LCY(i) i = 1 to 6	No of cycles for ith isotope (Cr 51, Mn 54, Mn 56, Co58, Fe 59, Co6)
6	V2	reactor coolant volume (hot conditions) (cc)
7	A6	total out of core surface area (cm^2)
8	A3	total in-core surface area (cm^2)
9	VIX	purification flow rate (cc/sec)
10	VELC	RCS coolant velocity-in core (cm/sec)
11	VELL	RCS coolant velocity-in loop (cm/sec)
12	DENF	RCS coolant density (g/cc)
13	CFSF	core flow splitting factor
14	CTF	factor to calculate transient in-core deposit
15	CP	Max. permanent in-core deposit (mg/dm^2 as oxide)
16	ETF	factor to calculate transient out-of-core deposit
17	EP	Max. permanent out-of-core deposit (mg/dm^2 as oxide)
18	OMR	oxide to metal ratio of crud
19	TOP	operating time during which out-of-core crud deposits grow faster due to high corrosion (sec)
20	PHIT	Avg. core thermal neutron flux (n/cm^2-sec
21	PHIF	Avg. core fast neutron flux (n/cm^2-sec)
22	TC	RCS coolant transit time-in-core (sec)
23	TL	RCS coolant transit time-out-of-core (sec)
24	DVOL	Demineralizer resin volume (cc)
25	DFP	Purification system DF for particulates
26	DFS	Purification system DF for solubles
27	TEMPH	Reactor coolant system core avg. temp. (deg F)
28	TEMPG	Reactor coolant system S/G avg. temp. (deg F)
29	CONTH	delta T in core (deg C)
30	CONTG	delta T in S/G (deg.C)
31	ID(I)	Identifier of ith isotope (e.g. Co58, Co60,..)
32	NOP(I)	Atomic number of ith parent element
33	XLAM(I)	decay constant of ith parent element (1/sec.)
34	SIGTH(I)	Thermal reaction cross section (cm^2)
35	SIGEP(I)	Epithermal reaction cross-section (cm^2)
36	SIGF(I)	Fast reaction cross-section (cm^2)
37	ABUND(I)	Abundance of ith parent isotope
38	EPDIS(I,i) with i=1 to 7	Gamma emission rate for E Group i (MeV/dis)
39	CRUDTYP	Type of crud- considered in calc. of solubility (MAG or FER)

40	SN	Substitution number for nickel in magnetite
41	CH2S	concentration of hydrogen in solution (cc/kg)
42	MNSOL	Corrosion behavior at high pH (>min solubility) 0-increase 1-constant 2-decrease
43	IP(I)	Identifier of parent element (e.g. Ni, Co,..)
44	NO(I)	Atomic number of ith parent element
45	XA(I)	Atomic weight of ith parent element
46	TITMA(i)	Alphanumeric identification of ith material
47	F(i,j) i=1 to NMAT j=1 to NP	Weight fraction of jth element in ith material
48	NCOB	No. of cycles over which the weight fraction of elements can vary in material compositions
49	IELM	Element number which varies from cycle to cycle
50	REL(i,j) i=1 to NMAT j=1 to NP	crud elemental release fraction of jth element in ith material
51	NRCM	Number of cycles over which the material corrosion releaes rate varies
52	RCM(i,j) i= 1 to NMAT j= 1 to N	Corrosion release of ith material during cycle 1 (mg/dm^2-mo)
53	AIN(i) i= 1 to NMAT	In-core area of ith material (sq.cm)
54	Aout(i) i= 1 to NMAT	Out-of-core area of ith material (sq.cm)
55	XSOL(i)	Solubility factor [sol.(i)/sol.(Fe)] for ith isotope (based on R&D at Westinghouse
56	DEPS	Constant for CL (subroutine COIN) RCS crud deposition constant (1/sec) normally=1.7E-4
57	CL4	constant for CL (subroutine COIN), period after which in-core crud layer thickness remains constant - does not affect results except coolant activity-
58	RCL4	Constant for RCL (subroutine COIN)
59	RCL7	Constant for RCL (subroutine COIN)
60	RE3	Constant for KP3 (subroutine COIN) particle deposition constant - in-core normally=2.52E-5
61	RE6	constant for KP6 (subroutine COIN) particle deposition constant-out-of-core normally=2.48E-5
62	REN3	Reynolds number in core

63	REN6	Reynolds number out-of-core
64	AREASP	constant for A52 and A82 (subroutine COIN)
65	B4CONT	Growth affinity factor for B4 (subroutine COIN)
66	B7CONT	Growth affinity factor for B7 (subroutine COIN)
67	LIMHCC	Cycle limit for high in-core crud growth
68	IFIXB	RCS Boron control option 1=constant boron 2=variable boron
69	N4STAB	Cycle no. after which Node 4 (permanent in-core metal inventory) has stabilized (coin) 0=no restriction on deposit growth
70	NRFF	No. of refueling factor sets
71	AREASOL	constant for C42 and C72 (subroutine COIN)
72	CONTPP	constant for surface precipitation (COIN)
73	AREASS	constant for A82 (subroutine COIN)
74	NCSTD	cycle number for standard TERM2
75	R1	Transient in-core crud activity (previous cycle) -not used if NRFF=1-
76	R2	Permanent in-core crud metal (previous cycle) -not used if NRFF=1-
77	R31	Permanent in-core crud activity (previous cycle-cycle 1) -not used if NRFF=1-
78	R32	Permanent in-core crud activity (previous cycle-cycle 2) -not used if NRFF=1-
79	R33	Permanent in-core crud activity (previous cycle-cycle 3) -not used if NRFF=1-
80	R4	Transient out-of-core crud activity (previous cycle) -not used if NRFF=1-
81	R6	Permanent out-of-core crud activity (previous cycle) -not used if NRFF=1-
82	R7	Purification system crud activity (previous cycle) -not used if NRFF=1-
83	R81	Structural core component activity , cycle 1 (previous cycle) -not used if NRFF=1-
84	R82	Structural core component activity, cycle 2 (previous cycle) -not used if NRFF=1-
85	R83	Structural core component activity, cycle 3 (previous cycle) -not used if NRFF=1-
86	NCY	number of operating cycles
87	CY(I)	operating time of the cycle (sec)
88	SDNT(I)	Shutdown time at end of cycle (sec)
89	RITH(I)	Initial RCS Lithium concentration at start of cycle (ppm)
90	BORF(I)	Initial RCS boron conc. at start of cycle (ppm)
91	NFUEL(I)	Refueling cycle option 1=no refueling 2=refueling at end of cycle
92	CCH2S	RCS hydrogen concentration (ml/kg)
93	TB1	cycle time associated with boron reduction (sec)
94	DELTA	Initial printout time (sec)
95	UDELTA	Upper limit of printout time intervals (sec)
96	TIMES	printout step size multiplier

97	MXCY	Number of cycles containing sub-periods
98	CHEM	chemistry changes in sub-periods y=yes N=no
99	JCY	Cycle no. which contains sub-periods
100	NSCY	Number of sub-periods within the cycle
101	STIME(i,j)	End of jth sub-period in cycle i (sec)
102	CAPS(i,j)	Fraction of full power of jth sub-period in cycle i

TITLE

K NMAT NP

LCY(1) LCY(2) LCY(3) LCY(4) LCY(5) LCY(6)

V2	A6	A3	VIX	VELC	VELL	DENF
CFSF	CTF	CP	ETF	EP	OMR	TOP
PHIT	PHIF	TC	TL	DVOL	DFP	DFS
TEMPH	TEMPG	CONTH	CONTG			
ID(1)	NOP(1)	XLAM(1)	SIGTH(1)	SIGEP(1)	SIGF(1)	ABUND(1)
ID(2)	NOP(2)	XLAM(2)	SIGTH(2)	SIGEP(2)	SIGF(2)	ABUND(2)
ID(3)	NOP(3)	XLAM(3)	SIGTH(3)	SIGEP(3)	SIGF(3)	ABUND(3)
ID(4)	NOP(4)	XLAM(4)	SIGTH(4)	SIGEP(4)	SIGF(4)	ABUND(4)
ID(5)	NOP(5)	XLAM(5)	SIGTH(5)	SIGEP(5)	SIGF(5)	ABUND(5)
ID(6)	NOP(6)	XLAM(6)	SIGTH(6)	SIGEP(6)	SIGF(6)	ABUND(6)
EPDIS(1,1)	EPDIS(1,2)	EPDIS(1,3)	EPDIS(1,4)	EPDIS(1,5)	EPDIS(1,6)	EPDIS(1,7)
EPDIS(2,1)	EPDIS(2,2)	EPDIS(2,3)	EPDIS(2,4)	EPDIS(2,5)	EPDIS(2,6)	EPDIS(2,7)
EPDIS(3,1)	EPDIS(3,2)	EPDIS(3,3)	EPDIS(3,4)	EPDIS(3,5)	EPDIS(3,6)	EPDIS(3,7)
EPDIS(4,1)	EPDIS(4,2)	EPDIS(4,3)	EPDIS(4,4)	EPDIS(4,5)	EPDIS(4,6)	EPDIS(4,7)
EPDIS(5,1)	EPDIS(5,2)	EPDIS(5,3)	EPDIS(5,4)	EPDIS(5,5)	EPDIS(5,6)	EPDIS(5,7)
EPDIS(6,1)	EPDIS(6,2)	EPDIS(6,3)	EPDIS(6,4)	EPDIS(6,5)	EPDIS(6,6)	EPDIS(6,7)
CRUDTYP	SN	CH2S	MNSOL			

IP(1)	NO(1)	XA(1)
IP(2)	NO(2)	XA(2)
IP(3)	NO(3)	XA(3)
IP(4)	NO(4)	XA(4)
IP(5)	NO(5)	XA(5)

TITMA(1)	TITMA(2)	TITMA(3)
F(1,1)	F(2,1)	F(3,1)
F(1,2)	F(2,2)	F(3,2)
F(1,3)	F(2,3)	F(3,3)
F(1,4)	F(2,4)	F(3,4)
F(1,5)	F(2,5)	F(3,5)

NCOB

REL(1,1)	REL(2,1)	REL(3,1)
REL(1,2)	REL(2,2)	REL(3,2)
REL(1,3)	REL(2,3)	REL(3,3)
REL(1,4)	REL(2,4)	REL(3,4)
REL(1,5)	REL(2,5)	REL(3,5)

NRCM

RCM(1)	RCM(2)	RCM(3)				
AIN(1)	AIN(2)	AIN(3)				
AOUT(1)	AOUT(2)	AOUT(3)				
XSOL(1)	XSOL(2)	XSOL(3)	XSOL(4)	XSOL(5)	XSOL(6)	
DEPS	CL4	RCL4	RCL7	RE3	RE6	
REN3	REN6	AREASP	B4CONT	B7CONT	LIMHCC	IFIXB
N4STAB	NRFF	AREASOL	CONTPP	AREASS	NCSTD	
R1(N)	R2(N)	R31(N)	R32(N)	R33(N)	R4(N)	R6(N)
R7(N)	R81(N)	R82(N)	R83(N)			

NCY

CY(I)	SDNT(I)	RITH(I)	BORF(I)	NFUEL(I)	CCH2S	TB1
DELTA	UDELTA	TIMES				
MXCY	CHEM					

JCY NSCY STIME(1,1)

CAPS(1,1)

Fig C.3 Diagram of CORA Input Data

```
PCCL(CORA2R2) CASE USING FER CONSTANT LITHIUM AT 1.84,fast flux*2
          6          3          5
     1    1     1    1     1    1
    6.17 +2   2.414 +3    4.02 +2     8.3 -2    2.84 +2    3.18 +2   7.000 -1
 1.0000 +0    1.500 +1   5.000 -1   2.000 +1   5.000 +0   1.400 +0   0.000
   2.500+13   4.300+13   7.000 -1   4.500 +0   1.000 +2   1.000 +2   1.000 +2
   5.607 +2   5.616 +2   1.730 +1     5.5 +0
CR-51    24   2.880 -7   1.350-23   1.730-24   0.0        4.130 -2
MN-54    26   2.560 -8   0.0        0.0        1.013-25   5.820 -2
MN-56    25   7.460 -5   1.330-23   4.580-24   2.230-27   1.0
CO-58    28   1.130 -7   0.0        0.0        1.683-25   6.800 -1
FE-59    26   1.780 -7   1.200-24   4.440-25   1.820-27   3.300 -3
CO-60    27   4.180 -9   1.944-23   2.132-23   4.830-27   1.0
   2.880 -2   0.0        0.0        0.0        0.0        0.0        0.0
   0.0        8.350 -1   0.0        0.0        0.0        0.0        0.0
   0.0        0.0        8.390 -1   0.0        0.0        0.0        0.0
   0.0        9.550 -1   1.210 -2   1.000 -2   0.0        0.0        0.0
   6.520 -3   0.0        1.180 +0   0.0        0.0        0.0        0.0
   0.0        0.0        2.510 +0   0.0        0.0        0.0        0.0
FER           0.600 +0   2.400 +1            1
   CR     24   52.01
   MN     25   54.93
   FE     26   55.85
   CO     27   58.94
   NI     28   58.69
   SS-304      ZIRC 4     INC 600
   0.1000      0.0010     0.1500
   0.0200      0.00005    0.0100
   0.5000      0.0020     0.0630
   0.0005    0.0000007    0.00037
   0.1000      0.00001    0.7600
          0
   2.000 -2   2.000 -2   2.000 -2
   5.000 -1   5.000 -1   5.000 -1
   5.000 -1   5.000 -1   5.000 -1
   5.000 -1   5.000 -1   5.000 -1
   5.000 -1   5.000 -1   1.000 -1
   1          RCM
   1.0000+0   0.0001-4   4.0000+0
   0.0        2.7300+2   0.0
   4.7230+2   1.3700+2   1.9420+3
     0.05+0     1.00+0     0.50+0   1.000+0     1.0+0     1.00-3
     1.70-4      1.0+0     0.50+0    0.50+0   2.52-5     2.48-5
      1.5+5    1.47+5     5.00+1     1.0+0     1.0-1          1          0
          0         1     2.50+1    1.50-2    5.00+1          1
      1.0+0      1.0+0      1.0+0     1.0+0     1.0+0      1.0+0      1.0+0
      0.0+0      1.0+0      1.0+0     1.0+0
1
    31.5+6     0.00+0   1.840+0   8.000+2          0     24.0+0     31.5+6
 4.320 +6   4.320 +6   1.000
          1          N
    1     1     31.5+6
                1.0
```

Fig C.4 Diagram of CORA Input Data for MITPCCL (1 year run, $pH_{300°C}$=7.0)

Table C.3 Description of CRUDSIM Input Variables (ref (1)

No.	Variable	Description
1	DAYS	duration of operation (day)
2	IN	time step size of numerical calculation (day):0.1 recommende
3	NTMA	number of time steps per printing output
4	NTS	number of meshes in numerical integration of solubility by temperature (normally 1<nts<50): 10 recommended
5	BETAC	crud transport factor in CRUDSIM/MIT
6	BETAA	activity transport factor in CRUDSIM/MIT
7	BORON	concentration of boron (ppm)
8	ALIT	concentration of LiOH (ppm)
9	CH2	hydrogen concentration (cc/kg-H_2O)
10	FLOW	coolant flow rate (kg H_2O/day)
11	ONOFF	coolant flow, on or off (1 or 0)
12	P1	% power for calculation of neutron activation
13	TIN	core inlet temperature (° C)
14	TOUT	core outlet temperature (° C)
15	DTBL1	temperature difference across the boundary layer in the core (°C)
16	DTBL3	temperature difference across the boundary layer in the S/G (°C)
17	FPUR	bypass flow rate of purification system (kg H_2O/day)
18	DEN	average density of the coolant (kg/m^3)
19	VIS	average viscosity of the coolant (n.sec/m^2)
20	IH	initial crud inventory in the core (kg-Fe)
21	IC	initial crud inventory in the S/G (kg-Fe)
22	AH1	initial Co-60 activity in the core (Ci)
23	AH2	initial Co-58 activity in the core (Ci)
24	AC1	initial Co-60 activity in the S/G (Ci)
25	AC2	initial Co-58 activity in the S/G (Ci)
26	AD1	initial Co-60 activity in the purification system (Ci)
27	AD2	initial Co-58 activity in the purification system (Ci)
28	IREF	refuelling of fuel assemblies, on ro off (1 or 0)
29	IPAR	particulate precipitation in the coolant, on or off (1 or 0)
30	INPRIN	printing of input data and detailed output, on or off (1 or 0)
31	DE1	hydraulic diameter of core fuel channel (m)
32	DE3	printing of input data and detailed output, on or off (1 or 0)
33	AR1	hydraulic diameter of core fuel channel (m)
34	AR3	hydraulic diameter of S/G tube (m)
35	AF1	coolant flow area in the core (m^2)
36	AF3	coolant flow area in the S/G (m^2)
37	DSOL	diffusion coefficient of soluble species (m^2/sec)
38	DPAR	diffusion coefficient of particulates (m^2/sec)
39	ALPH1	Co-60 production rate in core (Co60 Ci/kg-Fe.day.%power)
40	ALPH2	Co-58 production rate in core (Co58 Ci/kg-Fe.day.%power)
41	LAMD1	decay constant of cobalt-60 (day^{-1})
42	LAMD2	decay constant of cobalt-58 (day^{-1})
43	RR58	fractional direct recoil release of Co-58 produced by (n,p)
44	RR60	fractional direct recoil release of Co-60 produced by (n,r)

45	HCRYSC	crystal growth coefficient of corrosion productsin the core (m/sec)
46	HCRYSA	crystal growth coefficient of activity in the S/G (m/sec)
47	HDISSC	dissolution coefficient of corrosion products in the S/G (m/sec)
48	HDISSA	dissolution coefficient of activity in the core (m/sec)
49	CR	corrosion rate of the S/G (kg/day)

DAYS,IN,NTMA,NTS,BETAC,BETAA
BORON,ALIT,CH2,FLOW,ONOFF,P1,TIN,TOUT,DTBL1,DTBL3,FFUR,DEN,VIS
IH,IC,AH1,AH2,AC1,AC2,AD1,AD2
IREF,IPAR
INPRIN
DE1,DE3,AR1,AR3,AF1,AF3
DSOL,DPAR
ALPH1,ALPH2,LAMD1,LAMD2
RR58,RR60
HCRYSC,HCRYSA,HDISSC,HDISSA
CR

Fig C.5 Diagram of CRUDSIM Input Data

```
365.,0.1,10,10,0.01,0.005
800.,1.84,25.0,5914.,1,100.,273.9,315.6,23.23 ,-5.57,4.617,723.,9.278e-5
1.e-10,0.250e-4,0.,0.,0.,0.,0.,0.
1,0
1
0.652e-2,0.6159e-2,0.026,0.097,3.34e-5,2.98e-5
1.08e-8,6.9e-10
2.400e-3,3.94e-2,3.6e-4,9.78e-3
0.0 ,0.0
1.e6,1.e6,1.e6, 1.e6
3.55e-7
-1,-1,-1,-1,-1,-1
```

Fig C.6 Diagram of CRUDSIM Input Data for MITPCCL (1 year run, $pH_{300°C}$=7.0)